TITLE Silicon Molecular Beam Epitaxy: Doping and Material Aspects

AUTHOR Govind Pindoria
(formally Govind Patel)

INSTITUTION and DATE University of Warwick, 1990

Silicon Molecular Beam Epitaxy: Doping and Material Aspects

Govind Pindoria
(formally Govind Patel)

Thesis submitted in partial fulfilment of the requirements for the degree of Doctor of Philosophy.
University of Warwick, Department of Physics.

April 1990.

Summary

Silicon Molecular Beam Epitaxy (Si-MBE) allows independent control over the dopant and matrix species, offering the possibility of engineering device structures with resolution down to the monolayer level. However, significant improvements in material quality and doping capability are essential before the potential of the growth technique for applications in VLSI technologies and in evaluating new device designs can be assessed.

Three key areas have been identified in this study, where advances were considered feasible in the time scale of this project: particulate contamination, the modelling of the co-evaporation dopant incorporation process and an evaluation of a new dopant in Si-MBE, phosphorus. A fourth area, that of metallic contamination, was also investigated.

Particulate contamination in Si-MBE epilayers is of increasing concern, as the possible applications of this layer growth technology to VLSI are assessed. A systematic study of several hundred epilayers correlated the particulate contamination in the epilayers with the high electron flux in the deposition region arising from the electron beam evaporator and with the unstable excess silicon deposits in the growth chamber. Reduction of silicon accumulation in the deposition zone by containment of the silicon flux significantly reduces particulate densities in the epilayers. Two types of particulate-related features have been identified. The first type thought to be due to microscopic particulates is decorated by crystallographic defects, whereas the second type, which is free of these defects, appears to be related to shadowing by larger particulates. A correlation in the densities of both types of particulate defects in epilayers grown under a variety of experimental conditions suggests a common source.

The incorporation of dopants in Si-MBE has proven to be the most difficult aspect of this growth technology. In this study it is shown that the atomic size of a dopant relative to the matrix, is the key parameter which determines whether or not a dopant exhibits surface accumulation behaviour during molecular beam epitaxy. Specifically, surface accumulation only occurs if the dopant atoms are larger than those of the matrix atom substituted. In compound and alloy matrix systems, this size effect strongly influences the net site occupation of a dopant, a process previously believed to be dominated by site availability. The physical basis of this phenomenon is discussed with particular reference to theories of equilibrium surface segregation and the nature of the surface stress.

Although p-type doping in Si-MBE with boron is now well established, allowing high doping concentrations and good dopant control, n-type doping using antimony has not matched these achievements, the problems becoming acute at low growth temperatures, ($\leq 500^{o}C$). A possible alternative is the use of phosphorus instead of antimony. In this study the first phosphorus doped Si-MBE epilayers were grown, using a tin phosphide source. Bulk-like mobilities were demonstrated. The behaviour of phosphorus as a function of growth parameters and of "potential enhanced doping" indicates a non-unity, almost growth temperature independent incorporation efficiency. Preliminary evidence indicates that phosphorus does not accumulate on the growing silicon surface, in line with the predictions of the empirical model.

Metallic impurities can have a variety of influences on semiconducting devices, the majority of them detrimental. A preliminary investigation into the levels of metallic impurities in MBE grown silicon was carried out and a methodology developed aimed at reducing these levels.

Contents

Tables and figures

Acknowledgements

This research was initiated at the City of London Polytechnic in the Department of Physics which, sadly, no longer exists. I wish to thank the technical staff at the polytechnic for their help during my brief time there, in particular Pat Driscoll and William Hugglestone.

I also wish to thank my supervisor, Evan Parker, for seeing me through this work and to the research staff at both departments. Particularly Richard Kubiak, Yee Leong, Richard Houghton, Tim Naylor, Carl Parry and Mark Hopkinson. Other members of the research staff to which I am indebted are; Bob Barlow, Robin Biswas, Mark Dowsett, Simon Newstead and Phil Woodruff. My thanks also go to Bruce Hamilton at UMIST for organising my stay there.

I would like to acknowledge Philip Ashby (Mullards, Southampton) for the surfacan analysis.

The initial part of this work was funded by the Alvey Directorate, project 024 and carried out in association with the General Electric Company (Hirst Research Centre) and British Telecommunications (Martlesham Heath).

Declaration.

The work presented in this thesis was carried out either by or at the instigation of the author. It is presented according to the guidelines laid done in the regulations of the University of Warwick, see document Phys/PG3 (1988).

Several parts of this study have been or are in the process of being published. These are:

1) Pindoria. G, Houghton. R.F, Hopkinson. M, Whall. T, Kubiak. R.A.A, Parker. E.H.C, (1990), Particulate contamination in silicon grown by molecular-beam epitaxy, J. Vac. Sci Technol. B8(1). p21-27. Incorporated into chapter 3.

2) Pindoria. G, Kubiak. R.A.A, Newstead. S.M, Woodruff. D.P, The Influence of Atomic Size on Dopant Accumulation and Site Occupancy in Molecular Beam Epitaxy, Surface Science, July/August 1990. Incorporated into chapter 4.

3) Kubiak. R.A.A, Patel. G, Leong W.Y, Houghton R, Parker E.H.C, (1986), Co-evaporation Doping in Si Grown by Molecular Beam Epitaxy, Appl. Phys. A41. p233-235. Incorporated into chapter 5.

CHAPTER 1.

Introduction.

Silicon Molecular Beam Epitaxy (Si-MBE), (Parker 1985, Iyer 1986, Kubiak & Parker 1988, Kasper & Bean 1988), involves the growth of single crystal layers of silicon on a moderately heated (400°C to 850°C) single crystal silicon substrate, by an impinging flux of silicon. The growth is carried out in an ultra high vacuum environment, which allows a single crystal of extremely high purity to be grown. The electrical properties of the silicon epilayers are modified by adding current carriers. Doping by Group III elements on substitutional sites results in the addition of holes (p-type doping). Doping by Group V elements results in the addition of electrons (n-type doping).

An electron beam evaporator is used as the source of silicon and thermal effusion source cells are used to provide the dopant flux. This independent control over the dopant and matrix species offers the possibility of engineering a device structure with resolution down to the monolayer (~5 Å) level. Indeed initial attempts have come close, eg. Mattey et al (1990) report the growth of a ~20 Å dopant spike. However, to achieve the maximum resolution and exploit it to produce novel devices, there are still several problems to be overcome. These obstacles are two fold. (i) Improvement of the controllability of dopants and increasing the maximum doping level achievable with n-type dopants and (ii) reduction of the impurity and crystallographic defect levels, which can influence the final device properties.

Before these problems are discussed the basic theory of MBE growth will be described.

1.1 MBE Growth.

The MBE growth process involves a change of state, a transition from the vapour phase to the solid phase. In principle this process can be used to obtain thin films of any material, as long as the requisite building blocks are present in the vapour phase. Indeed MBE has been used to grow semiconductors, superconductors (Kwo et al 1988) and insulators, (Stenin 1986). To obtain a thin, single crystal film requires a greater degree of control over the growth conditions and the composition of the vapour arriving at the substrate, the primary requirement being that growth is carried out at a temperature, such that the adsorbed species are mobile enough to form the required single crystal. Other considerations are the surface finish of the substrate and the influence of impurity species on the growth kinetics.

1.1.1 *Crystal growth.*

The Burton, Caberra and Frank (BCF) theory (Burton et al 1951), is used as a basis for the description of two dimensional (2D) crystal growth. Other growth regimes are possible (eg. 3D growth), however as monolayer resolution is not possible in these regimes, they will not be considered here.

If the crystal surface is in contact with its vapour phase at thermal equilibrium, the BCF theory proposes that the growth of the crystal surface will occur as the result of 3 mechanisms. (1) Exchange of molecules between adsorbed layer and vapour, (2) diffusion of adsorbed molecules towards a step, leading to incorporation and (3) possible diffusion of molecules in the edge of the step towards kink sites before incorporation, shown in figures 1.1a & 1.1b.

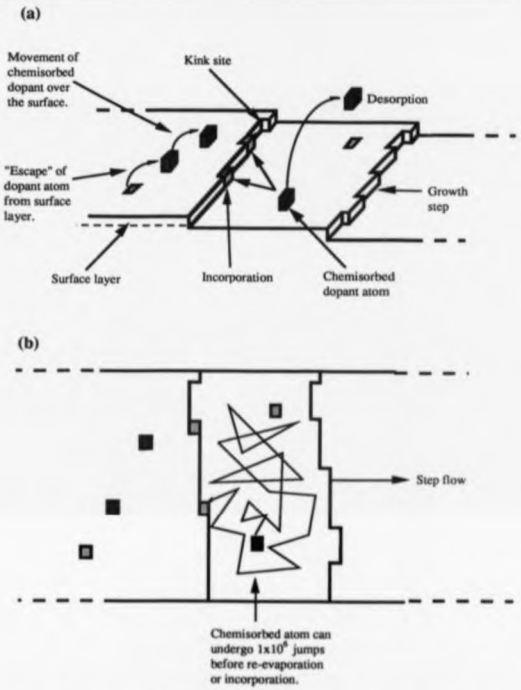

Figure 1.1. Schematic of the 2D layer by layer growth on the surface of a semiconductor, (a) illustrates the possible mechanisms that can occur on the surface and (b) illustrates the "free" movement of an atom on the surface before it incorporates at a step edge. Even for dopants with high vapour pressure at typical growth temperatures (400 °C to 850 °C), the surface lifetime of the adlayer atoms is long, allowing for ~$1x10^6$ jumps before re-evaporation, (Joyce et al 1988).

This process relies on the presence of steps on the single crystal surface. This is not a limitation as the surfaces of commercial silicon substrates are generally mis-oriented from the desired direction. This gives rise to reconstruction of the surface and the introduction of steps. The step separation (L_s) and hence their density can be calculated by equation 1.1 (Allen & Kasper 1988).

$$L_s = \frac{h}{\sin i} \qquad \ldots\ldots\ldots\ldots \quad 1.1$$

Where i = angle of mis-orientation and h = step height. For an angle of 0.250° and h = 3.84 Å Allen & Kasper calculate that the step density is,

$$\frac{1}{L_s} = 1 \times 10^5 \text{ steps cm}^{-1}$$

Continuation of the growth process requires the nucleation of islands on the surface and step flow. Under the supersaturation conditions prevalent in MBE the condensation rate of silicon onto the substrate is high enough for this to occur.

In the BCF theory the growth rate is dependent on the diffusion coefficient of the silicon atoms and their lifetime, on the surface of the substrate. Under this assumption, the velocity of the step across the crystal surface and hence the growth rate can be deduced. However, as MBE growth occurs under conditions of extreme supersaturation, description of the movement of the silicon atoms across the crystal surface by diffusion equations is no longer considered realistic. The BCF theory can be extended to account for these situations by assuming that in the immediate vicinity of each growth step, the local population is well below the overall level, due to continual incorporation into the step edge, (Mullins & Hirth 1963). A recent description of the 2D growth process (based on the BCF theory), is presented by Chen & Iyer (1988).

The 2D stepwise growth mechanism has been directly observed by Neave et al (1983), who investigated MBE growth of GaAs. MBE growth of silicon has been investigated using the techniques of Reflection of High Energy Electron Diffraction (RHEED), (Sakomoto et al 1985) and Low Energy Electron Diffraction (LEED), (Horn et al 1988). Both show monolayer growth regimes. Recent Scanning Tunnelling Microscopy (STM) results confirm these observations by directly imaging the Si(100) surface during MBE growth, (Hoeven et al 1989).

An interesting consequence of this 2D growth mechanism is the development of surface features on (100) orientated epilayers $\geq 1\mu m$ thick, generally described as ripple. This surface ripple (illustrated in figures 3.3 and 3.4), is attributed to the growth steps building up a periodic structure which, if growth is continued for a sufficiently long period, will develop into surface ripple. This is discussed in detail by Pidduck et al (1990).

1.1.2 *Transport of dopant to the substrate.*

The kinetic theory of gases (Atkins 1982, Collis 1982), describes the vapour phase of the growth flux, provided; (a) the species are in random motion, (b) experience elastic collisions with each other and (c) their diameters are much smaller then their mean free paths. These conditions are satisfied in MBE, due to the UHV conditions ($<10^{-8}$ Torr) used. The kinetic theory relates the pressure of a vapour to the number of collisions made by the constituents of the vapour on a plane surface, (I), equation 1.2.

$$I = \frac{P}{(2\pi mkT)^{1/2}} \quad m^{-2}\,sec^{-1} \qquad \ldots\ldots\ldots\ldots\ldots\ldots \quad 1.2$$

Where m = mass in Kg, P = pressure in Nm^{-2}, k = Boltzmann's constant and T = absolute temperature of the vapour, (K). Therefore the vapour pressure of the species over the substrate directly determines the

number of molecules arriving at the substrate surface. The vapour pressure of the dopant or silicon flux can be measured using a suitably positioned cross beam mass spectrometer (Stolt et al 1985).

In MBE, the dopant vapour is emitted from a thermal effusion source cell with an orifice of finite dimensions. The partial pressure of the species inside the source cell being much greater than that outside the cell. An ideal orifice of an effusion cell is one of area A (m^{-2}), in a diaphragm of negligible thickness, such that the linear dimensions of A are not greater then the mean free path of the species at either pressure and that the internal dimensions of the cell are greater then the mean free path. If the cell, at operating temperatures contains the condensed phase of the species in equilibrium with the vapour phase, then it is termed a Knudsen cell. The flux of molecules emitted from an ideal orifice in a Knudsen cell is given by equation 1.3.

$$I = \frac{P}{(2\pi mkT)^{1/2}} \frac{A}{\pi l^2} \quad m^{-2} sec^{-1} \qquad \text{..... 1.3}$$

where l (m) is the distance from the orifice to where the flux of the species is measured. Equation 1.3 is only valid for an axial geometry, illustrated in figure 1.2a. For a more realistic geometry, shown in figure 1.2b, the flux at the centre of the substrate (point Z), is given by equation 1.4, (Herman 1982).

$$I_z(\phi) = I \cos\phi \qquad \text{..... 1.4}$$

Where ϕ is the angle the flux from the source cell makes with the normal to the substrate at point Z. The flux intensity at points away from the central line of fire (eg. point Y) is given by equation 1.5.

$$I_y(\varphi) = I_z \cos\theta \cos(\varphi+\theta) \frac{l^2}{r^2} \qquad \text{..... 1.5}$$

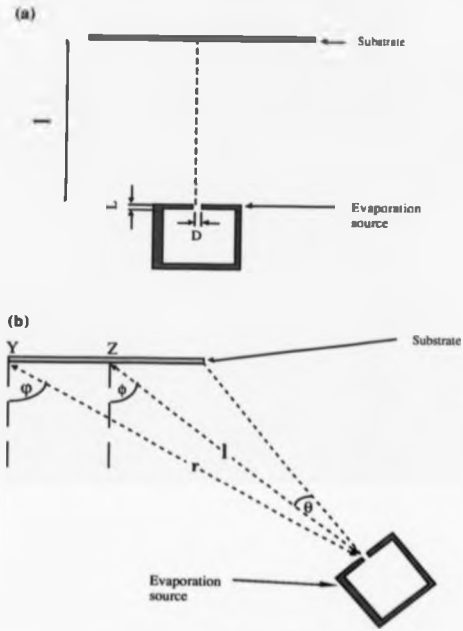

Figure 1.2. Schematic diagrams of dopant source cell-substrate geometry.
(a) Dopant source cell positioned directly below substrate.
(b) Dopant source cell in a more realistic orientation.

The angles φ and θ are illustrated in figure 1.2, r is the distance from the source cell to point Y.

Obviously a practical Knudsen source cell will deviate from the ideal situation. The extent of this deviation is determined by the dimensions of the orifice. The ideal case being when $^{L}/_{D} = 0$, where L = thickness of walls defining the orifice and D = the diameter of the orifice, illustrated in figure 1.1a. Practical MBE source cells are designed to achieve $^{L}/_{D}$ ratios ≤ 0.1, which gives a non-ideality factor $W \geq 0.91$. Inserting this factor into equation 1.3 results in equation 1.6.

$$I_y(\varphi) = \frac{W\ P}{(2\pi mkT)^{1/2}} \frac{A}{\pi l^2} \cos^2\varphi \quad m^{-2}\,sec^{-1} \qquad \ldots\ldots\ldots\ldots\ 1.6$$

1.2 Crystallographic Quality.

Three crystallographic defects are present in the majority of MBE layers investigated in this study, particle related defects (PRD's), (illustrated in figures 3.3 and 3.7), saucer pits (s-pits) and dislocations, (both illustrated in figure 1.5). Other defects occasionally seen are stacking faults and hillocks.

1.2.1. *Assessment of crystallographic defects*

On the as-grown epilayer, only large defects and general surface features can be discerned. To reveal finer detail the epilayers were preferentially etched. Various chemical etches were used, the predominate one being dilute Schimmel etch (1.5 H_2O : 1 CrO_3 (0.75M) : 2 HF), (Schimmel 1979), as it avoids staining problems with highly doped material, (Schimmel & Elkind 1978). The revealed defects were evaluated using several techniques. An optical microscope using Nomarski interference contrast was used to routinely assess the density of defects. A more detailed examination was made using a

Scanning Electron Microscope (SEM) and the Energy Dispersive Analysis by X-rays (EDAX) facility on the SEM, to investigate the presence of impurity elements at defect sites. EDAX however, has a high detection limit of $\sim 10^{18}$ atoms cm^{-3}.

During the course of this study the etching process was characterised and standardised to allow confident comparison of the results between epilayers. To avoid spurious features appearing during etching, the silicon surface has to be clean .ie. free of hydrocarbons, dust etc. Previously a complicated 7 step cleaning procedure was used before etching, (Leong 1985). Investigation of this cleaning procedure revealed it was unnecessary for routine assessment as this was generally done within 24 hrs of the epilayer being removed from the vacuum system. In this case a two step clean was employed, a 1:1 self heating solution of $H_2SO_4 : H_2O_2$ for 10 mins followed by an overflowing rinse in de-ionized (DI) water. To avoid possible re-contamination from particulates during blow drying, the sample was etched "wet". The small amount of water adhering to the surface made no discernible difference to the etch rate. If etching was carried out as soon as the sample is removed from the system no cleaning was found to be necessary.

Factors to be aware of when etching are the evolution of hydrogen during the reaction and the dependence of the etch rate on the doping level, doping type and the density of defects.

The hydrogen is a result of the reduction of the SiO_2 by HF during the reaction,

$$SiO_2 + 6HF \rightarrow H_2SiOF_6 + H_2O + H_2$$

It adheres to the silicon surface, masking it from the etchant, resulting in non-uniform etching. To avoid this, vigorous agitation was normally applied manually. This step was not reproducible and

raised doubts about comparisons. To standardise it a mechanical agitator was constructed principally out of PTFE and polypropylene.

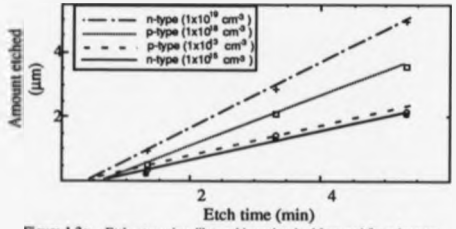

Figure 1.3a. Etch rates using dilute schimmel etch. Measured for substrates with various doping.

The preferential nature of the etchant is the result of the oxidation of silicon by CrO_3 to give SiO_2. This reaction is enhanced at areas of strain and by the presence of excess electrons, resulting in the etch rate being dependent on the doping level and type, (see figure 1.3a). Further investigations of this point discovered that the etch rate was also a function of the doping element, illustrated in figure 1.3b. An interesting consequence of this is the variation of the etch rate with the doping profile in the epilayer, illustrated in figure 1.4.

Empirically it was found that the best delineation of defects was achieved if the etching reaction was timed to remove between 1/2 and 2/3 of the total thickness of the epilayer. Obviously to achieve this control the factors mentioned above have to be taken into account.

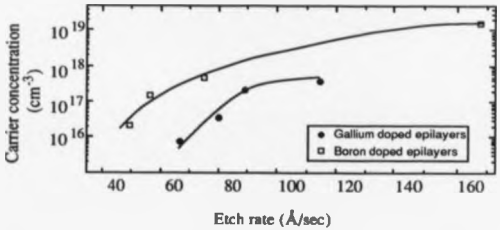

Figure 1.3b. Etch rate variation for boron and gallium doped epilayers as a function of carrier concentration. Using dilute achimmel etch.

Under an optical microscope, the error in counting of the individual defects is ± 20%. However, this will vary with the actual density of the defects and the delineation achieved. For example in thin epilayers, (≤ 0.5 μm), dislocations and a-pits are difficult to distinguish and hence the error in calculating both their surface densities will increase.

1.2.2 *Dislocations.*

Dislocations in Si-MBE have been the subject of intense research and several groups around the world have reported achieving zero dislocations (Ishizaka et al 1982, Tatsumi et al 1985, Sugiura & Ymaguchi 1981). However, in a parallel study, attempts to reproduce similar results using the reported surface cleaning procedures were unsuccessful, (Houghton et al 1987). In fact it was found that the surface cleaning procedure which gave the lowest dislocation density ($\sim 1 \times 10^3$ cm^{-3}), was different to all the reported procedures, (see later).

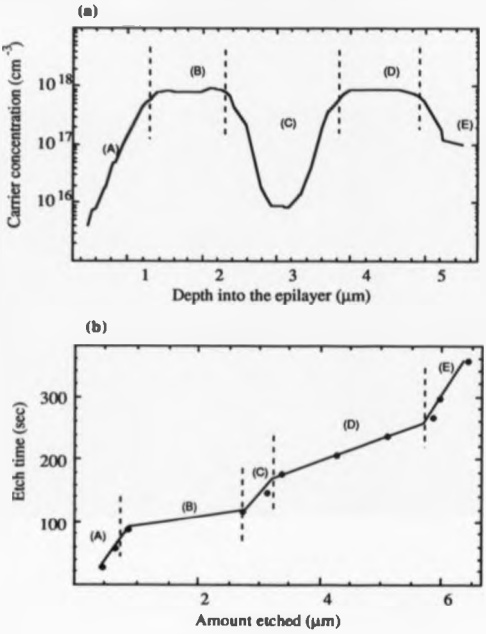

Figure 1.4. Illustration of changing etch rate in an epilayer as the doping profile varies.
(a) Electrochemical capacitance voltage (eCV) profile of a boron doped epilayer, 54/8.
(b) Plot of the etch rate as it varied through 54/8. The regions (A) to (E) correspond directly to those illustrated in (a). The shallower the slope, the faster the etch rate.

The investigation found that the dislocation density was dramatically influenced by growth conditions, the main parameter being the growth temperature. The optimum growth procedure generally used was as follows:

1) Ex-situ chemical clean consisting of a 5 minute dip in 2.5% HF solution (semiconductor grade) followed by a 45 minute rinse in overflowing DI water. The substrate was spun dry before loading into the vacuum system.

2) In-situ clean consisting of heating the substrate to ~400°C and playing a low flux of silicon (1 - 2 Å/sec), on the substrate for 10 to 20 secs. This was followed by immediate warming to 770°C. The substrate was kept at this temperature for ~7 minutes. Growth was initiated at this temperature before the substrate temperature was reduced to the required value, generally ≤ 700°C, over 1 minute. For a fuller description and explanation of these procedures see Houghton et al (1987) and Parker & Whall (1988).

The other growth procedure used involved no ex-situ chemical clean but a thermal in-situ clean. This involved slowly heating the substrate to ~890°C, (the maximum temperature achievable with the tantalum strip heater), to attempt to desorb the native oxide. Growth was initiated at this temperature before the substrate temperature was lowered to the required level. As complete desorption of SiO_2 requires temperatures ≥ 950°C, (Kasper 1987), a graphite meander substrate heater was designed and built that could reach these high temperatures, (see chapter 2).

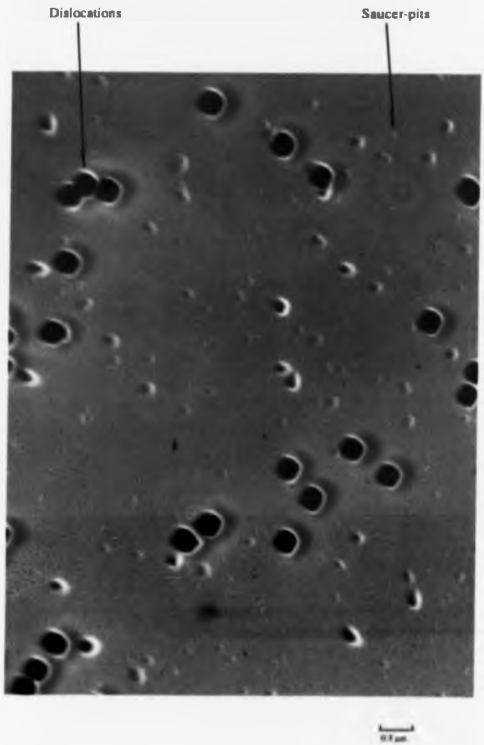

Figure 1.5. Scanning electron microscope image of an etched Si(100) epilayer, illustrating the difference between dislocations and saucer pits.

1.2.3 *Saucer pits.*

Topographically an s-pit is a shallow circular depression in the surface of the epilayer, typically 1/2 μm in diameter, see figure 1.5. Transmission Electron Microscopy (TEM) investigations of these defects have discovered small dislocation loops at their base (Pearce & McMahon 1977), caused by relaxation of the lattice around a precipitate. The nature of the precipitate is uncertain. Ota (1983) correlated a high density of s-pits with a variety of factors:

1) Poor vacuum.

2) Non-uniform heating of the substrate.

3) The presence of strain in the substrate due to thermal stress.

4) Excess dopant vapour.

5) Low growth temperature.

6) Unstable electron beam in the silicon source.

7) Copper contamination.

Other investigations have correlated the concentration of specific metals in the epilayer with the surface haze ie. high density of s-pits. Stacy et al (1981) have determined an empirical formula relating the copper concentration (n) with the surface density of s-pits ($\sigma_{s\text{-pits}}$).

$$n = \frac{v}{t} n' \sigma_{s\text{-pits}} \qquad \ldots\ldots\ldots\ldots\ 1.7$$

where n' is the copper concentration in the precipitate (atoms cm^{-3}), v is the average volume of the precipitate (cm^{-3}) and t is the wafer thickness (cm). They calculated that a copper concentration of 5.2×10^{13} atoms cm^{-3} is needed to produce a s-pit density of 1×10^{4} cm^{-2}, which was their background level. This contamination level varies with the element, eg. Sparks & Chapman (1986), have calculated that the minimum concentration of iron required to form s-pits is only 10 atoms cm^{-3}. The difference between copper and iron being

ascribed to their different solid solubilities. However, the diffusion coefficient of the metal has to be high enough for the metal to form precipitates. Therefore metals, such as copper, with high diffusion coefficients, (at the low growth temperatures of Si-MBE), will be the principle causes of s-pits.

If the metal impurity decorates an existing defect site, such as a dislocation, it will not form an s-pit. Therefore the relative densities of s-pits and dislocations should show an *inverse* proportionality. Figure 1.6 plots the s-pit density as a function of dislocation density.

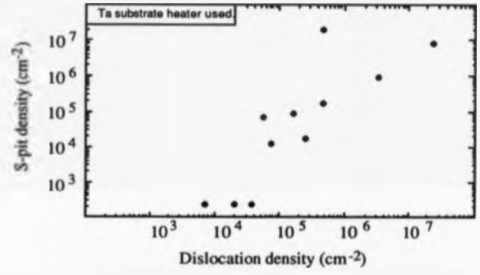

Figure 1.6. Variation of s-pit density as a function of dislocation density, for undoped layers, grown at temperatures in the range 600° C - 700° C. The tantalum strip substrate heater was installed.

As the defect levels are *directly* proportional, it is apparent that the mechanisms of s-pits formation and their effects are not so clear cut. Other factors, such as those listed earlier need to be considered.

There have been claims of zero s-pit densities and hence very low metallic concentration levels, in Si-MBE material (Higgs 1989).

However, these claims are open to question due to the difficulties in measuring their densities. Due to their size, s-pits have to be counted under high magnification in an optical microscope to enable their features to be discerned. This is especially the case in thin epilayers, ≤ 0.5 µm, where dislocations can have a similar appearance under the optical microscope. The detection limit can be estimated by, calculating the s-pit density if only one etch pit is observed in 20 fields of view (the average number of fields assessed for defect evaluation in this study). This gives density between $1x10^2$ and $1x10^3$ defects cm^{-2} for magnifications from 100x to 1500x. Translating these values using equation 1.7 results in ~$4x10^{12}$ copper atoms cm^{-3} and greater levels of other metals with lower solid solubility limits, eg. iron. The lowest densities of s-pits observed during this study were in this range of detection limits, as illustrated in figure 1.6.

1.2.4 *Particulate Related Defects.*

Of the three main imperfections, particulate related defects (PRD) have been the least studied. This was principally due to their low densities, being on average several orders of magnitude below the densities of dislocations. However, as the efforts towards ever higher yields continue and new device designs are assessed, even these comparatively low levels of particulates are unwelcome (Bellavance & Liu 1987). An indication of the limited work carried out on PRD's being the uncertainty surrounding the various types of PRD's. A systematic study of all PRD's has been carried out during this study. The results are presented in chapter 3.

1.3. Unintentional impurities.

The term unintentional impurity covers every other element present in the epilayer apart from silicon and the dopant. Elements

such as carbon and oxygen are present in high concentrations in the substrate and source materials, e.g. ~$1x10^{16}$ cm^{-3}. The source of metallic impurities are varied. Obvious sources are impurities in ; the chemicals used to clean the substrate, the dopant/silicon source material and/or from components that come in contact with the substrate. Other sources, intrinsic to the MBE growth process are investigated in chapter 6.

There is a growing realisation that a greater understanding of all the sources of impurities from each of the steps in the production process is required, from the growth of the epilayer to processing and encapsulation. The thermal history of the epilayer right up to the point the measurement is taken will influence the distribution and environment of the impurity. The concentration and distribution of other impurities and defects in the epilayer can result in complex inter-relationships between different impurity elements. More intractable limitations to the studies that can be carried out on the effect of specific impurities are the detection limits of analytical techniques available to directly measure the concentration of these impurities. In epilayers these limits are significantly higher than when analysing bulk material due to the reduced amount of material available for study.

1.3.1 *Effect of unintentional impurities*

The influences of unintentional impurities on the intrinsic properties of silicon epilayers are varied. Often detrimental, but in a few special cases beneficial. For example switching devices which use the deep levels in the band gap of silicon, caused by metallic impurities, as recombination centres to adsorb introduced carriers arriving at the collector (Ravi 1981).

Impurities can also manifest themselves as a variety of precipitates. Silicides, oxides (due to the high concentration of oxygen

in the raw material) and occasionally metallic precipitates can form. These usually occur in areas of high lattice strain, such as an extended defect, where the volume change occurring on precipitation can be accommodated (Ravi 1981). The formation of the precipitates themselves is a complicated process, dependant not only on the obvious factors such as temperature and solid solubilities of the respective impurities (Graff 1983, Weber et al 1985, Zhu et al 1989), but also on chemical interactions with point defects, (Goorski et al 1988, Gosele & Tan 1985).

The electrical effects of unintentional impurities are due to two processes: (a) Decoration of extended crystallographic defects by metallic atoms, which can provide a leakage path for carriers, hence leading to low breakdown voltages. (b) Formation of energy levels deep in the energy gap of silicon which can act as stepping stones for current carriers to cross the band gap and recombine. Deep levels are due to the formation of charged complexes involving point defects and/or impurity atoms.

The relative importance of the effects are dependent on the impurity. For example, in solar cells all the molybdenum impurity atoms can be electrically active as opposed to ~23% of chromium atoms, (Hopkins & Rohatgu 1986).

1.3.2 *Threshold concentrations of impurities*

In order to assess the effectiveness of any attempts at reducing impurities, it is desirable to know the threshold concentrations below which they have no observable effect. These concentrations vary from impurity to impurity and from device to device, though in general they are low. Solar cells are very sensitive to recombination centres and as such can serve as an indication of the threshold levels, see figure 1.7 (Hopkins & Rohatgu 1986)

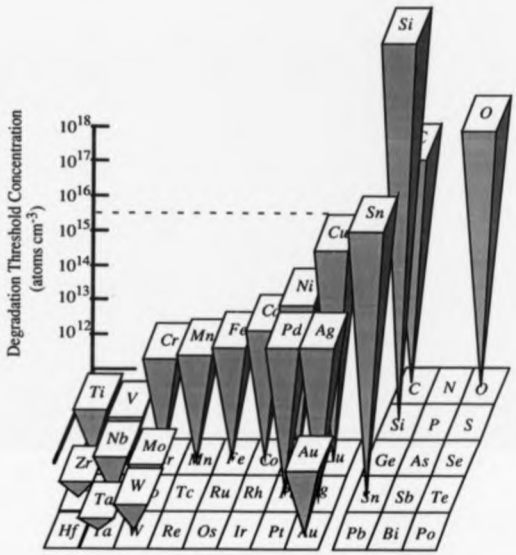

Figure 1.7. Threshold impurity concentrations for reduction in silicon solar cell perfomance, (after Hokins & Rohatgu 1986)

1.3.3 *Gettering Techniques*

Various gettering techniques have been developed to form a "denuded zone" of impurities around the effective working area of the device and trapping the impurity at a "sink" a safe distance away. The techniques are generally separated into intrinsic and extrinsic gettering process.

(i) Intrinsic gettering involves the formation of micro-crystals of SiO_2 which provide strain sites at which other impurity atoms can precipitate, (Craven 1985). The standard process involves 3 (high-low-high) temperature annealing steps to; (a) de-nude the surface region of oxygen, (b) nucleate the oxide precipitates and (c) form the precipitates, (Wong et al 1985). The final trapping process has to be carried out at the end of the production run, as it is possible that further temperature anneals could "re-melt" the gettered metallic precipitates and allow them to diffuse back to the active region of the device, (Borland 1985). Variations of this process have been developed for specific applications, (Wong et al 1985, Forbes et al 1985).

(ii) Extrinsic gettering is generally considered to proceed via the introduction of interstitial silicon (I_{Si}) at the back of the silicon substrate which enhances the dissolution of metal atoms into interstitial sites and hence aid the diffusion of the metal to getter sites, (Bronner & Plummer 1985, Hartzell et al 1985, Sparks et al 1986). The I_{Si} being induced by backside damage, (Sadana 1985, Matsumoto 1985, Lecrosnier et al 1980).

It has to be remembered that even in float zone silicon there is some oxygen present so the intrinsic gettering process is always present. Indeed Shimura et al (1981) and Tsuya et al (1982) have found that they can activate an intrinsic gettering process by the right thermal anneal in low oxygen content wafers. Nauka et al (1985) claim this proceeds via the precipitation of I_{Si} causing strain sites.

Other factors that could influence this process is the carbon and nitrogen content of these wafers.

Dopant atoms have also been used as gettering sites. Polignano et al 1988 found that the smaller dopant atoms, phosphorus and boron, were the most effective as there is more "space" around them to accommodate the formation of impurity complexes, eg. $Au^{+}B^{-}$. The basis of this argument, the nature of strain around the dopant atom, is discussed in detail in chapter 4.

A modified method of gettering is the use of misfit dislocations in SiGe alloys, (Salih et al 1985 and 1986). Misfit dislocations in the range $1x10^{6}$ to $1x10^{8}$ defects cm^{-2} are required within 4-8 μm of the device structure. The exact distance is a compromise between having them close enough to getter, but far enough away to avoid carriers being driven into the misfits during operation of the device. Kikuchi et al (1989), have developed this concept by inducing misfit dislocations in silicon substrates by heavily doping with boron.

1.4 Doping.

The dopant can be added to the growing epilayer in two ways:
1) Co-evaporation of the dopant onto the growing surface.
2) Low energy ion implantation during growth, (Ota 1980). The first method is used in this study. Co-evaporation of a dopant, as with the matrix flux, leads to supersaturation of the dopant vapour above the growing solid phase. The resultant condensate on the substrate surface is a precursor state to accommodation at a step edge. It is mobile at growth temperatures ($\leq$ 850°C) and has a high probability of being evaporated from the surface before accommodation. The relative mobilities, evaporation rates and ease of accommodation will evidently differ between species. The ideal situation is that every

dopant atom that condenses on the growing surface will incorporate into the epilayer as it arrives, however this is not the case for the majority of dopants in Si-MBE. Often the dopant accumulates on the growing silicon surface. This surface accumulation of a dopant can act as a reservoir, from which doping can occur after the dopant flux has been removed. Similarly as the accumulation is building up, the doping level achieved in the epilayer will be lower than would be expected for the dopant flux supplied. This limits the depth resolution of dopant profiles. The kinetics of this process have been investigated for a variety of dopant-semiconductor systems, (Alexandre et al 1980, Collins et al 1982, Harris et al 1984, Parker 1985, Wood 1985, Rockett et al 1985, Barnett & Greene 1985, Ekyholt & Srolovitz 1986, Rockett et al 1986). However, little consideration has been given to the physical process behind the phenomenon. This process is considered in chapter 4 together with an empirical model evolved during this study to predict the surface accumulation behaviour of dopants in MBE.

Several growth procedures have been developed to minimise this dopant profile "smearing":

(i) ***Flash off and Build up*** This technique requires interruption of growth to either build up the surface accumulation to its equilibrium level or evaporate it off. However, growth interrupts have been shown to cause increased incorporation of carbon (Houghton 1989), which is considered detrimental to the final usefulness of a device.

(ii) ***Solid Phase Epitaxy*** Taking the previous technique to its logical conclusion results in Solid Phase Epitaxy (SPE). This technique is currently used to grow delta doping devices (Zeindl et al 1987, Matley et al 1990, van Gorkum et al 1989), with monolayer dopant spikes. In essence it involves growing a thin silicon epilayer, interrupting growth, playing a dopant flux on the surface sufficient to achieve

monolayer coverage and depositing an amorphous silicon layer on top. This structure is then crystallized in situ under conditions designed to limit diffusion of the dopant. To date, dopant profiles of between 1 and 2 nm have been reported for various dopants. However, the problem of impurity incorporation during the interrupt has not yet been overcome.

(iii) *Potential enhanced doping, (PED).* This technique involves applying a negative potential to the substrate during growth. In the case of antimony doping, this method can enhance the doping level by up to 3 orders of magnitude, with extremely abrupt transitions, (Kubiak et al 1985b). It is less effective with arsenic and gallium doping and totally ineffective with boron doping. Jorke (1986) originally proposed that the enhancement was due to secondary implantation of the dopant atoms from the adlayer by Si^+ ions in the growth flux emitted from the electron beam evaporator. Houghton (1989) calculated that the flux of Si^+ ions emitted from the evaporator is insufficient to account for the observed enhancement. He proposed that a more realistic mechanism is that the Si^+ ion damages the silicon surface causing extra sites at which the dopant can incorporate. The differing effectiveness of PED is considered to be related to the differing surface accumulation behaviour of the dopant species. The lower the surface coverage the less effect PED has.

The "standard" n-type dopant in Si-MBE is antimony, despite the fact that it has a comparatively low solid solubility limit, $\sim 1 \times 10^{19}$ atoms cm^{-3}. This limits the maximum electron concentration achievable in the epilayer. The other possible n-type dopants have higher solid solubility limits, eg. $\sim 1 \times 10^{20}$ cm^{-3} in the case of phosphorus doping and $\sim 4 \times 10^{20}$ cm^{-3} for arsenic doping. Concern about their high vapour pressures (which limits the controllability of

the dopant), has so far limited their use in Si-MBE. However the use of compound dopant sources helps to alleviate this problem. Indeed, arsenic doping has been demonstrated in Si-MBE using a compound source, (Kubiak et al 1985b). The first investigation into phosphorus doping in Si-MBE was carried out during this study. The results are presented in chapter 5.

1.5 Applications.

A range of standard devices structures have been grown by Si-MBE. For example p-i-n switching diodes (Ota 1977), MOS transistors (Katayama et al 1979), hyper-abrupt diodes (Ota 1983) and IMPATT diodes (Luy 1990).

However, the advantages of MBE have made it the technique with which to grow experimental devices. The atomic layer doping has already been mentioned. Other recent experimental structures grown include the camel diode (Shannon 1979) and the doping superlattice (Nakagawa & Shiraki 1986). All of which require control over the dopant profile down to the nanometre level.

1.6 Aims of this Thesis.

As this project was funded as part of a directed, national research program, it was constrained in its scope. The primary aim of this thesis was to improve the understanding of the MBE growth process and progress the associated technology to allow growth of doped structures which are suitable for Very Large Scale Integration (VLSI) of devices.

The problems to be overcome have been introduced above. These areas are broad and substantial effort is being expended around the world in these fields.

Within the Advanced Semiconductor Research group at Warwick University, several people are involved in these and related areas. As only one MBE system was available, there were certain limitations on the research that could be undertaken by an individual. The principal one being the time the MBE system could be dedicated to the specific experiments of individuals. In the light of these limitations, three specific areas were identified where tangible improvements were considered feasible (and were achieved), in the time period of this study.

Chapter 3. A systematic study of the particulate related defects in Si-MBE material is presented and techniques aimed at eliminating PRD contamination assessed.

Chapter 4. The surface accumulation behaviour of various dopants in both Si and III-V MBE investigated. An empirical model, predicting the surface accumulation behaviour and site occupancy of dopants in III-V MBE, is introduced and its predictions compared to empirical evidence. One of the predictions being that phosphorus in Si-MBE will not exhibit any surface accumulation behaviour.

Chapter 5. In this chapter the results of the first study on phosphorus doping in Si-MBE is presented and the evidence on its surface accumulation behaviour is discussed.

Chapter 6 In this chapter initial investigations into the metallic impurity content of Si-MBE material are discussed.

The conclusion will draw together the results and discuss the overall effect of this study on its principle aims.

CHAPTER 2

MBE Technology.

2.1. The growth system

The epilayers were grown on (100) silicon substrates in a Vacuum Generators (VG) Semicon V80 MBE system, which over the period of study has been modified significantly, as described below. To clarify the experimental procedures, figure 2.1 shows a schematic diagram of the system, comprising a deposition chamber, a preparation chamber which contains the wafer transport mechanism, and a fast entry lock for wafer loading and exit without effecting processing pressures. Both the growth and preparation chambers were pumped separately by closed cycle helium cryo-pumps, and a Ti sublimation pump. The growth chamber was also pumped by a 400 l/sec ion pump. The load lock was pumped by its own 100 l/sec ion pump. The rough pumping was achieved by an oil free, vane pump which evacuated the system to ~100 Torr, then sorption pumps were used to evacuate the system to $\leq 1 \times 10^{-3}$ Torr, at which point the cryo-pumps could be switched on. After the cryo-pumps achieved their working temperature of ~15K, a pressure of less then 5×10^{-7} Torr, could be achieved. After baking the system to ~200°C for ≥ 50 hrs the background pressure went down to $\leq 1 \times 10^{-10}$ Torr. Originally, a liquid nitrogen shroud surrounded the growth area, although in later experiments, this was removed and the system cooling was affected by water flowing in pipe work welded to the exterior of the deposition chamber. Little difference was observed in the characteristic properties of the material (such as background doping) on transfer to the more convenient water-cooling.

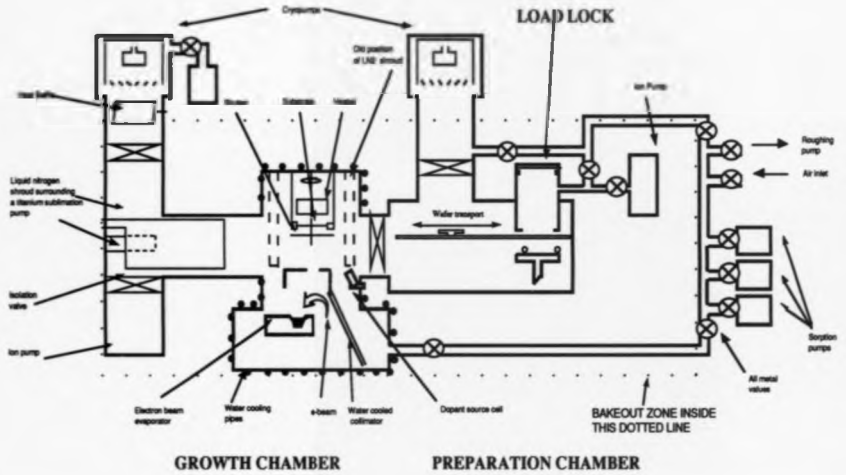

Figure 2.1. Schematic diagram of the V80 silicon MBE system used in this study.

The silicon flux was generated by an Airco Temescal 40cc electron beam evaporator. A 7-8 KV electron beam was used to melt the central part of the silicon source, ie. using the rest of the silicon source as a crucible. This minimises the contamination from the hearth.

The flux control system utilized Electron Impact Emission Spectroscopy, (Inficon Sentinal III). This technique involves detecting photons emitted from the growth flux after electron impact induced excitation.

Doping could be achieved by two Knudsen sources positioned in the growth chamber, illustrated in figure 2.1. The residual gases in the vacuum system were monitored by a quadrupole mass spectrometer.

The VG substrate heater used was capable of accommodating 76mm samples, and the rotation facility was generally employed to ensure lateral uniformity. The substrate temperature was measured by an infra red pyrometer. The maximum temperature achievable by the heater was ~890°C which is considered to be too low for complete thermal desorption of SiO_2. For this, temperatures $\geq$ 950°C are required, (Kasper 1987). Another problem with the tantalum strip heater is the possibility of it contaminating the silicon epilayer with tantalum. This possibility is assessed in the context of the investigation into unintentional impurities discussed in chapter 6.

At the time of this study a non-metallic heater module for MBE growth systems was not commercially available, therefore it was decided to design and build such a replacement substrate heater, that would have the capability to raise the substrate to temperatures in excess of 1000°C.

2.2 Replacement substrate heater.

2.2.1 *Design considerations.*

Other design criteria used for the new heater module were:
(i) No rotating mechanisms so as to avoid the presence of bearings in the vacuum system that could give rise to particulates, (see chapter 3).
(ii) Computer control via a thermocouple feedback.

The material chosen for the heating element was graphite. It is a well characterised heating material, used routinely in chemical vapour deposition (CVD) systems. It is available in extremely high purity (≤ 5 ppm impurity levels), several orders greater than tantalum and is easily machinable. Other advantages over tantalum are its longevity and increased emmisivity.

The structural support was constructed out of stainless steel, (american iron and steel institute grade 316). Other construction materials used near the heating element were silicon for the heater stage and molybdenum for its supports and contact to the heating element.

To reduce the contamination by contact with other materials, the heating element was designed to be self supporting .ie. to be held only at the electrical contact points. This design, however, has a penalty of a minimum thickness for the graphite used. The first test structure chosen was a one piece zig zag pattern, illustrated in figure 2.2.

To minimise the heat loading on the rest of the vacuum system from this more powerful substrate heater, the heating element was surrounded by a water cooled shroud constructed out of stainless steel tubing. This was lined with molybdenum reflectors, see figure 2.2. As with the tantalum strip heater a quartz disc was placed between the heating element and the substrate. This prevents line of sight to the substrate for any impurities outgassing from the graphite.

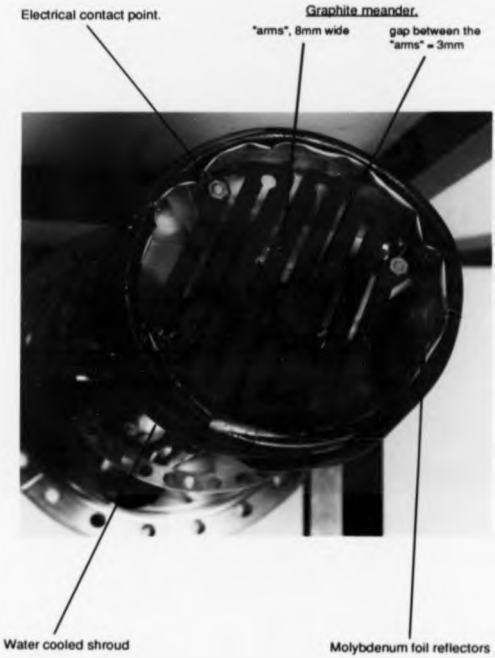

Figure 2.2. Photograph of the graphite meander heater. The heater stage was removed for clarity.

The substrate shutter was a 150 mm diameter silicon wafer held in a molybdenum clamp. Tungsten/rhenium thermocouples were used for the feedback control of the heater power supply. The electrical feedthroughs were isolated using lengths of high purity quartz tubing. The intention was to reduce outgassing from the more traditional ceramic insulators, see figure 2.3.

Calculation of the power required to achieve a certain heater temperature involves consideration of the radiative losses from all the surfaces, and the variation of resistivity of the graphite with temperature. This can be estimated by balancing the electrical input power, with the radiative power loss.

$$\text{Electrical input power} = I^2R = \frac{I^2 L \rho(T)}{A_x} \qquad \text{..... 2.1}$$

Where I = current, R = resistance, L = length, A_x = the cross sectional area of the heating element and $\rho(T)$ = resistivity at temperature T.

$$\text{Radiative power loss} = \sigma \varepsilon T^4 A_s \qquad \text{..... 2.2}$$

Where σ = Stefan's constant, ε = emissivity of the graphite and A_s = the surface area of the heating element. Combining equations 2.1 and 2.2 gives equation 2.3.

$$I^2 = \frac{A_x A_s \sigma \varepsilon T^4}{L \rho(T)} \qquad \text{..... 2.3}$$

Using equation 2.3 the power required for the graphite meander to reach a certain temperature can be calculated for a variety of meander designs, see figure 2.4.

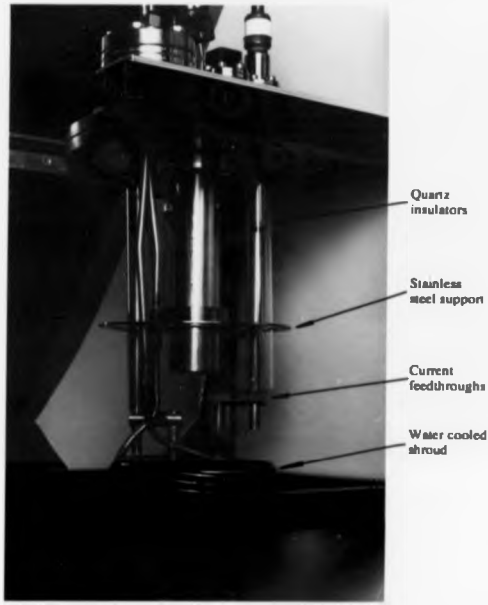

Figure 2.3. Photograph of the graphite meander heater module. The heater stage has been removed.

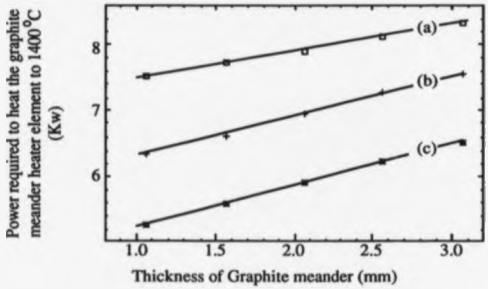

Figure 2.4. Calculated power consumption for various designs for a graphite meander heater.
(a) For a graphite meander with 10 mm wide "arms" and a 1 mm gap between the "arms". Figure 2.2 illustrates the "arms" and the gap.
(b) For a graphite meander with 8 mm wide "arms" and a 3 mm gap between the "arms".
(c) For a graphite meander with 6.5 mm wide "arms" and a 5 mm gap between the "arms".

In the first test element, (shown in figure 2.2), the spacing of the arms was 3 mm with their width 8 mm. The thickness of the whole element was 2 mm and its overall diameter 107 mm. It was found that the zig zag meander accommodated the thermal expansion occurring on heating without the need for movement of the contact points. The edges of the meander arms were thinned to a width of 6.5 mm. This caused an increase in the heat output from the edge of the meander to counteract the heat loss from the substrate to the heater stage. Testing of this element showed an increase in temperature of ~50°C at the edge, as measured by a pyrometer.

The graphite was machined out of a 2 mm x 110 mm diameter disc. To prevent damage due to vibration during machining it was held on a metal plate by beeswax and subsequently cleaned using a

heated solution of 1 H_2O_2 : 1 NH_4OH for ~15 minutes and rinsed in overflowing DI water. This cleaning procedure was repeated twice before it was left in a class 100 workstation to dry for several days.

2.2.2 *Assessment of the graphite meander heater.*

The graphite meander proved to be a stable heat source, which controlled the temperature of the substrate reproducibly. The essential results are:

(i) *Heater calibration*. The maximum substrate temperature was found to be >1000°C, (see figure 2.5), limited only by concern about the level of heat input into the water cooled growth chamber.

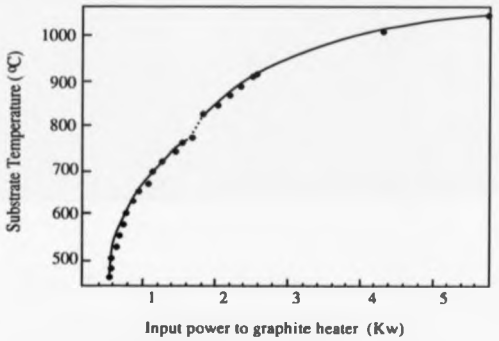

Figure 2.5. Calibration of the graphite substrate heater.
The break in the calibration curve was due to the second stage of the power supply cutting in. The temperature was measured by a pyrometer.

(ii) *Temperature uniformity over the substrate*. Figure 2.6 illustrates the temperature uniformity over the substrate. The variation, ± 40°C,

compares favourably with that obtained with the tantalum strip heater, ± 30°C. The coolest part of the substrate is at the gap in the heater stage through which the substrate was loaded. A possible hot spot in the meander at point A (due to non-uniform machining of the "arms"?), could be adding to the temperature gradient across the substrate. The obvious solution was to plug the source of the heat loss. A silicon "gate" that allowed the "wobble stick" to place and remove the substrate in vacuo was designed, but due to the limited time available, was not tested.

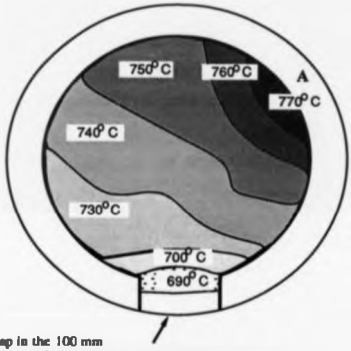

Figure 2.6. Temperature uniformity obtained over a 76mm diameter substrate using the graphite meander heater.

(iii) *Outgassing of the graphite meander.* It was found that for effective outgassing of the meander, it had to be held at its maximum temperature for a total of 5 hours, spread over a couple of days to prevent excessive temperature rise of the vacuum chamber. Curve (a) in figure 2.7 shows the change in the background pressure in the growth chamber during the initial step of this outgassing procedure. Curve (b) shows the change in the background pressure with the temperature of the graphite meander heater, after several hours of outgassing had been carried out.

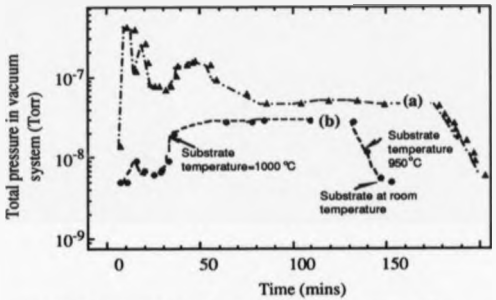

Figure 2.7. Variation in the growth chamber pressure during outgasing of the graphite meander heater.
(a) Pressure increase when the graphite was first used. The fluctuations are due to changes in the input power.
(b) Pressure increase when the graphite heater had been outgassed for ~5 hrs. Note that the pressure rise when the substrate is heated to 950° C from room temperature, Δ p~8x10 $^{-9}$Torr. The gases causing this pressure rise are shown in the residual gas spectrum shown in figure 2.8.

Note that when the substrate is heated to 950°C from room temperature, the pressure rise, Δp, is $\sim 8 \times 10^{-9}$ Torr. Unfortunately, it was found that this long outgassing procedure had to be undertaken every time the graphite meander was exposed to atmospheric pressure.

Figure 2.8 shows the mass spectra of the residual gases in the growth chamber during the outgassing procedure. The major constituents were carbon monoxide and other carbon containing compounds such as carbon dioxide and various alcohols. These larger hydrocarbon species were not present during use of the tantalum heater. The impact of these extra species on the carbon and oxygen impurity content of the epilayers was investigated using Secondary Ion Mass Spectrometery (SIMS), (described in appendix A). The results are illustrated in figure 2.9. The carbon and oxygen content remained unchanged, (staying well above the the saturation level), at $\sim 1 \times 10^{18} cm^{-3}$, indicating that these low partial pressures of hydrocarbons, ($< 1 \times 10^{-9}$ Torr), did not increase the contamination levels in the epilayers. The growth temperature varied from 795°C for epilayer 79/2 to 480°C for epilayer 79/4. No correlation is evident in this study between growth temperature and the carbon and oxygen contamination levels.

Also present in the residual gas spectrum were small peaks ($\sim 3 \times 10^{-10}$ Torr), attributable to HCl. The source of this acid may have been residue left in the growth chamber, as the growth chamber was commercially cleaned with an acid etch before this experiment. The major source of the other species is likely to be the wax used to hold down the meander during machining. To reduce this source a new meander was designed and machined without recourse to bee's wax, to eliminate the need for a chemical cleaning procedure.

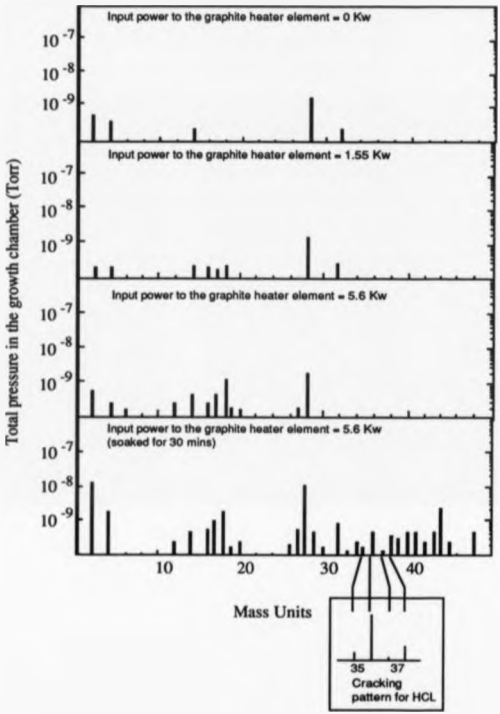

Figure 2.8. Mass spectra taken as the graphite heater was outgassed.

Outgassing in a high vacuum evaporator was envisaged to be sufficient before use. This would reduce the source of the larger hydrocarbon species. However, as graphite has a porous structure, it will still require rigourous outgassing after every exposure to air. This problem can be significantly reduced by the application of an impervious coating of SiC on to the graphite meander surface.

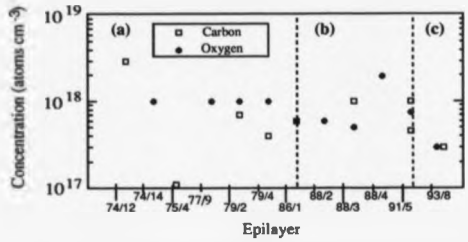

Figure 2.9. Variation of oxygen and carbon content of silicon epilayers as a function of substrate heater design. The substrate temperature was not kept constant in these samples, (see text).
(a) Epilayer heated using the tantalum substrate heater.
(b) Epilayer heated using the graphite substrate heater.
(c) Epilayer heated using the renovated tantalum substrate heater.

(iv) *Summary*. Technically the introduction of the graphite meander heater into the MBE growth environment was successful. It allowed substrate temperatures ≥ 950°C to be achieved to facilitate the desorption of the native oxide from the substrate surface, with a pressure rise of only ~8×10^{-9} Torr. However, the effect of this high temperature treatment of the substrate on the dislocation levels could not be unambiguously determined during this assessment of the graphite meander heater.

The long outgassing times required for this first prototype can be reduced by the application of an impervious coating such as SiC.

The effect this graphite heater had on metallic contamination levels in the epilayer will be discussed in chapter 6.

Chapter 3

Particulate contamination.

3.1. Introduction.

Due to their size (≤ 0.1μm to ~20 μm), particulate related defects are of concern, despite their low densities (≤ $1x10^3$ cm^{-2}). However, they have not yet been studied extensively in Si-MBE. In this chapter the results of a detailed study into the nature and influences of particulates in Si-MBE material and the procedures designed to remove them are presented.

3.1.1 *Effect of particulates on devices.*

The effect of particulates on device properties has been studied to a much greater extent, especially during the device processing stages. There are two principle mechanisms by which PRD's can influence device properties:

(i) By obstruction of lithographic masks. It has been estimated that up to half the yield loss in devices was due to this mechanism (Duffalo & Monkowski 1984). The extent of the mechanism is dependent on the size of particulate. The general consensus being that the largest dimension of the particulate can be as small as 0.1 x the smallest device dimension and still adversely affect the device. As sub-micron line-widths are now common, particulates down to tenths of a micron can now be a problem. (Bellavance & Liu 1987).

(ii) A more subtle mechanism is via the chemical nature of the particulate. It has been suggested that they can act as sources of impurities which can lead to breakdown of oxides (Duffalo & Monkowski 1982). The influence of metallic impurities on device properties will be discussed in chapter 6.

3.1.2 *Current understandings on particulates in MBE.*

There has been limited research on sources of particulates in the MBE growth process, the principle conclusions are;

1) Silicon forms unstable deposits on the stainless steel vacuum chamber walls. These powdery deposits of silicon lead to a continuous "shower" of silicon particulates (Houghton et al 1987, Kubiak et al 1985c, Robbins et al 1985, Leong 1985, Bellavance & Liu 1987, Matteson & Bowling 1988), which can be seen by the scintillation of the particulates when a bright light is shone into the chamber.

2) Several mechanisms by which these particulates reach the growing epilayer have been put forward (Leong 1985, Matteson & Bowling 1988), all related to the electron beam evaporator. The lack of an electron beam in gas source MBE has been highlighted as the reason why there is an absence of particulates in epilayers grown by this method, (Hirayama et al 1987).

3) Two methods to prevent the particulates reaching the substrate have been proposed; (a) shielding of the chamber walls from the silicon flux to prevent the build up of deposits (Ota 1983) and (b) the use of charged deflection electrodes to divert the particulates away from the substrate (Tatsumi et al 1989). Only the second method is claimed to completely eliminate particulates from the epilayers, however, this claim is unsubstantiated and the introduction of a charged electrode compromises the effectiveness of potential enhanced doping, (see section 1.4).

These points will be discussed in detail in this chapter.

3.2 The Nature of Particulate-Related Defects.

Particulate features are sometimes evident, on the as-grown epilayers as shown in figure 3.1. To further identify their nature, all samples were subjected to a preferential etch and examined initially by an optical microscope. A more detailed examination was carried out in many cases with an SEM. The particulates on the epilayers were found to have a wide range of diameters, ranging from < 1μm to greater than 20μm. They are randomly distributed over the epilayer, see figure 3.2.

Two distinct particulate features (PF) are apparent.

1) Some particulates were surrounded by mis-oriented regions of silicon, resembling micro-twin lamellae, as shown figure 3.3a, and reported elsewhere (Kubiak et al 1985c, Robbins et al 1985). The mis-oriented area contains multiple stacking faults which lie in the (111) plane, with some evidence of dislocations. The multiple stacking faults are often evident before defect etching but become more pronounced after treatment. These features will be referred to as Particulate-Induced Multiple Stacking Faults (PIMSF). The absence of material in the centre of the PIMSF in figure 3.3a, is probably caused by the rapid etching of this region which has been shown to be polycrystalline by Robbins et al (1985).

Figure 3.4 shows a seemingly different particulate feature. This star shape defect is the result of over etching a PIMSF defect. The dislocations at the ends of the stacking faults etch faster than the main body of the PIMSF defect. This manifestation of a PIMSF defect is normally evident in thinner layers (≤ 2μm) where the PIMSF are small and the normal etching time to reveal the other defects in the layer is sufficient to over etch them.

Figure 3.1. An as-grown silicon epilayer, as observed by Normarski interference contrast, showing particulate features.

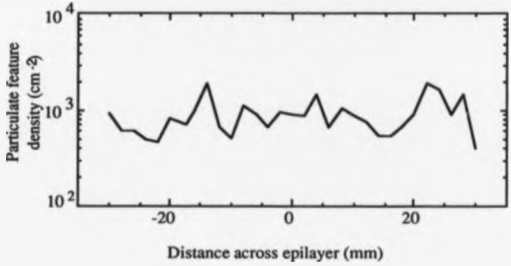

Figure 3.2. Illustration of the random distribution of particulate features over a 76 mm diameter silicon epilayer.

As shown in figure 3.3b, epilayers contain PIMSF with a range of stacking fault lengths, (the surface ripple evident in this photograph was discussed in the Introduction).

The length of the stacking fault can be related to its depth of origin by equation 3.1(Mendelson 1964),

$$\text{Depth of origin} = \frac{1}{\sqrt{2}} \text{(stacking fault length)} \qquad \ldots\ldots\ldots\ldots \quad 3.1$$

Therefore, the length of the outermost stacking fault of a PIMSF can be related to the depth at which the associated particulate resides. Equation 3.1 can only be used with measurements of stacking faults on unetched epilayers as the etch preferentially attacks the strained region around the defect and obscures the size of the defect. The depth of the particulates below the epitaxial surface were obtained by measuring the size of the stacking fault associated with the particulates using equation 3.1. This yields the rate of accumulation of particulates leading to PIMSF growth.

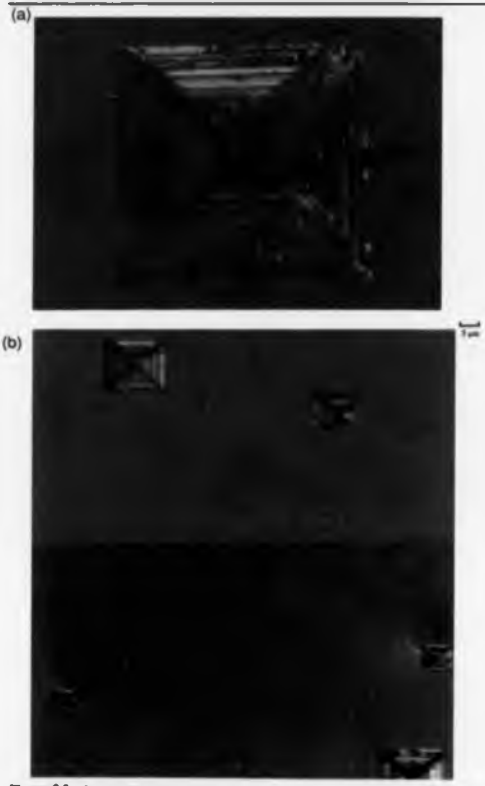

Figure 3.3. Particulate related defects revealed by using a preferential etch (dilute schimmel) and observed by nomarski interference contrast.
(a) A Particulate Induced Multiple Stacking Fault (PIMSF) decorated by dislocations.
(b) PIMSFs due to particulates arriving at different stages during the growth of a 25 µm epilayer.

Figure 3.4. Over-etched particulate-induced multiple stacking fault, as observed by Normarski interference contrasts.

Figure 3.5, shows these results for two different system configurations ie. with and without source collimation, (see section 3.4). The figure shows a near linear increase of PIMSF defects with increasing thickness of the epilayer, indicating that the particulates causing the PIMSF are arriving at a constant rate. Shielding the vacuum chamber walls reduces this rate significantly but not to zero. The range of rates of accumulation of the PIMSF defects, with or without a collimator, indicates that there are other factors which are influencing this accumulation process, though not to the same extent as collimation.

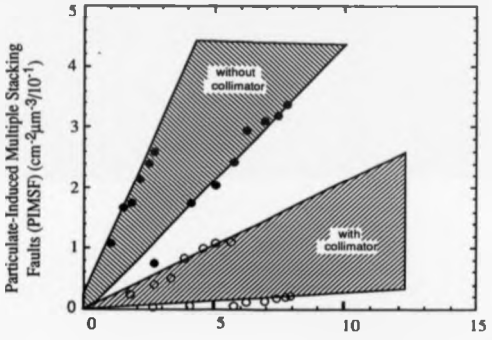

Figure 3.5. Range of rates of accumulation of PIMSFs densities with and with out growth flux collimation.

An interesting point is that there appears to be noticeable PIMSF defects nucleating at the substrate-epilayer interface. These points will be discussed in section 3.4.

2) The second particulate features, are large (typically 1 to 20μm) irregular lumps of material, an example of which is shown in figure 3.6a. They are denoted Macroscopic Particulate Features (MPF). They often protrude beyond the epitaxial surface, do not induce crystallographic defects and generally shadow growth. During defect etching this type of particulate can detach from the surface, leaving "holes" (illustrated in figure 3.6b). EDAX analysis failed to detect any element other than silicon in MPF's, indicating that if any impurities are present, they have a density $\leq 1 \times 10^{18}$ atoms cm^{-3}.

The accumulation of MPF's with growth time cannot be assessed, since the size of the particulate cannot be related to its depth of origin.

3.3 Sources of Particulates.

To investigate the origin of the particulate contamination, wafers were subjected to progressively more steps of the layer growth process and then inspected using a laser particle counter, (Tencor Instruments Surfscan 100 Analyser). The counter scans the whole wafer (excluding a region around the edge). It detects scattered light from particulates with a diameter of > 1μm in grids of area 100μm^2 and calculates the particulate density as the number of 100μm^2 grids that contain scattering centres. Therefore the scanner sensitivity is limited to one particulate per 100 μm^2 by the software control.

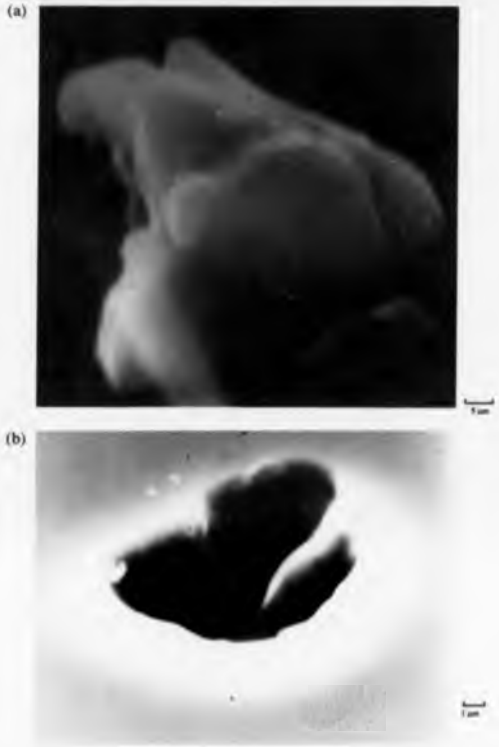

Figure 3.6. Particulate related defects revealed by using a preferential etch (dilute schimmel) and observed by the scanning electron microscope.
(a) Macroscopic Particulate Feature (MPF). Note the shadowing along its edge.
(b) A hole left by a MPF that has "fallen" out during the etching process.

For a random distribution of particulates, the density would have to be $> 4 \times 10^6$ cm^{-2} before this sensitivity limit becomes a problem. As the particulate density calculated by the laser scanner was several orders of magnitude below this level, this limit will not affect this discussion of the results, which are summarised in figure 3.7. Ex-situ handling of the wafers (steps 1a, 2, 3) apparently contributed only a few particulates, (significant contamination did accrue on a wafer from a container previously opened and stored in a clean room, step 1b). The first vacuum step, (step 4), involving evacuation of the fast entry lock with subsequent venting to nitrogen, increased the particulate count significantly (~50 counts cm^{-2}). However handling of the wafer within the UHV system, including loading and unloading from the growth chamber and substrate manipulator (step 5) appears to be a relatively clean process. Energisation of the electron beam evaporator for a time period comparable with pre-growth preparation, whilst keeping the substrate shutter closed (i.e. no line of sight between the substrate and the electron beam evaporator), caused another large increase in the particulate density (step 6a) This suggests that charging effects by the stray electron flux from the electron beam evaporator plays a significant role in particulate accumulation, (both the heater stage and the substrate were earthed).

The simple expedient of keeping the substrate closely shielded, with a second wafer, through out in-vacuo process protects it from particulate fluxes (step 6b). The deposition step (step 7) itself produces major particulate contamination and this is further exacerbated by substrate rotation (step 8), presumably due to the vibration loosening the silicon deposit from the heater assembly.

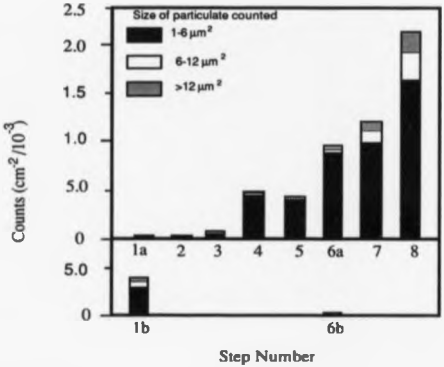

Figure 3.7. Comparision of the relative particulate density on silicon epilayers that have been subjected to progressively more steps of the SI-MBE process, (as counted by a Surfscan laser scanner).
Step 1a. Wafer removed from a previously unopened wafer box.
Step 1b. Wafer removed from a previously opened wafer box stored in a clean room.
Step 2. Wafer chemically cleaned and spun dry.
Step 3. Wafer transferred to the load lock from the fume cupboard.
Step 4. After been subjected to evacuation and "soft" venting of load lock.
Step 5. After transportation through the preparation chamber to the substrate heater stage in the deposition chamber.
Step 6a. After energizing the electron beam evaporator with the substrate shutter closed.
Step 6b. Step 6a repeated, but with a shield in front of the cleaned wafer.
Step 7. After 0.1 μm epilayer growth, with no substrate rotation.
Step 8. After 0.1 μm epilayer growth, with substrate rotation.

Utilizing equation 3.1 the number of PIMSF defects nucleating at the substrate-epilayer interface was investigated for a variety of conditions. Leaving a substrate in the vacuum chamber overnight before the epilayer was grown led to a dramatic increase of PIMSF at the interface. Compare figure 3.8a with figure 3.8b.

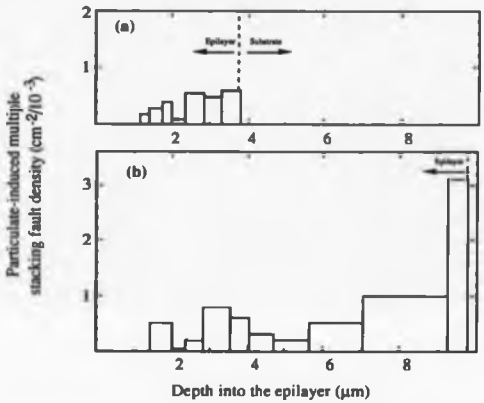

Figure 3.8. Investigation of the depths origin of particulate-induced stacking fault density, utilizing equation 3.1.
(a) Epilayer grown immediately after loading into the MBE system.
(b) Epilayer grown on a substrate which was left in the deposition chamber overnight before growth commenced.

On the basis of these experiments, it can be concluded that there were three main sources of particulates, namely:

(i) Wafer loading into vacuum. This can be improved by soft pump procedures which reduce the turbulence of the air flow, as employed in other wafer processing equipment and/or by providing a shield close to the wafer during evacuation.

(ii) The silicon electron beam evaporator.

(iii) Wafer rotation. The mechanism employed was a first generation model and improvements in its design should reduce this source to acceptable levels. For example by minimizing the use of bearings in vacuum and removing any gears or linear bearings.

It is clear that the primary source is the electron beam evaporator, however, the mechanisms involved are unclear.

3.4 Factors influencing the density of particulate contamination.

3.4.1 *Correlation with MBE technology.*

Figure 3.9 shows a plot of total particulate densities of the silicon epilayers grown over the period 1983-1989. It should be noted that the particulate densities have been normalised per micron of epilayer growth. These epilayers were not grown specifically to study particulate contamination and a wide range of conditions were used, even within a growth run. This contributed to the wide range of densities observed in a given growth series. This spread of densities within a growth series can be reduced if growth conditions and system configurations are optimised for the study of particulates, (see section 3.4.3). The plot in figure 3.9 is subdivided into a number of sets of epilayers, identified as A to H.

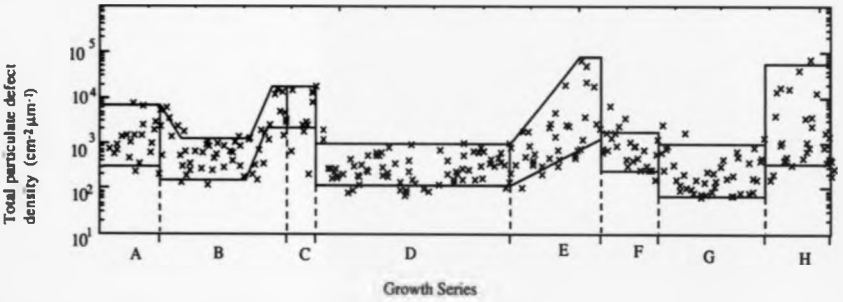

Figure 3.9. Particulate density on silicon epilayers grown in the period 1983-1989.
A. As recieved MBE system. No collimators were used and a liquid nitrogen shroud surrounded the growth area. **B.** With a Ta box collimator in position. The changes at either end of the growth series were due to conditioning and cleaning of the Ta, respectively. **C.** Ta box collimator removed and electron beam scanning introduced for source evaporation. Higher energies were used (8KV) for these growths **D.** With a Ta-lined water cooled collimator. **E.** With instabilities in the power supply to the electron beam evaporator. **F.** Power supply fault rectified. **G.** Liquid nitrogen shroud removed and replaced by exterior water cooling pipes on the growth chamber. Silicon lined water cooled collimator was introduced near the end of this series. **H.** Collimator removed.

Each set represents growth runs between which the configuration of the growth system has been changed significantly. (These changes are described fully in the figure caption). The main observations are:

(i) The reductions of approximately one decade between growth series A and B and growth series C and D were associated with the collimation of the silicon flux by restricting the area of the deposition chamber over which silicon could accumulate. This was accomplished by surrounding the electron beam evaporator by an assembly which restricted the flux so as only to reach the substrate, substrate holder and flux detector, (shown schematically in figure 2.1).

Due to the relatively large area of the source melt, simple geometrical considerations preclude the use of extremely tight collimation (to achieve further reductions), as this would lead to highly non-uniform epilayer growth. In series C however, such over tight collimation was attempted whereby the flux only intersected the substrate and gave minimum particulate densities of ~50-60 cm^{-2}. This coincided with the removal of the LN_2 shroud.

Several types of collimator were used. A tantalum box assembly placed on the electron beam hearth was used in series B. It was subjected to constant thermal cycling, due to its proximity to the silicon melt, resulting in flaking of the silicon deposits. This is assumed to be the cause of the slow decrease in particulate density on introduction of the collimator and the rise at the end of period B when the silicon deposits on the collimator were removed. This collimator was replaced by a tantalum collimator surrounded by a water cooling jacket, held above the electron beam hearth to prevent any interaction of the primary electron beam and keep the tantalum at a constant temperature, period D. Note the sharp drop in PRD density on the introduction of this collimator. Silicon deposits of several

millimetres thick were obtained on this collimator at the end of this period.

Concerns that the tantalum collimator may be adding to the metal content of the epilayer (see chapter 6) led to a variety of designs using quartz and silicon. However, large structures of quartz surrounding the electron beam evaporator suffered from problems of charging, which prevented stable deposits of silicon from forming. At the start of period G a tantalum collimator surrounded by improved water cooling was used, while a silicon lining for the water cooling was manufactured out of 6" silicon wafers. This was installed near the end of period G. Due to close contact with the water cooling no charging problems were encountered and deposits of millimetre thickness, (similar to those obtained on the tantalum collimator), were obtained.

An added advantage of earthing the collimator is that the reflected and secondary electron flux emanating from the electron beam evaporator into the growth environment will be reduced.

(ii) The primary electron beam of the electron beam evaporator appears also to play a role in particulate contamination in the epilayers. The dramatic rise during series E coincided with instabilities in the electron beam due to gradual degradation in the high voltage stabilisation of the power supply. The decrease in series F resulted from rectification of the fault. The higher baseline is probably due to an increase in unstable silicon deposits on the vacuum chamber walls caused by the fluctuating silicon flux. In addition, the higher level in series C compared with series A, during which time there were no significant differences in system design, were found to be associated with either the use of higher primary electron energies in series C or through scanning of the

beam over the charge during growth. Scanning of the beam obviously influences the "melt" area and will, to some extent, lead to fluctuations in the boundary of this melt. The local stress introduced could give rise to large particulates causing MPF defects. This situation would be exacerbated by an unstable power supply. (see section 3.4.2).

(iii) For growth series G (and subsequent series), the liquid nitrogen cryo-panel surrounding the growth region was removed, and system cooling was effected using water passed through pipes welded to the outer chamber walls. Original speculation that the source of particulate material was related to the powdery silicon deposit on liquid nitrogen surfaces (Kubiak et al 1985c) was thus refuted since comparable levels of particulates in the collimated and uncollimated system in the water cooled and liquid nitrogen configurations are apparent, and only slightly less powdery deposits were found on water-cooled surfaces.

3.4.2 *Relationship between particulate related defects.*

The existence of the two distinctive particulate defects raises the question, whether the particulates share a common source. Figure 3.10, correlates the densities of PIMSF and MPF's using representative data from growths carried out under a range of experimental conditions, (see earlier). The data indicates that the primary electron beam energy instabilities of period E tended to increase MPF accumulation with respect to PIMSF's, but in general a near unity slope is apparent, for both collimated and uncollimated system configurations. This suggests that the particulates have a common source, but manifest themselves in different ways, depending, presumably on the size of the particulate. The larger particulates shadow growth of the epilayer (although growing

themselves from flux incident on them), thus precluding the epilayer growth planes from interacting with their crystallographic faces.

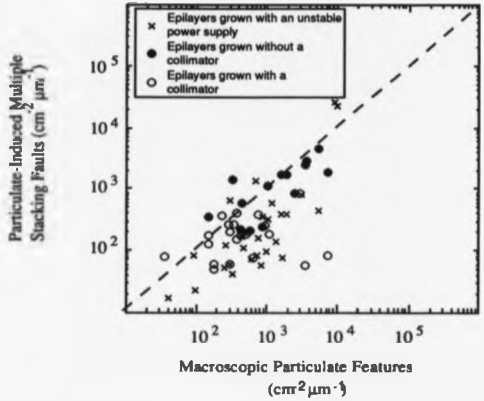

Figure 3.10. Variation of PIMSFs density as a function of MPF density, for three different sets of growth conditions. The dashed line indicates the 1:1 correlation.

Konig et al (1981) has observed what they call poly stacking faults (PSF) on heavily antimony doped silicon epilayers. In appearance the PSF defect is the same as a PIMSF defect indicating that the nucleation mechanisms are related. Konig et al (1981) imply that precipitates involving antimony are nucleating these PSF's, suggesting that the particulates causing the PIMSF must originally have been of a similar scale ie. a few nanometres, (Werkhoven 1983).

However, Robbins et al (1985) observed a 1 μm silicon particulate at the base of a particular PIMSF defect by cross sectional TEM. Possible reasons for this apparent contradiction are; (a) that the particle grew to its present size as the epilayer grew or (b) it arrived on the epilayer surface at its present size but that it has surfaces which interact directly with the growth steps, disrupting the growth mechanism and generating defects at the edges. More detailed electron microscopic study is required to clarify the mechanisms involved.

3.4.3 *Transport of particulates to the epilayer*

Matteson et al (1988) has suggested that the silicon atoms and molecules in the growth flux will provide enough "pressure", by exchanging their momentum with the silicon particulates, to propel them up onto the substrate. There are limitations to the applicability of this mechanism in MBE, as a density of silicon atoms and molecules sufficient to achieve a growth rate of 10 Å/s was required to levitate a particulate of < 0.5 μm diameter. This is at least twice the rate used in practice in this study and this mechanism cannot explain how particulates, > 0.5 μm diameter, reach the substrate. The model does however provide a plausible explanation for the observed dependence of PIMSF on the growth rate (Robbins et al 1985), since as seems likely, PIMSF are caused by microscopic particulates ≤ 0.5 μm.

The most likely mechanism for the larger particulate (> 0.5 μm) to reach the substrate is via the electrostatic fields in the growth chamber. A particulate could become positively charged by secondary electron emission, the magnitude of the charging effect would depend on the size of the particulate, as the larger the particulate the greater charge it can accommodate. The existence of charging in these particulates can be inferred from the results presented in figures 3.11 and 3.13. The results shown in these figures

are averages for epilayers that were grown in a random order and indicate systematic increases in particulate densities when negative substrate potentials were applied. This correlation was evident with and without a collimator.

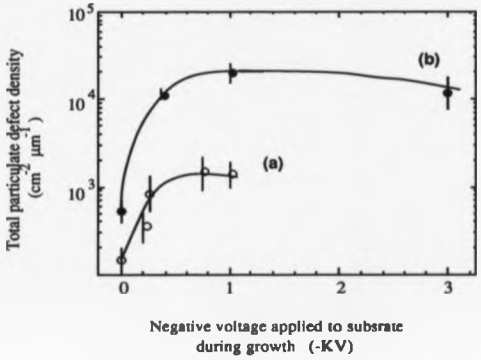

Figure 3.11. Variation of total particulate defect density with applied voltage on the substrate.
(a) During growth series G (in figure 4.9), i.e. silicon water cooled collimator in place.
(b) During growth series H, i.e. no collimator.

In the case of negatively charged particulates, Leong (1985) showed theoretically that a 2 μm particulate falling into an electron beam of 7KV can gain enough potential energy by electron irradiation to overcome the pull of gravity and reach the substrate. The presence of negatively charged particulates is shown experimentally by the results of Tatsumi et al (1989) and further substantiated by results in the next section.

The field distribution in the growth chamber will be influenced by electron space charge effects, the existence of various charged species (e.g. secondary electrons and ions), the surface charge of the silicon source, charging of insulating surfaces such as silicon deposits in the system and by the existence of magnetic fields in the deposition chamber. This field will also be influenced by the silicon growth rate. Kubiak (1985) has shown that an increase in the emission current from the electron filament sufficient to increase the evaporation rate from 3.3 Å/sec to 4.9 Å/sec will more then double the negative current arriving at the substrate, (280 nA → 600 nA). Note that due to differences in design of electron beam evaporators, the presence or absence of collimators etc, the electrostatic field in each growth chamber will be different eg. Knall et al (1989) observed a maximum electron current density of 17.5 nA over the area of a 3" substrate.

3.4.4 *Reduction of particulate related defects.*

An electrode positioned in the deposition chamber will influence these charged particulate trajectories and depending on the position and design of the electrode possibly reduce the density of particulates in the epilayer. Using this method Tatsumi et al (1989) claim to be able to eliminate particulate contamination in their epilayers. Their results suggest that starting from a base line of

~35 particulates cm^{-2}, a reduction to zero particulates cm^{-2} is possible when -6 KV or +4 KV was applied to the tantalum electrode. As particulates of both polarities can exist, it is surprising that both polarities individually prevented all particulates from reaching the epilayer. They restrict their observations to macroscopic particulate contamination (MPF's) in a 1μm epilayer. As shown earlier particulates > 1 μm are present in significant quantities.

Figure 3.12a, shows a schematic representation of a tantalum plate in our system, in a similar configuration to that reported by Tatsumi et al (1989), showing the approximate field lines due to the applied voltage. For a negative potential on the plate some negatively charged particulates are deflected away from the substrate, but others that would otherwise have missed, will be deflected on to the substrate. Its influence on positively charged particulates will be reversed. Corresponding arguments apply for a positively charged plate. Figure 3.13, plots the total particulate density (curve (a)) vs the applied voltage with the plate as shown in figure 3.12a. For voltages up to -3 KV there is no dramatic change in the particulate level, but at higher voltages there is a significant increase in the level of particulates reaching the substrate. A potential of +8 KV on the plate produces a significant increase, of over a decade, in the particulate density in the epilayer. This confirms Tatsumi et al's (1989) conclusion that there are greater numbers of negatively charged particulates.

Repositioning the plate (illustrated in figure 3.12b) to achieve a more optimum deflection field pattern produced no reduction in particulate densities, (compared to the densities observed when the deflection plate was earthed), see figure 3.13.

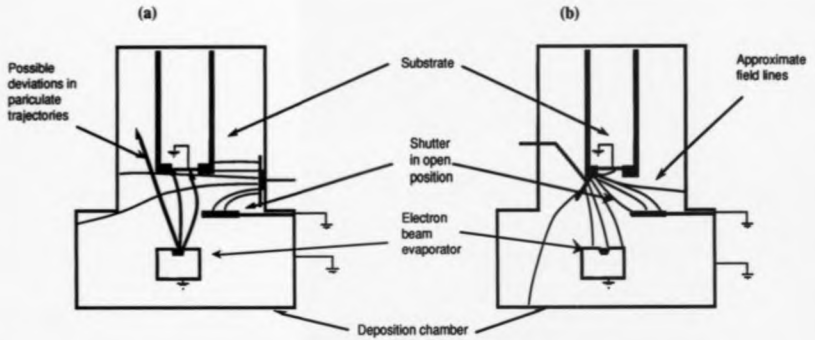

Figure 3.12. Schematic of the deposition chamber showing the approximate field lines due to an applied voltage on a tantalum plate electrode.
(a) Similar configuration to that used by Tatsumi et al (1989). Possible deflection of trajectories of charged particulates due to the electrode are shown, the extent of deflection will obviously depend on the strength of the applied field.
(b) Illustrates a better position for the plate electrode.

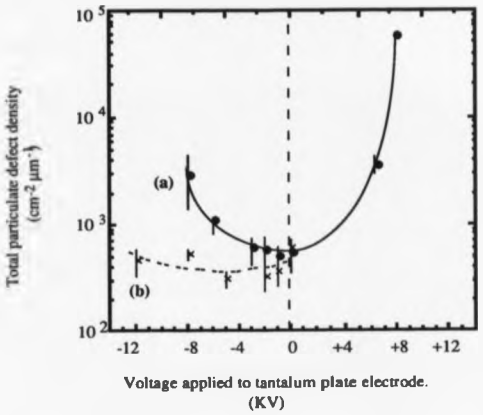

Figure 3.13. Variation of particulate density as a function of applied voltage to the tantalum plate electrode.
(a) For the tantalum plate electrode in the position shown in figure 3.12a.
(b) For the tantalum plate electrode in the position shown in figure 3.12b.

Improvements in the design and positioning of the electrode should result in reduction in the PRD densities. A possible example is illustrated in figure 3.14. The use of grids and the angle with respect to the substrate are chosen to reduce the possibility of species sputtered from the electrodes reaching the substrate and contaminating it.

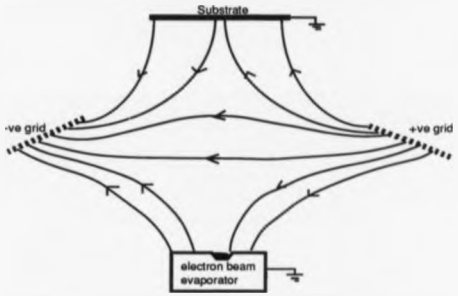

Figure 3.14. Schematic of the configuration of a compromise deflection electrode. The use of a grid is intended to limit the probability of sputtering events.

3.4.5 *Dependence of particulate features on growth parameters.*

The dependence on growth rate was discussed earlier. No statistical evidence could be found for variation of particulate density in the epilayers with the other growth parameters, such as growth temperature. In addition, there appears to be no correlation between the particulate defect density in the epilayers and the type of silicon charge used, (e.g. single crystal or polycrystalline), or the growth flux monitoring systems.

3.5 Conclusions and further work.

Particulate contamination of epilayers grown by MBE has been shown to be due to the build up of flaky deposits of silicon in the growth region. The deposits give rise to a "shower" of particulates which reach the substrate by some mechanism(s) associated with the electron beam evaporator. Any action which disrupts this "atmosphere" of particulates can lead to increased accumulation in the epilayer ie. evacuation of the load lock and transport of the wafer to the heater stage. A close shield in front of the substrate, while it is transported from the class 100 workstation, through the vacuum system to the heater stage and during the electron beam hearth warm up process, is shown to dramatically reduce the particulate density.

When the particulate reaches the substrate it can cause one of two types of defect. Particulate-induced multiple stacking faults (PIMSF), associated with microscopic particulates causing crystallographic defects, and macroscopic particulate features (MPF's) associated with larger particulates causing disruptions to the growth. The densities of both types are related, suggesting a common source. Further characterisation of the interaction of particulates of various sizes with the growth step on the substrate is required. Cross-sectional TEM studies of a series of thin epilayers, (100-1000Å), would help elucidate the mechanism of PIMSF formation.

Reviewing the possible mechanisms, it becomes evident that, contamination with particulates depends on the particulate shape and charge and the existence of an electrostatic field between the silicon charge and the substrate produced by the primary electron beam of the electron beam evaporator. Particulates $\leq 0.5\ \mu m$ can reach the substrate by the pressure of the silicon flux alone (implying a dependence on the growth rate). However, the introduction of a

negative voltage on the substrate also influences these smaller particulates, indicating that more than one mechanism must exist for transport of these particulates to the epilayer. The relative importance of these mechanisms will depend on the ratio of charged to neutral particulates and the distribution of the electrostatic field in the growth chamber.

Containment of the silicon growth flux reduces the particulate density in the epilayers. A stable growth environment and silicon source allows low levels of particulate contamination to be maintained.

Electrodes placed in the growth chamber were found to affect the particulate densities, the extent of which depended on the position and design of the electrode. In these experiments no useful reductions in particulate contamination were observed. However, improvements in the design and positioning of the electrodes could reduce the PRD density in an epilayer. The ratio of charged to neutral particulates could be deduced by systematically retarding the electron current arriving at the substrate by a grid directly in front of the substrate and comparing the reductions(?) in the relative densities of PIMSF and MPF. This obviously cannot be used routinely due to shadowing of the growth flux.

Chapter 4.

Dopant accumulation and site occupation.

4.1 Introduction.

The monolayer resolution in doping profiles promised by MBE can only be achieved by ensuring the dopant incorporates at the time of arrival at the substrate. However, many dopants demonstrate a reticence to direct incorporation, leading to their accumulation in a surface adlayer. The resultant smearing of doping transitions due to this gradual build-up in and depletion from the adlayer are well documented, (Ploog & Fischer 1978, Iyer et al 1981, Kubiak et al 1985b). There already exist good quantitative descriptions of the kinetics of the dopant accumulation, (Alexandre et al 1980, Collins et al 1982, Harris et al 1984, Parker 1985, Wood 1985, Rockett et al 1985, Barnett & Greene 1985, Ekyholt & Srolovitz 1986, Rockett et al 1986), but these rely on experimentally determined parameters which preclude their use for general predictions. A microscopic description of the thermodynamic driving force for surface accumulation does not exist for the non-equilibrium situation existing during MBE growth.

In this chapter a simple predictive, qualitative model of the process is developed. The factors which influence the dopant incorporation and surface accumulation process during MBE growth are examined. ***It is proposed that the relative size of the dopant and matrix atoms is a key parameter in determining the propensity to surface accumulation.*** This is discussed with respect to the existing experimental evidence. It was found that this is a general observation to the MBE growth process, which is demonstrated by extending the discussion to include dopant

incorporation during MBE growth of other elemental and compound semiconductors. In the case of compound/alloy systems, the relative size of dopant and matrix atoms is also found to be a key parameter in determining the site occupancy during MBE .

4.2 MBE growth, dopant incorporation and equilibrium segregation.

The 2D step growth process proceeding via the formation of an intermediate adlayer of atoms is clearly not an equilibrium one, as it results in the net accumulation of solid material, ie. growth. Indeed sharp changes in composition (e.g. dopant concentration) are only possible if the growth rate is high compared with the rate of bulk diffusion of the dopant species at the growth temperature. However, an understanding of the problems of dopant incorporation, can be achieved by considering the physical processes governing the equilibrium situation. In particular, the factors influencing the equilibrium concentrations of a dopant species in the bulk solid, the surface phase and the vapour.

The problem of surface equilibrium is one which has been studied mainly in metallic systems in order to understand the propensity of some solutes to preferentially accumulate at free or internal surfaces of solids ie. surface segregation. The equilibrium between the surface and bulk phase is governed by the relative energies of the dopant species on the surface and in the bulk. It is described by two influences, the local chemical or bonding energy (which includes the influence of the different co-ordination of surface and bulk sites) and the strain energy induced by incorporating atoms of different sizes into the crystalline lattice. In this situation it is well-established that some species do segregate

strongly (i.e. their surface composition is much higher than that of the bulk solid with which they are in equilibrium), while in other cases species prefer to occupy matrix sites and the surface composition is negligible. (Seah 1979, Abraham & Brundle 1981, Wynblatt & Ku 1977)

Assuming the system is at equilibrium, with the surface richer in one species, the addition of a flux of matrix and dopant species, in the same concentration as in the bulk solid, will disturb the overall equilibrium. However, local equilibrium can be maintained between the surface phase atoms and those of the immediately underlying (new) bulk layers, hence a steady state can be established in which the new material grows with the underlying bulk composition, whilst the surface phase remains enriched in dopant. If the dopant flux is switched off, but the growth flux maintained under the same conditions, the excess dopant in the surface phase would start to be accommodated in the newly grown material in order to maintain this local equilibrium. The dopant concentration of the new material would fall as this surface excess is depleted ie. the dopant concentration falls off after the flux has been removed. A similar argument leads to the conclusion that if the dopant flux were increased, the newly grown material would increase in dopant concentration by a smaller amount. (Indeed, if the surface phase were highly enriched it is possible that the dopant sticking coefficient at this surface composition would be so low as to lead to no enhancement of the bulk composition).

The situation resulting from this local equilibrium model is clearly very similar to that found in "real" MBE growth. Therefore factors which dictate which species should segregate in equilibrium should also allow a prediction of those species which will accumulate on

the surface during MBE growth. There are several competing factors, however it is proposed that the dominant one is the influence of atomic size. The other factors only being of importance when the mismatch of dopant and matrix size is small. This situation will be discussed later.

Intuitively, increasing the atomic size mismatch will increase the strain energy. For substitutional sites this strain energy is significantly greater if the foreign atom is larger than those of the matrix, due to a greater force being required to compress a bond than to stretch it. This conclusion is implicit in the potential energy curve of a bond, illustrated in figure 4.1.

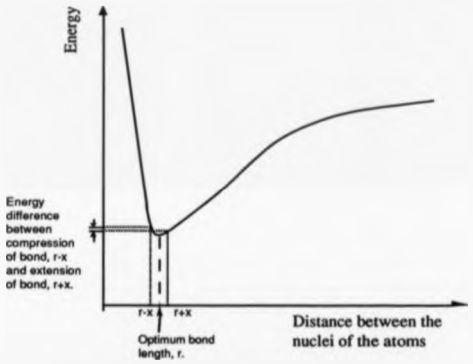

Figure 4.1. Schematic representation of a potential energy well for a bond. It illustrates the difference in energy when the bond is extended or compressed.

Using this as a basis it is proposed that surface accumulation in MBE growth occurs only for dopant species with atomic sizes larger than those of the matrix atoms they replace. This simple picture can be extended to predict site occupancy in III-V semiconductors which also serve as a more rigourous test of the predictions of this "model".

4.3. The Atomic Size Model.

In the following comparison with the existing experimental data, two assumptions are made: (i) the discussion is confined to MBE growth under "normal" BCF conditions, and to doping levels below those where the solubility limit effects eg. precipitation, become pronounced and (ii) only elemental and III-V semiconductors which are predominantly covalently bonded (the ionic contribution being small (Phillips 1970)), will be considered. Similarly, the dopants which have a significant degree of ionic bonding, i.e. elements in Groups II, VI and in the transition series are not considered.

4.3.1 *Elemental matrix systems.*

The atomic size model is particularly simple to test for the case of elemental semiconductor growth, although the experimental data is limited to the silicon matrix. All the dopants investigated to date, namely, boron (Kubiak et al 1985a), aluminium (Becker & Bean 1977, Hasen et al 1990), gallium (Iyer et al 1981, Becker & Bean 1977), indium (Rockett et al 1985), phosphorus, arsenic (Kubiak et al 1985b) and antimony (Kubiak et al 1985a, Iyer et al 1981, Kubiak et al 1985b) match the behaviour predicted by this hypothesis. Note that the data for phosphorus doping in Si-MBE is presented in the next chapter. Figure 4.2, plots the ratio of dopant to matrix size (σ) for each dopant.

$$\sigma = \frac{\text{atomic radius of dopant}}{\text{atomic radius of matrix}}$$

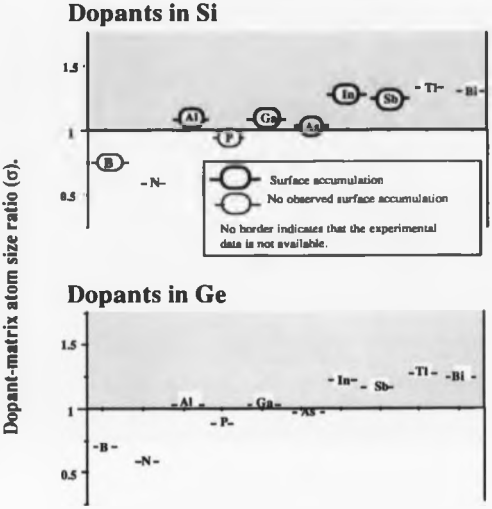

Figure 4.2. Schematic representation of the ratio of dopant and semiconductor atom size (σ) for the possible dopants in Si and Ge.

The dopants in the shaded region (σ > 1) are those predicted to accumulate on the surface. The predictions agree with experiment for all available data.

Note that the experimental data is for elemental dopant fluxes arriving at the semiconductor surface.

As shown in the figure the line $\sigma = 1$ does, as predicted, separate the known cases of surface dopant accumulation from those not showing this behaviour ($\sigma < 1$). In the case of the germanium matrix, the predictions are similar except for arsenic doping. In germanium, $\sigma = 0.99$ for arsenic doping, hence it is predicted that it will not exhibit any surface accumulation behaviour.

The normal covalent radii of the elements (Dean 1985), are used to calculate σ. This estimate is considered appropriate for an adatom on the surface and for the surface of a bulk layer, where tetragonal bonding does not occur.

At this stage, only whether surface accumulation does or does not occur and not its degree, is of concern. The incorporation probability in silicon for antimony and indium and for gallium and aluminium should be similar on the basis of the size effect alone, whereas they differ significantly. (At a growth temperature of 550°C, the incorporation efficiencies are 0.5 for antimony (Ni et al 1989) and $\sim 5 \times 10^{-5}$ for indium (Knall et al 1989), 0.01 for gallium (Becker & Bean 1977) and 0.2 for aluminium (Hasan et al 1990). Other effects clearly modify the quantitative degree of accumulation, these will discussed in section 4.4.

4.3.2 *Compound/alloy matrix systems.*

The situation for compound/alloy matrix systems is more complicated, since a dopant may occupy one of several lattice sites. The most relevant example is the doping of III-V compound semiconductors with group IV elements. To date, it has been generally accepted that the most important factor governing dopant site occupation in these compounds is the relative availabilities of the two matrix sites. For example, the amphoteric behaviour of silicon and particularly germanium in GaAs as a function of the gallium and

arsenic surface coverage (Wood 1985, Cho & Hayashi 1971, Chai et al 1981). The surface coverage can be influenced by the growth conditions. Substrate temperature (Chai et al 1981), growth rate and flux rate (Cho & Hayashi 1971) have all been shown to influence the site occupancy of dopants in III-V compounds.

However, although other III-V materials are deposited under closely analogous surface conditions (i.e. usually group V flux rich conditions), the relative surface coverage fails to explain the observed doping behaviour in many cases. For example, tin is a n-type dopant in GaAs (Wood 1985, Alexandre et al 1980), but in GaSb it exhibits p-type behaviour (Chang et al 1981). The choice of matrix site favoured by these dopants in III-V materials, is the result of competing incorporation at the two sites. It is proposed that the atomic size ratio σ, influences this choice in the following way.

Consider a matrix system AB, where A is larger than B and assume that the surface dopant accumulation in a compound/alloy system occurs from each sub-matrix site independently. The size effect "model" suggests that a dopant larger than either would tend to segregate more from the smaller B-site, leading to net incorporation on the A-site, and also to surface accumulation as $\sigma_A > 1$. For an intermediate sized dopant, the larger A-site would again be favoured, but surface accumulation would not be observed as $\sigma_A < 1$, unless some other mechanism promotes preferential B-site incorporation. Finally, for a dopant smaller than either matrix site, surface accumulation would be absent; in this case the dopant atom will incorporate on the larger A-site. This can be summarised in the statement; the site with the lowest σ is the predicted incorporation site. This means, of course, that the predicted site is not necessarily the site on which the dopant atom will cause the least strain (see discussion).

Figures 4.3(a), 4.3(b) and 4.3(c) compare the predicted and where available, experimental surface accumulation and site occupancy for silicon, germanium, and tin in the III-V semiconductor compounds of technological interest. Returning to the example of tin incorporation given above, good agreement between experiment and prediction is achieved; tin is n-type in GaAs (Wood 1985) and InP (Stanley et al 1985), since incorporation is favoured on the larger group III site, whereas p-type doping prevails in GaSb since the antimony provides the larger matrix site.

The most direct confirmation of the size effect comes from the observation of a gradual shift from p-type to n-type doping of tin in $GaSb_{1-y}As_y$ with increasing y, (Chang et al 1977), as incorporation shifts between the group III site in GaAs to the larger group V site in GaSb. The surface accumulation of tin has only been extensively studied in GaAs, although preliminary results indicate significantly reduced or absence of accumulation in InSb (Newstead 1989) in qualitative agreement with our hypothesis. The site occupation of silicon in III-V compounds also confirms the hypothesis (see figure 4.3a), being n-type in GaAs (Wood 1985), InAs (Oh et al 1989) and InSb (Newstead 1989) but p-type in GaSb (Newstead 1989) and AlSb (Subbanna et al 1989). No evidence for surface accumulation of silicon (except at concentrations near the solubility limit (Beall et al 1988)), has been reported.

Although further verification of the hypothesis awaits more complete mapping of the behaviour of the group IV dopants in the complete matrix of III-V compounds and their alloys, it is evident that the size effect plays a key role in determining dopant incorporation behaviour during MBE growth.

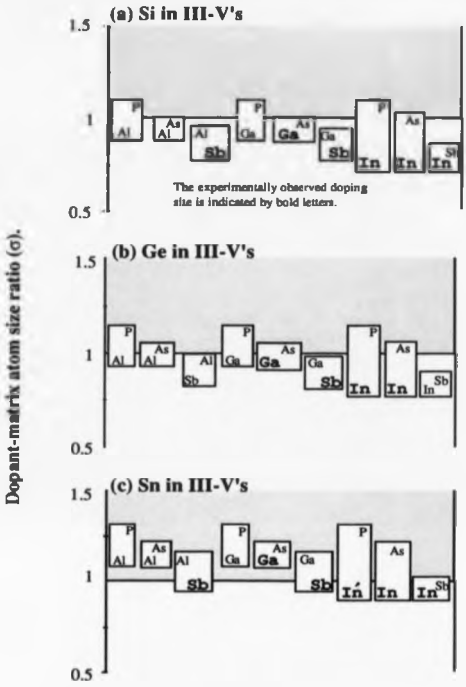

Figure 4.3. Schematic representation of the predicted site occupancy and surface accumulation behaviour for Si, Ge and Sn in various semiconductors.
The lower site (i.e. the larger matrix atom site), is the predicted preferred site.
The dopants in the shaded region ($\sigma > 1$) are those predicted to accumulate on the surface.
The model accurately predicts the preferred site occupancy and accumulation behaviour in all known cases.

The influence of site availability in compound semiconductors, will play a significant role only in the special (and most extensively studied), cases of GaAs and AlAs, where the close similarity in size of the matrix species minimizes the size effect. The case for germanium doping of other III-V materials would be particularly revealing. It is expected that germanium will be n-type in the indium compounds and not exhibit any accumulating or amphoteric behaviour. But in AlSb it will be a p-type dopant.

This model is also applicable to the growth of $Si_{1-x}Ge_x$ alloys on silicon substrates. Germanium being bigger than silicon is predicted to accumulate on the growing surface. Recent observations have confirmed this prediction (Gravesteijn et al 1989) and shown that the extent of the surface accumulation decreases as the growth temperature is decreased, see discussion.

4.4. Discussion

In section 4.2 it was proposed that the atomic size of a dopant, relative to that of the appropriate matrix species was the key factor determining the tendency of the dopant to accumulate on the surface, or the preferred site in a compound or alloy matrix. The physical basis for this proposal was that this is known to be *one* of the factors governing equilibrium segregation in metallic matrices, larger atoms producing excessive strain energy if incorporated into the bulk. The basis is one of energetics alone. It includes no specific *mechanism* of incorporation or rejection, although local equilibrium between the (enriched) surface phase and the freshly grown material might be possible at the interface, even though bulk diffusivities are too low to allow equilibrium to be maintained with deeper layers. (This is an

(This is an intrinsic requirement of MBE growth to produce, for example, 'delta-doped' layers). For the purposes of this study the interest lies in the question; is the apparent dominance of this single influence on the energetics of segregation fortuitous and can the picture of the local kinetics at the interface of the growing solid be refined?

4.4.1 *Comparison with bimetallic alloys*

As mentioned earlier, the local chemical energy (local bonding energy), as well as strain energy, controls the equilibrium balance between bulk and surface dopant concentration ('segregation'). Although several theories have concentrated on only one of these influences, unified theories have been presented by Seah (1979) and by Abraham and Brundle (1981). The more microscopic description of the latter authors is more appropriate in this case. The essential features of these models of equilibrium segregation are based on consideration of the location of the dopant-matrix combinations in $\sigma-\varepsilon$ space, where ε is given by,

$$\varepsilon = \frac{\text{dopant-dopant bond strength}}{\text{(matrix atom)-(matrix atom) bond strength}}$$

Consider the influence of strain energy alone, it is clear that *any* deviation of σ from unity will introduce strain energy and so might be expected to induce segregation. Introducing some threshold energy below which this effect is unimportant leads to a region of stability (in which dopant segregation is not expected) around a value of unity for σ independent of ε. As interatomic repulsive interactions are much stronger than attractive ones, (illustrated in figure 4.1), the excess strain energy for a given deviation of σ from unity is greater for $\sigma > 1$ than for $\sigma < 1$, so the region of segregation will be asymmetric about $\sigma = 1$. This is shown schematically in figure

4.4a. If, on the other hand, only the local bonding energy influence is considered, segregation will occur if the dopant-matrix bond strength is less than the matrix-matrix bond strength. For a regular solution situation (in which the dopant-matrix bond strength is the mean of the dopant-dopant and matrix-matrix bond strengths) this corresponds to $\varepsilon < 1$. The dopant segregation-free region, in this model, corresponds to the whole area $\varepsilon > 1$ (see figure 4.4b). If we combine the two influences, retaining the asymmetry of the strain energy effect but returning the threshold strain energy to zero, Abraham and Brundle (1981) arrive at a new dopant segregation-free region shown in figure 4.4c. Re-introducing the strain energy threshold would pull the segregation boundary line down to lower values of ε (i.e. below $\varepsilon = 1$ at $\sigma = 1$).

Figure 4.4. Schematic diagram of the region of ε (bond strength ratio) and σ (atomic size ratio) space in which no dopant segregation is expected (shaded regions) for three models:
(a) strain energy only, including asymmetry as a threshold,
(b) bond energy only,
(c) both effects but setting threshold to zero.
(after Abraham & Brundle 1981).

Figure 4.5a shows the actual data for MBE accumulation used in section 3 displayed on such a plot. The bond strengths are estimated as the single bond strength of the respective elements in discrete molecules (Huheey 1978, Weast 1988). A striking feature of this plot is that while all those systems which do show accumulation behaviour lie outside

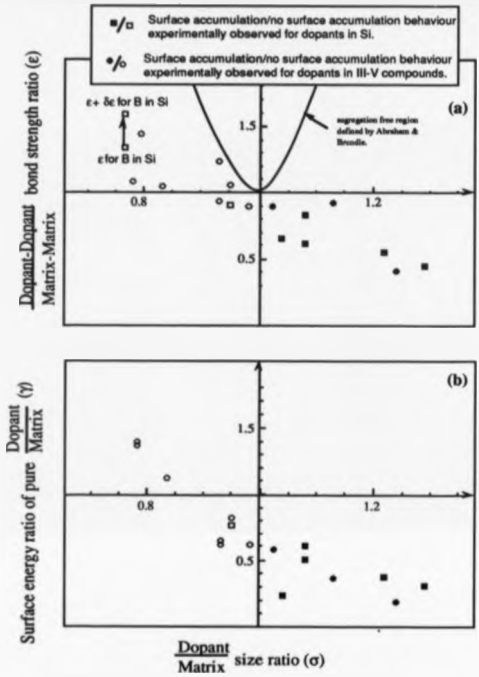

Figure 4.5.

(a) Variation of the ratio of dopant-dopant/matrix-matrix bond strengths (ε) as a function of the ratio of dopant/matrix atomic sizes (σ).

(b) Variation of the ratio of dopant/matrix surface energies (γ) as a function of the ratio of dopant/matrix atomic size (σ).

γ was calculated using data from Gschneider (1964) and Sirota (1968).

the predicted segregation-free region, so too do the data points corresponding to no accumulation behaviour in MBE!. Indeed figure 4.5a clearly shows that the key dividing line between systems which do or do not show accumulation behaviour is the $\sigma = 1$ line which formed the basis of the discussion in section 4.2. In an attempt to investigate the physical basis behind this $\sigma-\varepsilon$ plot, Abraham and Brundle (1981) plot γ vs σ, where γ is the ratio of the surface energies of pure dopant to the surface energy of the pure matrix.

$$\gamma = \frac{\text{surface energy of pure dopant}}{\text{surface energy of pure matrix}}$$

Surface energy is determined by several factors including, the bond strengths, atomic size and the nature of the surface/adlayer. The $\gamma-\sigma$ plot reproduces the predictions of the $\sigma-\varepsilon$ plot. As before, dopants that show no surface accumulation behaviour in MBE lie outside the predicted segregation free region and the $\sigma = 1$ line is still the key dividing line, (see figure 4.5b).

The failure of the unified bond-strength/atomic size theory apparent in figure 4.5 may be due to one of two possible reasons; either the theory fails in some way for semiconductor systems, or the *dynamic* equilibrium at the growing interface modifies the importance of the contributing factors relative to true equilibrium, (or both). In fact there is some evidence that the former explanation might be sufficient. The regular solution theory, implicit in the ε parameter, is probably particularly inappropriate for covalently bonded semiconductor systems. The theory assumes the heat of mixing is zero ($\Delta H = 0$) whereas in these systems there is considerable dopant-matrix interaction (ie. $\Delta H \neq 0$). In the only case in which we could find a dopant-matrix bond energy to plot onto a modified ε

parameter plot (B in Si), the relevant point is displaced very considerably in ε. The correction was of the form

$$\varepsilon - \delta\varepsilon$$

$$\text{where } \delta\varepsilon = \frac{\varepsilon_d + \varepsilon_m - 2\varepsilon_{dm}}{\varepsilon_m}$$

ε_d = dopant-dopant bond strength, ε_m = matrix-matrix bond strength and ε_{dm} = dopant-matrix bond strength. It is therefore possible that only the σ values of the experimental points in figure 4.5 are reliable. Nevertheless, the atomic size ratio σ alone appears to provide qualitatively, an adequate accumulation-defining parameter. To provide a quantitative description, clearly requires a more realistic basis for calculating the chemical energy effects in covalently bonded semiconducting systems then is currently available. Other factors such as; the propensity for island formation (Harris et al 1984), surface compound formation (Iyer et al 1981), atomic or molecular nature of the dopant in the surface phase (deFresart et al 1988) and structural anisotropy effects, need to be considered.

4.4.2 *Stress in semiconductor systems.*

A particularly striking feature of the compound semiconductors is that dopants appear to prefer to occupy the largest site, (section 4.3.2), even in the case in which the dopant atom is smaller than either of the matrix species. This is contrary to a simple strain energy prediction of the kind discussed above because a large mismatch in atom size in substitutional sites should lead to a net increase in strain energy, be the strain compressive or tensile. One possible explanation of this effect, which may also account for the considerable influence of dopant size in compound semiconductors, concerns the sign of the *surface* stress. Little is known about this quantity for solids, but recent calculations and

some experimental evidence suggests, that at metallic surfaces, the surface stress is *tensile*, (eg. (111) surfaces of aluminium, iridium, platinum and gold), whilst for equilibrium (covalent) semiconductor surfaces (notably Si(100) (2x1) and Si/Ge(111) (7x7) it can be *compressive* (Payne et al 1989). Incorporating a small atom in a substitutional site *in* the surface could then lead to an energy lowering. Support for this view is provided by recent structural studies of the Si(111)/B system in which the boron atoms apparently occupy sites just below the surface (Headrick et al 1989, Lyo et al 1989, Bedrossian et al 1989). They compare the preferred sites for boron and gallium on a Si(111) surface and find that the stretched bonds surrounding the smaller boron atom (σ = 0.75) in the immediate bulk layer will allow relaxation of surrounding silicon atoms towards the boron atom leading to a lower energy orientation. However, it is energetically unfavourable for the compressed bonds surrounding the larger gallium atom (σ = 1.07), to allow similar movement, hence its preferred site is on the surface where the surrounding silicon atoms have a greater degree of freedom to accommodate it. These results are for a specific equilibrium reconstruction on a Si(111) surface, however, arsenic on Si(100) (an accumulating system), is also believed to involve overlayer adsorption (Uhrabera et al 1986). Relief of compressive surface stress could therefore be a significant additional factor in semiconductor systems favouring accommodation of smaller atomic adsorbates into, or below the surface. Even if these species are not favoured as *bulk* substitutional species, they could become trapped in growth much more readily than if their preferred adsorption site was above the surface.

4.4.3 *Equilibrium during MBE growth*

Another issue of importance is the nature of the surface-substrate equilibrium during growth. The recognition that atoms at

the surface are much less constrained in their movements than those in the bulk. This leads to the idea that the dopant concentration in the surface phase might be in equilibrium with the freshly deposited solid immediately below it, even though bulk diffusivities may be too low to achieve this situation over any significant distance. In fact this problem, of the extent to which the surface concentration may be in true equilibrium with the growing substrate, has been addressed in a series of papers by Greene and co-workers as described by Barnett and Greene (1985). These studies set out to provide a quantitative description of the surface accumulation phenomenon in MBE. The key factors in determining the accumulation, the activation energies for desorption into the gas phase and into the solid matrix (the enthalpy of segregation) are entered as parameters. The values of which are either estimated from other experiments or chosen to optimise the fits of the computational results to experimental growth measurements. An important conclusion of this work is that at sufficiently high growth temperatures there is evidence that true local equilibrium is established during growth, leading to the characteristic Gibbs or Langmuir behaviour, in which the surface accumulation increases as the temperature is lowered. They also, however, find evidence for non-equilibrium or dynamic equilibrium behaviour in some dopant-temperature regions of the growth parameters. It is accepted that if the growth rate was sufficiently high, or the growth temperature sufficiently low, then place exchange at the interface would be too slow to prevent dopant atoms from being buried causing a suppression of the surface accumulation below the level expected in equilibrium.

The actual mechanism of achieving (or failing to achieve) equilibrium incorporated into the theory of Barnett and Greene (1985)

is not, however, that of local surface place exchange between dopant and matrix species, but enhanced *bulk* diffusivity in the outermost few atomic layers. This physical picture may be appropriate in the case of low energy ion implantation during growth, (Bajor & Greene 1983), in which substantial temporary damage of this sub-surface region must occur. However, in the case of simple thermal beams and growth rates of little more than 1Å/sec (0.4 μm/h), such enhanced diffusion over 10 or 20Å below the growing surface is unlikely. These limitations have been largely overcome by a more physical description of this near surface region based on several different potential wells, (Ni et al (1989). However, as this model relies on experimentally determined parameters, it can not be used to obtain general predictions.

4.5. Conclusion and further work.

It is proposed that the relative atomic size of a dopant and its matrix is a key parameter influencing the propensity of the dopant to surface accumulate during MBE growth. This hypothesis has been successfully tested by comparison with the existing experimental data for doping in MBE. By extending the hypothesis, this study has shown that the size effect also influences site occupation in compound/alloy systems. Indeed, with the exception of GaAs and AlAs where the size differential between the matrix sites is small, the size effect appears to dominate over the site availability in controlling site occupation. Prediction of the occurrence or absence of surface accumulation, and of dominant site occupation (for the case of compounds) for all the common dopants in silicon, germanium and III-V MBE provides a basis for further tests of this hypothesis.

This model does not rely on any specific mechanism for the dopant incorporation. However, it is proposed that the same factors

which influence the local equilibrium between a dopant atom and the surface layer also determines the propensity of the dopant to incorporate or accumulate at the vapour-solid interface during MBE growth. Previous quantitative descriptions of the kinetics of this phenomenon have been based on this assumption and have used the enthalpy of segregation as the key parameter determining the degree of surface accumulation of the dopant. However, in considering the factors influencing this enthalpy, it was found that a regular solution model, which has previously proved adequate for describing metallic segregation phenomena, is inadequate for covalently bonded semiconductor systems. To adapt this description for covalently bonded systems, the matrix-dopant bond strengths and surface energies of these systems need to be elucidated. This can be done empirically for surface accumulating systems by desorption studies or semi-empirically using ab-initio molecular orbital calculations.

A full physical description of the dopant incorporation process will involve consideration of several other factors. For example ; (a) nature of the surface stress. Recent evidence suggests that the sign of the surface stress and the tendency of a particular dopant species to equilibriate in surface or sub-surface sites maybe responsible for the surprising dominance of atomic size in determining the qualitative accumulation behaviour, (b) lattice orientation, (c) nature of the dopant species arriving at the substrate, eg. atomic or molecular, (d) influence of impurity species, eg. oxygen from a boric oxide source can stabilise boron on the growing silicon surface, (e) effect of ionised species such as Si^+ or Mo^+ from the electron beam hearth. Knall et al 1989 found that Mo^+ from an electrostatically focused electron beam hearth increased the incorporation efficiency of indium in Si(100) by several orders of magnitude, (f) growth conditions, (g) entropy effects.

Chapter 5.

Phosphorus doping in MBE by co-evaporation.

5.1 Introduction.

Table 5.1a and figure 5.1b present the important properties for possible dopants in silicon. The n-type dopants all have low ionization energies allowing high activation efficiencies. But, as antimony has a lower solid solubility limit, phosphorus and arsenic have been the preferred dopants in silicon.

However, dopants in MBE also have to fulfil other criteria. A good technological dopant in MBE would be one whose vapour pressure; (a) is low at bakeout temperatures (150°C to 300°C), to avoid increasing the background doping already present in the MBE system, (Kubiak and Parker 1988) and (b) at relatively low source cell temperatures, (~300°C to 500°C), gives a sufficient vapour pressure to dope the growing silicon at a level ranging from $\sim 1x10^{15}$ to $1x10^{20}$ atoms cm^{-3}. Both phosphorus and arsenic, have very high vapour pressures, (if elemental sources are used), at bakeout temperatures. Antimony on the other hand, fits these conditions. However, it suffers from a major drawback, namely, surface accumulation. At low substrate temperatures, ($\leq$ 500°C), antimony can reach greater than one monolayer coverage of the silicon surface (Metzger and Allen 1984a). This surface accumulation behaviour leads to problems in dopant profile control, (see chapter 4), although developments such as PED, (see chapter 1), have increased the controllability of antimony to the extent that it is an acceptable n-type dopant in Si-MBE.

Dopant	Source [a] composition	Evaporation[a] temperature range (°C)	Maximum[b] concentration (cm^{-3})	Ionization[c] energy (eV)
B	B	1300 - 2000	$5x10^{19}$	0.045
	B_2O_3	700 - 1150		
	B/Si	1000 - 1400		
	BF_3	Gaseous	$7x10^{20}$	
Al	Al	1000 - 1100		0.067
Ga	Ga	750 - 1100	$2x10^{20}$	0.072
P	PH_3	gaseous		0.045
	P	25 - 100 [d]		
As	GaAs	500 - 750		0.054
	InAs	500 - 650		
	AsH_3	gaseous		
Sb	Sb	250 - 500	$1x10^{19}$	0.039

(a) Kubiak & Parker, 1988.
(b) Iyer, 1986.
(c) Sze, 1985.
(d) Kubaschewski & Alcock, 1979.

Table 5.1a. Properties of the common dopants in silicon

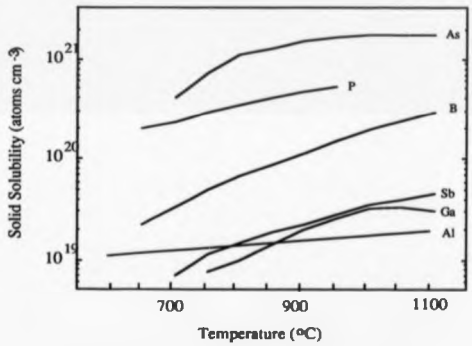

Figure 5.1b. Solid solubilities of the common dopants in silicon. (Data from references Sze 1985, Nobili 1988, deCogan 1988).

However, due to its low solubility limit phosphorus or arsenic doping will have to be developed to achieve higher electron concentrations in the silicon epilayers.

5.1.1 *Possible dopant sources.*

Fears of memory doping effects has impeded the use of phosphorus in Si-MBE and most of the experience of the use of phosphorus in MBE is derived from InP and GaP MBE, (Lippens et al 1982, Lau and Gosele 1986, Stanley et al 1985).

Elemental sources use solid phosphorus (i.e. red form), with the vapour phase composed of P_4 molecules, which condenses as white phosphorus and is inflammable in air at room temperature. This drawback can be circumvented by thermally cracking the P_4 molecule to P_2, (in a baffle structure directly above the source cell), which then condenses as red phosphorus, (Huheey 1978). Its high vapour pressure ($\sim 7 \times 10^{-4}$ Torr at 200°C, (Panish 1970)), necessitates cooling of the source cell during bakeout and prevents the use of outgassing procedures to remove adsorbed contaminants.

The use of phosphine gas (PH_3) avoids these problems (Chow and Chai 1983). Thermal cracking of the PH_3 molecule produces P_2 and H_2, but large volumes of H_2 are difficult to pump and PH_3 itself is extremely toxic, requiring extensive safety precautions.

Another alternative is low energy ion implantation of P^+. At a beam energy of 100 eV, high quality InP films were reported by Mariuno et al (1987). However, the equipment required for ion implantation is both complex and expensive.

Technical solutions such as removable liquid nitrogen cooled cryo-panels (Tsang et al 1982) surrounding the growth area to limit its background doping effects have also been developed, though these necessitate involved growth procedures and limits throughput.

Solid sources such as InP, offer greater control over the phosphorus vapour pressure. In the case of InP the vapour contains appreciable concentrations of In and some P_4, (Farrow 1974). The presence of indium is obviously not a problem during InP growth, though in silicon it can cause degradation in the epilayer quality, (Kubiak et al 1985b).

Another compound source is tin phosphide. Using a tin rich, tin phosphide source Chai (1984) found that the partial pressure of P_4 to be over a decade lower than the P_2 vapour pressure in the temperature range 250°C to 400°C. In this regime the vapour pressure of tin was below the detection limit of the Quadrupole Mass Spectrometer (QMS), ie. $< 1 \times 10^{-12}$ Torr. These advantages led to this source being chosen for this study.

To enable comparisons to be made with Chai's vapour pressure data, the same source composition was used in this study, i.e. Sn_3P_4 + Sn. Chai formed his source by reacting phosphorus and tin, a process which resulted in excess tin being present.

5.2 Assessment of tin phosphide as a dopant source in Si-MBE.

5.2.1 *Tin phosphide source*

The construction of the source cell is shown schematically in figure 5.2. It is constructed principally out of tantalum. The heating was carried out radiatively using a tantalum wire heater. A pBN crucible sat in a wire cradle formed by the thermocouple. A tantalum shutter was positioned in front of the source cell to allow control over the dopant flux.

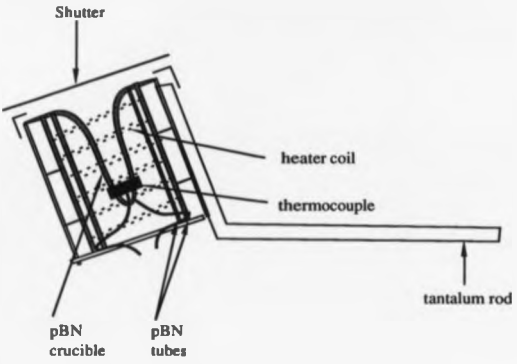

Figure 5.2. Schematic of the tin phospide source cell. All unlabelled parts were manufactured out of tantalum.

Two grammes of Sn_3P_4 (99.999% pure) was placed with 2g of Sn (99.9999% pure) into the pBN crucible. The source cell was outgass ed at 325°C for 30 mins before growth. During this period the background pressure rose to $2x10^{-7}$ Torr, consisting principally of phosphorus and hydrogen, (see figure 5.3). The QMS was positioned such that the dopant flux required several bounces before entering the ionizer. In agreement with Chai (1984), the vapour pressure of tin was found to be below the detection limit of the QMS, ~$1x10^{-11}$ Torr. The mass peak 31 (ie. P_1), produced by cracking of the predominant species, P_2, was monitored during this study. It showed a similar dependence on T_{Sn} as the doping level, (see figure 5.5).

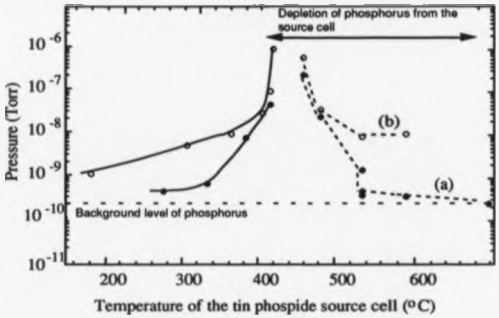

Figure 5.3. Plot of vapour pressures as a function of the temperature of the tin phosphide source, T_{SnP}.
(a) Partial pressures of mass 31, i.e. P
(b) Total pressure during growth.
The drop in partial pressure for $T_{SnP} > 400$ °C is discussed in the next section.

The partial pressure rose above the background at a T_{SnP} ~250°C. At T_{SnP} = 390°C the partial pressure of phosphorus was such that the system pressure rose above the normal growth pressure range 1×10^{-10} to 1×10^{-8} Torr, (normally mostly H_2), see curve b in figure 5.3. This high level of P_2 depositing over the growth chamber will obviously lead to increased doping due to the background vapour pressure of phosphorus.

During the outgassing procedure the tin was in the molten state (m.p = 231.9°C), leading to a fraction of it diffusing into the Sn_3P_4, (Vivian 1920). Therefore the Sn_3P_4 is unlikely to remain stoichiometric. The exact composition of the compound is uncertain,

though it is likely that there will be localised formation of Sn_4P_3, the phospide composition which is richest in tin. Despite this, at a given source cell temperature, the phosphorus flux emitted stayed reasonably constant. Secondary Ion Mass Spectrometry failed to detect any tin in the epilayers above its detection limit of $\sim 1 \times 10^{15}$ atoms cm^{-3}. Curve a in figure 5.4 shows the eCV profile of the first phosphorus doped silicon epilayer grown. It is evident from this example that the thermal response of the source cell is slow.

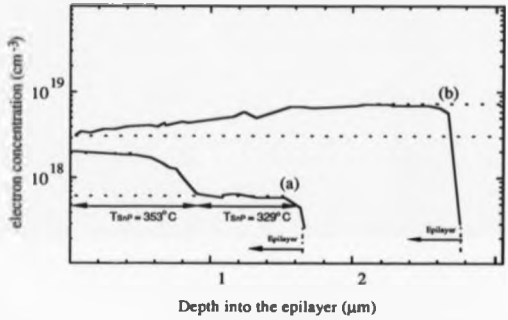

Figure 5.4. Electrochemical Capacitance Voltage profiles of two phosphorus doped epilayers illustrating the stability of the flux emmitted from the tin phosphide source.
(a) 51/1, the first epilayer grown. The broad translation in doping on changing the source cell temperature indictes the slow thermal response of the source cell. Note that when the temperature of the source cell stabilised the doping level remained constant.
(b) 51/17, during this layer the source cell became depleted of phosphorus, note the 1/2 decade drop in doping level. All growth conditions were kept constant, $T_{SnP} = 450°C$. (See section 5.2.2).

5.2.2 *Doping.*

Figure 5.5 plots the doping levels as a function of source cell temperatures, (T_{SnP}), as measured by electrochemical capacitance voltage (eCV) and four point probe.

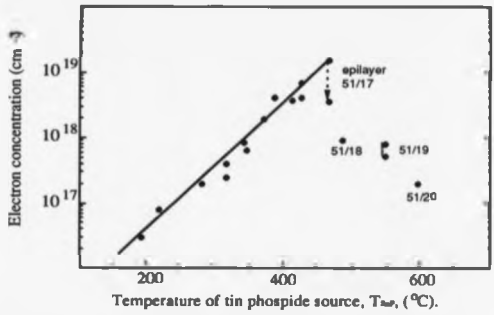

Figure 5.5. Carrier concentration as a function of the tin phospide source temperature. The reduction in doping for T_{SnP} > 480 °C was caused by depletion of phosphorus from the source, see text. Note that the highest doping level was not found uniformly over the epilayer, (see section 5.2.3).

The graph indicates a linear relationship up to 450°C, with doping levels from $3x10^{16}$ to $1x10^{19}$ cm^{-3} being achieved. For epilayer 51/17 (T_{SnP} = 450°C), a fall off in the doping level is evident, illustrated in figure 5.4. Subsequent attempts to vary the doping level as a function of T_{SnP} were unsuccessful. The initial explanation for the reduced levels was thought to be a phase change in the composition of the charge, occurring as the phosphorus depleted, leading to the formation of a eutectic. If this were the case then the eutectic

composition, (49.7 atomic per cent phosphorus, Vivian 1920, Hanson and Andreko 1958), will be evaporated from the charge i.e. approximately half the dopant atoms reaching the substrate would be tin. For example epilayer 51/17, which was doped at $3x10^{18}$ cm^{-3}, should have a similar concentration of tin. However, SIMS analysis of this layer found no tin above the detection limit, ($\sim 1x10^{15}$ cm^{-3}).

For the next two epilayers, 51/18 and 51/19, the source cell temperatures differed by 75°C (the maximum temperature being 550°C), but the doping level remained constant. This behaviour could be explained if during the growth of epilayer 51/17 the source cell became depleted of phosphorus. At this point the doping level would begin to decrease, (as shown by curve b in figure 5.4), to the background doping levels. The constant doping level in the subsequent epilayers is then explained as being entirely due to this background doping. The drop in the partial pressure of phosphorus down to the background level, (evident in figure 5.3), for $T_{SnP} > 480°C$ supports this assumption. An upper estimate of the background doping level, (obtained by shuttering the phosphorus flux, see figure 5.7), was found to be $\sim 1x10^{18}$ cm^{-3}, approximately the level observed above.

A feasibility check on this deduction could be obtained by calculating the flux of phosphorus leaving the source cell as a function of T_{SnP} and comparing the theoretical lifetime of the source with the observed lifetime.

Due to lack of data on the partial pressures of the constituents over the tin phosphide source, calculating this theoretical lifetime is non-trivial. Direct measurement of the phosphorus flux during growth was not possible with the QMS, as it was a direct beam analyser and as such, prone to contamination if used to measure the flux

directly. The doping level obtained at various values of T_{SnP}, cannot be related to the partial pressures of phosphorus as the overall sticking coefficient for phosphorus doping as a function of substrate temperature (Ts), in Si-MBE was not known. However, an estimate can be obtained using data presented by Chai (1984). For a source cell temperature of 350°C, the total partial pressure of phosphorus, (P_2 + P_4), measured at the QMS by Chai was $\sim 3 \times 10^{-5}$ Torr. This pressure can be translated to the number of P_2 molecules arriving at the QMS using the kinetic theory of gases, (see Introduction). Using equation 1.2, a partial pressure of 3×10^{-5} Torr of P_2 translates to 5.4×10^{13} molecules cm^{-2} sec^{-1} (I_p) impinging on the QMS head. The total flux of phosphorus atoms, (I_{P_s}), can be calculated by rearranging equation 1.6 and assuming W = 1. This gives the partial pressure of P_2 at the source cell (P_{P_s}),

$$P_{P_s} = \frac{I_{ps}]^2 (2\pi m k T)^{1/2}}{A \cos\phi} \quad Nm^{-2} \quad \text{..... 5.1}$$

P_{P_s} can be translated to the number of P_2 molecules leaving the source (I_{P_s}), by combining equations 1.2 and 5.1

$$I_{P_s} = \frac{I_{ps}]^2}{A \cos\phi} \quad \text{molecules } cm^{-2} \text{ sec}^{-1} \text{ ..... 5.2}$$

Therefore the total number of phosphorus atoms leaving the source cell at T_{SnP} = 350°C is

$$\frac{2I_{ps}]^2}{\cos\phi} \quad \text{atoms sec}^{-1} \quad \text{..... 5.3}$$

In the growth system used by Chai, the position of the source cell with respect to the QMS head was such that $l \sim 5$ cm and $\phi \sim 35°$. Inserting these values in equation 5.3 gives

$$1.4 \times 10^{17} \text{ atoms sec}^{-1}$$

The tin phosphide used as a source was Sn_3P_4 which has a molecular weight of 479.95g. Two grammes of Sn_3P_4 will therefore contain 1.4×10^{21} phosphorus atoms. Comparing this value with rate of depletion of this source gives a lifetime of the source for $T_{SnP} = 350°C$ to be ~170 mins.

Taking into account outgassing times etc, the tin phosphide source was at $T \geq 350°C$ for 195 ± 20 minutes before the drop off in doping concentration occurred. The estimate of the source cell lifetime is within the order of magnitude accuracy expected from this calculation, indicating that depletion of phosphorus from the source is a plausible explanation.

5.2.3 *Dopant uniformity*

The dopant uniformity across a 76 mm diameter substrate is shown in figure 5.6. The uniformity is very good at low doping concentrations, ± 6% in the doping range 1×10^{16} to 1×10^{17} cm^{-3}. This gets progressively worse the higher the doping concentration, reaching ± 40% in the doping range 1×10^{18} to 1×10^{19} cm^{-3}.

Closer examination of the non-uniformity indicates that at the higher doping levels there is a gradient in the doping concentration from one side of the 76 mm diameter epilayer to the opposite side. Further 4 point probe scans over these epilayers backed up this observation. It is possible that the variation in substrate temperature over the wafer, (± 30°C at the growth temperatures used), contributes to this non-uniformity.

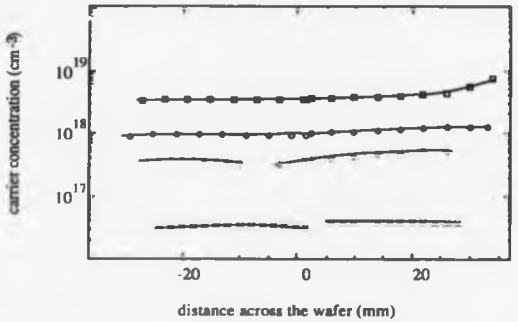

Figure 5.6. Graph showing the uniformity of doping achieved across a 76 mm diameter epilayer at different carrier concentrations.

5.2.4 *Doping Transitions.*

Figure 5.4 illustrates that variation of the source cell temperature is not sufficient to obtain "sharp" doping profiles. Two other methods of achieving greater control over the dopant profile were discussed in the introduction. These are shuttering of the dopant flux and the application of a potential to the substrate ie. PED.

Figure 5.7 shows a doping transition introduced by partially shuttering the SnP source without interrupting growth. The doping transition rate achieved was ~120 nm per decade. This is considerably more abrupt than can be achieved with gallium or antimony, (Kubiak et al 1985b). The instant drop in the doping level, at these high doping levels, without the normal "rounding" of the profile, evident with gallium and antimony doping suggests an absence of any

significant surface accumulation of phosphorus on the growing silicon surface.

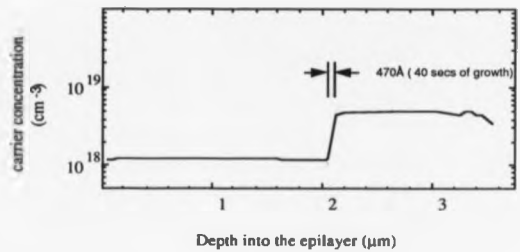

Figure 5.7. Doping transition induced by partial shuttering of the tin phosphide source during growth of epilayer 51/12, at a substrate temperature Ts = 750 °C and a growth rate of 4.3 μm hr⁻¹.

The response of the phosphorus doping to PED, was also investigated. For an applied voltage of -350 volts, the antimony doping level increases by 2 orders of magnitude and the arsenic doping level by 1/2 a decade, (Kubiak et al 1985b). In these experiments the same voltage had no influence on the doping level of phosphorus. This is illustrated in Fig. 5.8, the voltage was applied during growth at point A.

The trend of decreasing response to an applied voltage correlates with the decreasing surface accumulation behaviour from antimony to arsenic (see introduction), further indicates that the phosphorus adlayer coverage is negligible. However, if phosphorus formed 3D islands, then the effectiveness of PED would be limited, as is

the case for Ga doping, (Houghton 1989). This will be discussed in section 5.7.

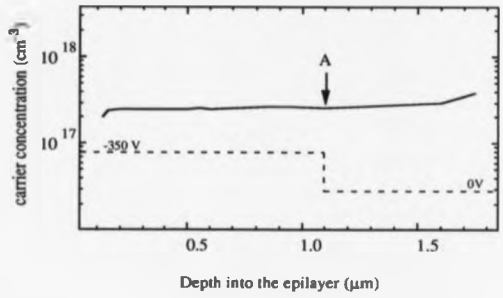

Figure 5.8. Illustration of the ineffectiveness of PED on phosphorus doping level. A voltage of -350 v was applied at point A.

5.2.5 *Background doping.*

Before the phosphorus growth series, 51/X, the background doping was $6x10^{14}$ to $1x10^{15}$ cm^{-3}, (curve a in figure 5.9). At the end of the series the background doping level was ~$1x10^{17}$ cm^{-3}, an increase of two decades, (curve b in figure 5.9). During the middle of the doping experiments the background doping reached ~$1x10^{18}$ cm^{-3}. A standard two day bakeout at ~190°C produced a small reduction in the background doping to ~$6x10^{16}$ cm^{-3}, (curve c in figure 5.9). However, by the eighth layer of the next growth series, the background doping was back down to ~$3x10^{15}$ cm^{-3}, (curve d in figure

5.9). This indicates that the deposition of silicon over the phosphorus deposits is more effective at reducing the phosphorus background doping. In this case 24 μm of silicon were deposited before the test epilayer was grown, but it is probable that significantly less silicon would have similar effect.

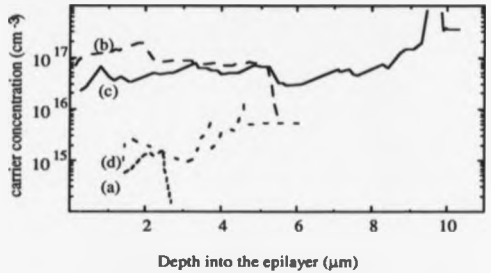

Figure 5.9. eCV profiles of unintentionally doped epilayers.
(a) epilayer 48/1 grown before the phosphorus source was used.
(b) epilayer 51/21 grown at the end of the phosphorus doping experiments.
(c) the first epilayer grown after a standard two day bakeout, 52/1.
(d) the eighth epilayer grown after the bakeout, 52/8.

5.3 Electrical assessment of phosphorus doped Si-MBE epilayers.

5.3.1 *Electron mobility.*

The epilayers grown showed bulk like mobilities both at room temperature and at 77K, indicating material of good electrical quality.

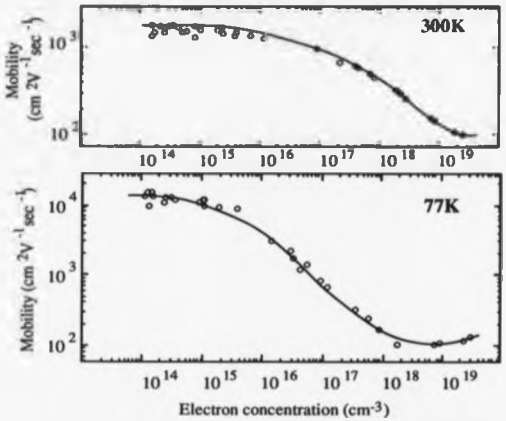

Fig 5.10. Electron mobilities in MBE-grown Si doped with P as a function of electron concentration, measured at 77K and 300K. Carrier concentrations in excess of $5 \times 10^{15} cm^{-3}$ have been obtained by controlled introduction of the dopant, whereas lower electron densities are associated with residual impurities. The solid line represents bulk mobility values derived from the measurements of Morin and Maita (1954) on Si doped with As. After Kubiak et al (1987).

Figure 5.10 shows the mobility measurements on these epilayers reported by Kubiak et al (1987).

5.3.2 Activation coefficient.

As mentioned earlier, one of the reasons why phosphorus is used as an n-type dopant in device fabrication is its high solid solubility limit. There have been various values in the literature for the solid solubility of phosphorus (C). Nobili (1988) has collated the data up to 1987 into the expression

$$C = A \exp\left(\frac{E}{kT}\right) \qquad \text{..... 5.4}$$

for the temperature range 750°C to 1050°C, (see figure 5.1b). The pre-exponential factor A = (1.8 ± 0.2) x 10^{22} atoms cm^{-3} and E = 0.4 ± 0.01 eV.

At the standard substrate temperature used this growth series, 750°C, the solid solubility limit is 1.9×10^{20} atoms cm^{-3}, increasing to 2.6×10^{20} atoms cm^{-3} at the highest substrate temperature used, 825°C. These values were found in equilibrium conditions using bulk silicon. The samples were either implanted with phosphorus and then annealed or the phosphorus was diffused-in from the surface. MBE, as discussed in the previous chapter, is a non-equilibrium situation so this limit, although thermodynamically possible, could be kinetically limited. Indeed there is evidence from other epitaxial growth techniques that the solid solubility limits found at equilibrium are not achievable when the dopant is "grown in", with the silicon matrix. Leong et al (1988) found that in UHV CVD the maximum phosphorus concentration was $\sim 1 \times 10^{18}$ cm^{-3}, 100% of which was active. Due to the depletion of phosphorus from the tin phosphide source the maximum level of electrically active phosphorus achievable in MBE was not found. However, a level of $\sim 1 \times 10^{19}$ cm^{-3} was achieved, (illustrated in figure 5.5), an order of magnitude higher than that so far achieved by UHV CVD.

To evaluate the degree of activation for phosphorus doping by co-evaporation in MBE, the total phosphorus content was assessed using SIMS and compared with the electrically active concentration found by eCV profiler and four point probe measurements. Figures 5.11a & 5.11b, compare the SIMS and eCV profiles for layers grown at two different substrate temperatures.

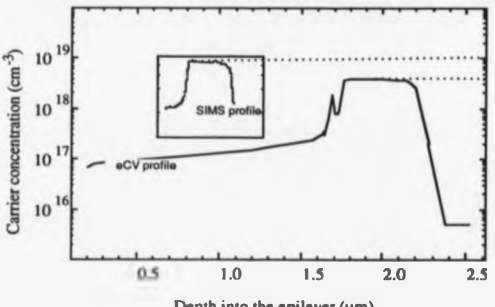

Figure 5.11a. Comparison of the chemical concentration (SIMS profile) and the electrically active concentration (eCV profile) of phosphorus in an epilayer grown with Ts = 750 C at growth rate of 2.26 μm hr , (T$_{RT}$ = 410 C).
As high resolution SIMS, of the full 2.46 μm of the epilayer would take a prohibitive length of time, the first 1.5 μm was chemically removed before the SIMS profile was taken, therefore the scales are different.

The analysis was done on neighbouring areas of the epilayer to minimise errors due to possible variation in the dopant incorporation across the epilayer. At Ts = 750°C the eCV profile shows that the electrically active phosphorus concentration is ~57% of the total phosphorus concentration shown by SIMS (see figure 5.11a). Even taking into account the maximum possible error in the techniques (~15%) the result indicates that full activation was not achieved. This is surprising as it is ~2 decades below the solid solubility limit at this growth temperature. At a higher growth temperature of 775°C and higher growth rate, (5.48 μm hr^{-1}), a similar level of activation efficiency was obtained, illustrated in figure 5.11b. This will be discussed in section 5.7.

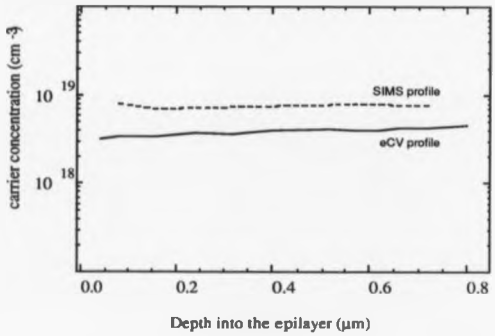

Figure 5.11b. Comparision of the chemical concentration and the electrically active concentration of phosphorus in an epilayer grown at Ts = 775 °C at a growth rate of 5.48 μm hr^{-1}, (T_{MP} = 450°C).

5.4 Growth temperature dependence.

The effect of Ts on doping concentration is illustrated by figure 5.12 which shows that the doping level varies by a factor of ~2 over a substrate temperature range of 650°C to 825°C. This is much lower then that observed for antimony and indicates a non-unity sticking coefficient and possibly the lack of surface accumulation of phosphorus on the Si(100) surface. It has to be noted that this Ts dependence is for electrically active phosphorus only and takes no account of the activation efficiency. Further SIMS analysis are required to ascertain the Ts dependence of the total phosphorus incorporation rate.

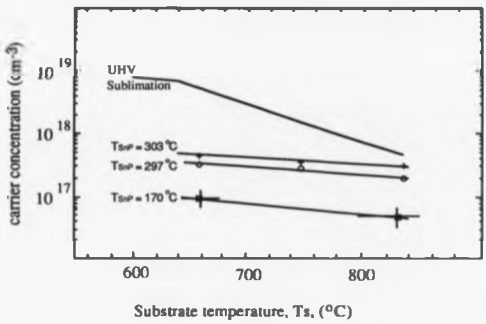

Figure 5.12. Variation of phosphorus doping level with growth temperature, Ts, at various source cell temperatures, T_{SnP}.

The variation in phosphorus doping level with Ts in the technique of UHV sublimation (see appendix B), over the same temperature range was greater at ~10x, (see figure 5.12, (Kuznetsov et al 1974). In this case the situation is complex and will be discussed later. The data presented in figure 5.12. was not corrected for intentional experimental variation in the growth rate and no systematic studies were undertaken on growth rate dependence of phosphorus doping.

The relative insensitivity of the doping level to substrate temperature is unlike the behaviour of other n-type dopants. Antimony and arsenic both show a change of ~20 times over the same temperature range, (Metzeger and Allen 1984a, 1984b, Kubiak et al 1985b). However, gallium (a p-type dopant), exhibits a similar

variation with substrate temperature, ~3x (Houghton 1989). This difference between gallium and the n-type dopants, arsenic and antimony, is probably related to their different surface accumulation behaviour. The antimony adlayer consists of complete monolayers, whereas the adlayer of gallium on Si(100) consists of 3D islands. The intimation being that a variation in substrate temperature will affect the desorption rate of the dopant from a 2D adlayer to a different extent then from 3D islands and hence vary the doping level to a greater extent. The possibility of phosphorus forming 3D islands on the silicon surface therefore has to be considered.

An estimate of the sticking coefficient (S), at Ts = 750°C can be obtained using Chai's vapour pressure data via equation 5.5

$$S = \frac{N\,r}{I} \qquad \text{..... 5.5}$$

Where S = the sticking coefficient and N = phosphorus content of the epilayer per cm^{-3} and r = growth rate. An epilayer grown with T_{SnP} = 350°C at a substrate temperature of 750°C, had a doping level of $2x10^{18}$ cm^{-3}. The growth rate r = $6.3x10^{-8}$ cm s^{-1} and the arrival rate of the phosphorus atoms on the silicon surface, I, (estimated from Chai's data) was $3x10^{13}$ atoms cm^{-2} s^{-1}. Inserting these values into equation 5.5 gives the sticking coefficent for phosphorus that becomes electrically active. The overall sticking coefficent will be ~2x this value, see section 5.3.2.

$$S = \sim 4x10^{-4}$$

This value is one of the lowest for any dopant in Si-MBE, (see figure 5.13).

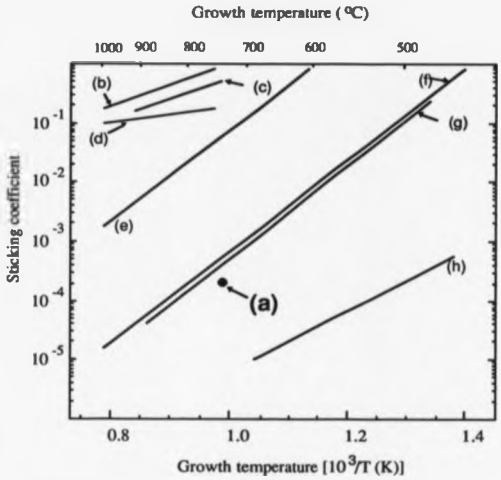

Figure 5.13. Comparision of the estimate of the sticking coefficient for phosphorus on Si(100) in MBE with other dopants and other techniques.

(a) The estimate for P on Si(100) in MBE.

(b) B on Si(111) in UHV Sublimation, (After Bennett & Parish 1974).

(c) P on Si(111) in UHV Sublimation, (After Bennett & Parish 1974).

(d) Sb on Si(111) in UHV Sublimation, (After Bennett & Parish 1974).

(e) Sb on (100) in MBE, (Bean 1984).

(f) Ga on Si(111) in MBE, (Iyer et al 1981).

(g) Sb on Si(111) in MBE, (Metzger & Allen 1984a).

(h) Sb on Si(111) in UHV Sublimation, using a separate doping source, (Tolomasov et al 1971).

The defect densities in the phosphorus doped epilayers was comparable with other doped epilayers grown at the same stage in the development of the MBE system.

Dislocation densities were in the range 2.6×10^4 cm^{-2} to $\sim 1 \times 10^8$ cm^{-2} depending on pre-cleans, substrate temperature etc. (see Introduction). The PRD densities were between 3×10^2 cm^{-2} to 4×10^3 cm^{-2}, (see period D in figure 3.9).

In the case of high antimony doping, unless the surface sdlayer is "flashed off", it gave very high surface defect densities after preferential etching. The defect density in the highest phosphorus doped epilayer was similar to that found in an unintentionally undoped epilayer, (ie. 6.4×10^6 cm^{-2}), further indicating that the phosphorus sdlayer is negligible.

5.6 Comparisons with unintentionally doped epilayers.

The background dopant found in unintentionally doped material grown by MBE, is considered to be phosphorus, at levels between 1×10^{13} and 1×10^{15} cm^{-3}. The source is assumed to be the stainless steel chamber (Iyer & Delage 1988). Recent evidence supporting this theory was reported by Houghton (1989). Unintentional bombardment of stainless steel with an electron beam increased the background levels by two orders of magnitude, whereas shielding of the region with silicon produced large reductions.

Experiments on background doping have been performed over a range of growth temperatures (550°C to 850°C), and PED potentials, (Houghton 1989, Kubiak and Parker 1988). However, due to the low doping levels encountered in the undoped material, characterization of the growth rate and substrate temperature

temperature dependencies were difficult to establish, so no direct comparisons are possible.

5.7 Discussion.

This study has shown that phosphorus is an unusual dopant in Si-MBE, its interesting features being;

(i) Phosphorus incorporation on electrically active sites has a low substrate temperature dependence in sharp contrast to other n-type dopants on Si(100).

(ii) Phosphorus has a low activation coefficient (significantly < 1), compared to near unity activation for Sb.

(iii) Phosphorus does not reveal any significant surface accumulation behaviour, unlike other n-type dopants in MBE.

These are now discussed by comparison with related systems.

5.7.1 *Comparison with phosphorus in bulk silicon.*

When phosphorus is diffused into bulk silicon at high concentrations an anomalous diffusion profile is obtained (Hu et al 1983, Mathiot and Pfister 1982, Richardson and Mulvaney 1988). Two different explanations have been put forward for this; (a) the formation of a +ve charged E-centre (vacancy-phosphorus pairs) that acts as a compensating agent or (b) the formation of small electrically inactive SiP precipitates, (Nobili et al 1982). The second case is generally accepted as the reason for the anomalous diffusion profile in bulk silicon, as mobility measurements do not show any reduction that the presence of an extra ionic scattering centre would cause, (Hu et al 1983). However the precipitates were only found with phosphorus levels close to the solid solubility limit and in the present case the phosphorus levels are ~2 orders of magnitude below this limit. However, it is possible that the presence of high concentration of

oxygen and carbon in Si-MBE material, (see figure 2.9), may enhance the formation of phosphorus oxides or carbides.

The former possibility is unlikely as measurements presented in section 5.3.1 showed that these epilayers exhibited electron mobilities comparable to those found in bulk n-type silicon, over a wide range of doping levels.

From the discussion in the chapter 1, it is possible that the presence of phosphorus precipitates will increase the density of s-pits and hence an their density would show a correlation with the activated phosphorus concentration in the epilayers. Figure 5.14 shows that the s-pit density is directly proportional to the activated phosphorus concentration, indicating that a constant fraction of the total phosphorus may be tied up at s-pits. However, due to the uncertainty of the mechanisms causing s-pits this is only a tentative explanation.

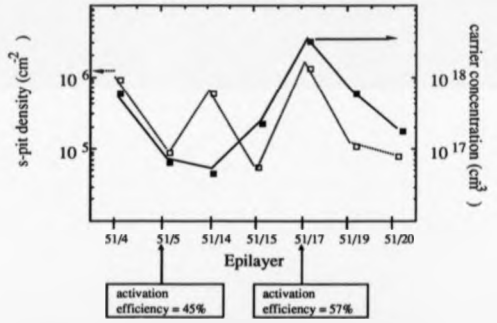

Figure 5.14. Comparision of the saucer pit (s-pit) density and electrically active phosphorus concentration.

Another possible mechanism that could reduce the activation efficiency is the diffusion of phosphorus atoms to dislocation cores where they can occupy electrically inactive sites. These are 3 fold co-ordination substitutional sites associated with a dislocation core, (Street 1982). Recent calculations showed that this 3 fold coordination site is energetically stable for phosphorus, (Heggie et al 1989). This mechaniam assumes that the phosphorus atoms are mobile enough in silicon for a significant percentage of them to reach dislocation cores during the growth period. Table 5.15 tabulates the relevant data for the two epilayers discussed in section 5.3.2.

Epilayer	Activation efficiency (%)	Substrate temperature (°C)	Growth time (sec)	Separation between dislocations (μm)
51/5	45	750	$3x10^3$	~323
51/17	57	775	$2x10^3$	~22

Table 5.15. Table showing the relationship between the activation efficiency and the possible diffusion of phosphorus atoms to dislocation cores.

Allen & Kasper (1988) calculated the diffusion distance for phosphorus in silicon at 700°C to be 3.9 Å hr^{-1}. Therefore even accounting for the slightly elevated temperatures in these samples, the average time required for a phosphorus atom to reach a dislocation core would be on the order of years, rather than the 10's of minutes available. ie. requires an enhancement in the diffusion coefficient of $\sim 1x10^4$. Therefore unless the diffusion of phosphorus is

significantly enhanced on the growing surface this mechanism cannot account for the low activation efficiency.

The most probable explanation for the low activation efficiency in as grown Si-MBE material, is that some of the phosphorus atoms incorporate on interstitial sites. The dopant incorporation process involves the P_2 dimer from the tin phosphide source, splitting on the growth surface. On the reconstructed Si(100) surface, it is probable that a significant fraction of these phosphorus atoms will then incorporate on interstial rather than substitutional sites. This mechanism can be tested by activating these inactive phosphorus atoms by rapid thermal annealing. Optimization of the temperature and time of anneal should allow differentiation between phosphorus activation from interstitial sites or from phosphorus percipitates.

5.7.2 *Comparison with co-evaporation doping of arsenic using compound source.*

The sources are similar technologically and arsenic is similar in its electrical and chemical properties. It emulates phosphorus's preference for the tetrahedron structure (As_4) in the vapour phase when evaporating from elemental arsenic. From compound sources such as InAs or GaAs it sublimes predominantly as As_2 (Kubiak et al 1985b). Unlike tin phosphide the vapour pressure of the other constituent (ie. In or Ga) is significant and can incorporate into the growing silicon layer at high doping levels. Farrow (1974) found that the presence of In increased the sticking coefficient of phosphorus during growth of InP, indicating that the "purity" of the phosphorus beam from the tin phosphide source could be contributing to a low sticking coefficient and hence the low T_s dependence.

Table 5.16 shows the trend in bond strengths for the n-type dopants. The trend is of increasing stability of the molecular dopant flux from Sb → As → P. This trend appears to correlate with the trend in the surface accumulation behaviour. Arsenic accumulates on the surface to a lesser extent than antimony (Kubiak et al 1985b). It is possible that this link between bond strengths and the tendency for surface accumulation extends to phosphorus, which shows no evidence of any surface accumulation.

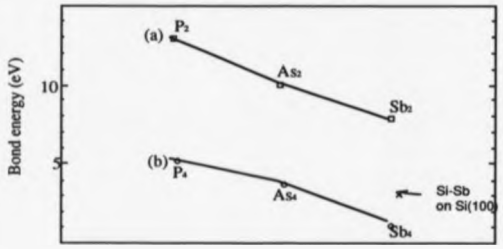

Figure 5.16. Trend in bond strengths for n-type dopants in silicon.
(a) Single bond strength in the diatomic molecule, *i.e.* P_2.
(b) Single bond strength in the tetrahedron structure, i.e. P_4.
(From references Wenzl 1988, Huheey 1978 and Metzger & Allen 1984a/1984b).

However, no difference in doping characteristics has been observed for a dopant flux consisting of Sb_4 or Sb_2 molecules whose bond strengths differ by ~6.5 eV! (Kubiak et al 1985b).

5.7.3. *Comparison with UHV sublimation.*

In this technique the silicon growth flux is the result of sublimation from directly heated silicon strips. The source-substrate

distance is normally a few millimetres and doping is carried out by using doped silicon as the source strips, (see appendix B). The growth environment is similar to MBE, .ie. a flux of silicon and dopant impinging on the substrate in UHV. Kuznetsov and Postnikov (1974) observed a decrease in the doping concentration of ~10x, as opposed to ~2x for MBE in the same temperature range, (see figure 5.12).

The surface accumulation behaviour observed for phosphorus doping under UHV sublimation conditions is discussed in detail in appendix B, the pertinent point being that Kuznetsov et al (1979) obtained indirect evidence that phosphorus accumulated on the silicon substrate during growth. This involved attributing a peak in the depth distribution of stacking faults to a similar distribution of phosphorus precipitates, caused by the build up of phosphorus on the surface exceeding the local solid solubility limit. Kuznetsov et al suggest the increased probability of gettering phosphorus at the peak in stacking fault concentration as the reason for an observed tail-off in the electrically active phosphorus. In the case of MBE no variation in stacking fault length, suggesting depth distribution of the point of origin, was observed. There are three significant differences between the techniques of UHV Sublimation and MBE that could explain these results:

(i) No charged species due to the electron beam evaporator are present.

(ii) The dopant flux is considered to consist of phosphorus atoms rather than P_2 or P_4 molecules.

(iii) Due to the small source substrate separation the phosphorus atom is likely to undergo repeated bounces between the sublimation source and the substrate, before incorporation or "escape" occurs. This has the effect of increasing the probability of the incorporation of a

phosphorus atom, ie. increases its sticking coefficient to near unity, (see figure 5.13) and hence its Ts dependence.

5.8 Conclusions and Further Work.

In this study the feasibility of achieving phosphorus doping by co-evaporation in MBE has been demonstrated for the first time. The tin phosphide source has been shown to provide a fairly stable phosphorus flux, giving good doping uniformity, (± 6%), over a 3" wafer at low doping levels. No contamination due to tin was observed.

At the highest doping levels so far achieved, $1x10^{19}$ cm^{-3}, (which is a decade higher than that achievable by UHV CVD), the uniformity deteriorates to ± 40%. The background doping level is high ($\sim 1x10^{18}$ cm^{-3}), but is most effectively reduced by depositing silicon in the growth chamber. A LN_2 shroud around the source cell and collimation of the P_2 beam would reduce the high background phosphorus pressures during growth and hence reduce the memory doping effects. The low sticking coefficient of phosphorus deduced in this study suggests a much larger capacity source cell would be required for practical work.

Phosphorus has been shown to be a reasonably well behaved dopant, which does not induce any extra crystallographic defects. Relatively good doping transitions are possible on shuttering the dopant flux. Bulk mobility levels are obtained at both 300K and 77K, despite the fact that the activation efficiency is significantly less than unity. It exhibits unusually low Ts dependence for n-type dopants in silicon. This together with the abruptness of the dopant profile with a change in dopant flux and the lack of any doping enhancement on the application of PED indicates a lack of surface accumulation, as predicted by the model in chapter 4. An alternative explanation is the

possibility of phosphorus forming 3D islands. Further work is required to further clarify these points. Possible experiments include;

(i) Use of a cross beam analyser in a quadrupole mass spectrometer will allow direct measurement of the phosphorus flux arriving at the substrate and hence its sticking coefficient. Monitoring the decay in the phosphorus vapour pressure above the substrate when the doping flux is removed, (as a function of substrate temperature), would allow investigations of the rate of re-evaporation of phosphorus.

(ii) The above experiment can be backed up by growing a phosphorus doped epilayer at room temperature, thereby preventing phosphorus from re-evaporating and depth profiling by SIMS.

(iii) High resolution TEM study of the epilayer is required to ascertain the existence or otherwise of SiP precipitates. SiP is coherent with the silicon lattice (Nobili et al 1982) and hence causes less disruption in the lattice then would otherwise be the case. Therefore, if the precipitates are present in low densities, distributed through the epilayer, this could make imaging them difficult. Analysising these epilayers by Small Angle Neutron Scattering, which has a resolution limit of ~100Å, is another possibility.

(iv) Rapid thermal anneal experiments to fully activate the phosphorus would provide an indication of the location of the inactive phosphorus.

(v) Analysis of the surface composition during doping would detect a surface adlayer, (if it existed), and whether it formed 2D layers as the other n-type dopants or 3D islands as gallium. Auger analysis would detect the chemical composition of the surface as a function of doping and diffraction experiments such as LEED or RHEED could detect any surface reconstruction due to an adlayer.

(vi) The maximum doping level achievable in Si-MBE and the growth rate dependence needs to be investigated. The influence of PED and the reduction of memory doping by burying the phosphorus deposits with silicon need to be investigated further.

Another possible approach to phosphorus doping is the use of other source materials for phosphorus. For example:

(i) The use of carrier molecules that only release the phosphorus atoms on the surface of the silicon. A possible molecule being the orthorhombic form of P_4O_{10}. This has the advantage that at the temperatures of the vacuum chamber walls, (<80°C), its vapour pressure is ~5 decades less than elemental phosphorus, (Kubaschewski & Alock 1979). This would significantly reduce any background doping effects due to re-evaporation from these surfaces. This advantage has to be balanced against the possible onset of surface accumulation of phosphorus (and resultant "smearing" of the dopant profile), due to its stabilisation on the surface by oxygen. Compare with boron which exhibits surface accumulation behaviour when evaporated from a B_2O_3 source (deFresart et al 1988). When using an elemental boron source no surface accumulation is observed (Kubiak et al 1985a).

(ii) The use of P/Si alloys as a separate dopant source with an electron beam evaporator providing the growth flux. This would maintain the existing geometry, avoiding the problems of UHV sublimation due to the close proximity of the source and substrate. The presence of silicon raises the sublimation temperature of phosphorus and hence increases the control possible over its vapour pressure. The maximum solubility of phosphorus in silicon is ~2.5 atomic percent. At this concentration its melting point is ~1150°C (Hanson and Andreko 1958), indicating that the possible temperature range for its use as a dopant source would be between 700°C and 1000°C.

Chapter 6.

Metallic Contamination.

6.1 Introduction.

A long standing problem in silicon device technology, is that of metallic impurities. Due to improvements in crystal frabrication technology, commercial silicon substrates are now specified to contain $\leq 1x10^{13}$ metallic impurity atoms cm^{-3}. At present MBE material cannot match this purity both in silicon and compound semiconductor growth. Added to this is the fact that to take full advantage of the monolayer resolution offered by MBE, the traditional high temperature gettering steps that a standard device structure undergoes, cannot be used. Therefore, recent innovations such as using rapid thermal transients, need to be developed.

In this chapter the results of investigations into the metallic contamination levels in MBE material is discussed. The actual growth process occurs in an environment surrounded with metallic components, some of which are subjected to radiant heating. It is therefore possible that a certain level of metallic contamination in the epilayers is unavoidable. In this situation, the relevant questions to ask are; (a) to what extent can the contamination levels be reduced and (b) can gettering techniques be developed to "clean up" the epilayer to an acceptable level, without compromising the dopant profile.

6.2 Investigations into the metallic content of SI-MBE material.

Several specialized techniques have been developed to determine the unintentional impurity content of silicon. Neutron

Activation Analysis (NAA) and Atomic Adsorption Spectroscopy (AA) are extremely sensitive techniques when analysing bulk silicon samples, capable of detecting ~$1x10^{10}$ atoms cm^{-3}. However, due to the restricted amount of material available for investigation of epilayers, the detection limits are significantly higher, eg. for NAA the detection limit is ~$1x10^{19}$ cm^{-3} for iron. Other techniques used are, SIMS and Deep Level Transient Spectroscopy (DLTS). These techniques are described in appendix A. The uncertainty of the results obtained are ~10% for all the techniques.

A batch of epilayers, grown during the period when a tantalum substrate heater was installed, were assessed using all the above techniques. The experimental details of these epilayers are listed in table 6.1, together with the results of the analysis. Due to the high detection limits of NAA it is impossible to determine exactly the absolute level of unintentional impurities in these epilayers. However, with the information available the minimum concentration of metallic impurities can be estimated. This was initially ~$4x10^{17}$ atoms cm^{-3}, the major impurity being copper. Epilayers grown later had lower metallic impurity levels, in the range $1x10^{16}$ to $7x10^{16}$ atoms cm^{-3}.

6.2.1 *Copper contamination.*

On several samples, SIMS analysis for the copper contamination gives differing values from those given by NAA and AA. Possible reasons for the discrepancies include; (i) variation in the copper contamination levels across the epilayers, (ii) the presence of a peak of copper observed at the substrate-epilayer interface by SIMS, (illustrated in figure 6.2). NAA relies on chemically etching off the epilayer for analysis, therefore if the interface region containing the copper spike is removed, the NAA

Sample	Growth temp. (°C)	Pre-growth preperation	Cu (cm^{-3})				Fe (cm^{-3})		Cr (cm^{-3})		Ta (cm^{-3})	
			NAA	AA	SIMS	interface spike	AA	SIMS	AA	SIMS	NAA	SIMS
13/1	850	in-situ heat treatment			$3x10^{15}$	$2x10^{17}$						
16/1	850	in-situ heat treatment			$1x10^{16}$	$2x10^{17}$						
74/11	650	chemical clean + in-situ heat	$3x10^{15}$	$3x10^{15}$	$1x10^{16}$	$3x10^{16}$	$7x10^{15}$	$<1x10^{14}$	$2x10^{15}$	$7x10^{14}$	$4x10^{15}$	$3x10^{15}$
77/8	570	chemical clean + in-situ heat	$1x10^{16}$		$7x10^{14}$	$6x10^{15}$		$<1x10^{14}$		$<1x10^{14}$	$<1x10^{15}$	$<1x10^{14}$
77/9	626	chemical clean + in-situ heat		$5x10^{14}$	$<1x10^{14}$	-	$2x10^{15}$	$<1x10^{14}$	$4x10^{14}$	$<1x10^{14}$		$<1x10^{14}$
79/2	795	chemical clean + in-situ heat		$1x10^{15}$	$2x10^{15}$	-	$1x10^{15}$	$1x10^{15}$	$3x10^{14}$	$4x10^{14}$	$2x10^{15}$	$1x10^{15}$
79/4	480	chemical clean + in-situ heat	$<1x10^{15}$		$3x10^{15}$	$6x10^{16}$	$<1x10^{15}$	$<1x10^{14}$	$3x10^{14}$	$<1x10^{14}$		$2x10^{15}$
79/5	690	chemical clean + in-situ heat	$<2x10^{15}$		$<1x10^{14}$			$<1x10^{14}$		$<1x10^{14}$		$5x10^{15}$
79/6 - Substrate, see note (a).			$6x10^{15}$								$4x10^{14}$	
Substrate, see note (b).			$<9x10^{11}$				$<5x10^{15}$		$<8x10^{13}$		$<2x10^{12}$	

Table 6.1. The major metallic contaminants in Si-MBE epilayers as measured by NAA, AA and SIMS. No nickel was observed above the detection limit in AA of $^{\sim}5x10^{14}$ atoms cm^{-3}.
(a) Substrate heat treated in the growth chamber, whilst shuttered from an energised electron beam hearth. NAA analysis removed the top 2.5 μm of the substrate.
(b) Substrate measured by NAA after the epilayer was removed.

analysis will give a significantly higher value for the level of copper contamination, eg. as in epilayer 77/8.

Considering the high diffusion coefficient of copper, eg. 9.3×10^{-5} cm^{-3} sec^{-1} at 1000°C, (Keenan & Larrabee 1983), the presence of the peaks of copper at the substrate-epilayer interface is unexpected, indicating that a gettering process has trapped the copper at the interface.

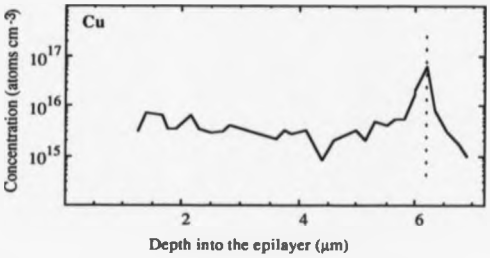

Figure 6.2. Depth profile of copper in epilayer 79/4, as measured by SIMS. The peak occurs at the substrate-epilayer interface, (shown by the dotted line).

Possible sources of copper are:

(i) Contaminant in the HF used to remove the native oxide on the substrate surface before growth, (Houghton 1989). This source can be ruled out as no reduction in the copper contamination is evident between epilayers grown on as-received or cleaned substrates. It is improbable that the copper arises from contamination left on the

substrate after the manufacturers final clean, as several different batchs of substrate were used.

(ii) The copper electron beam hearth used for the silicon evaporation, via localised heating by stray electron bombardment or diffusion of the copper into the silicon charge. During growth the top surface of the hearth is quickly coated with silicon. However, due to the design of the hearth there are areas where the silicon coating is slight, but the probability of stray electron impact high. The probability of copper diffusing from the water cooled hearth into the silicon can be estimated from its diffusion coefficient in silicon. The copper in intimate contact with the silicon charge will be at $\leq$ 80°C. Assuming that the copper atoms get onto the surface of the silicon charge, then at 80°C the copper atoms will diffuse through silicon at a rate of ~0.8 $\mu m\ sec^{-1}$, (Keenan & Larrabee 1983). Therefore it is probable that the initial outgassing of the electron beam hearth results in copper contamination of the silicon charge and hence the epilayer.

6.2.2 *Contamination from the stainless steel components.*

The elements that occur in the grade 316 stainless steel used to construct the MBE system are,

Fe (68% - 73%) : Cr (16% - 18%) : Ni (10% - 14%)

The levels of iron and chromium detected in these samples were approximately in the above ratios, though no nickel was detected above its detection limit in AA of $\sim 5x10^{14}$ atoms cm^{-3}. As the surface of stainless steel is mainly chromium oxide, it is unlikely that this contamination was caused by straight forward evaporation.

6.2.3 *Tantalum contamination.*

The levels of tantalum in the epilayers are in the range $1x10^{15}$ to $5x10^{15}$ atoms cm^{-3}. Note that these levels are close to the detection limit for NAA ($\sim 4x10^{14}$ atoms cm^{-3}) and SIMS ($1x10^{14}$ to

1×10^{15} atoms cm^{-3}). Due to its low vapour pressure, (it has to be heated to ~2000°C before its vapour pressure becomes sufficient to contaminate the epilayer by $\sim 1 \times 10^{15}$ atoms cm^{-3}), this contamination can not be due to straight forward evaporation. The vapour pressure of tantalum in the UHV system can be increased by:

(i) Incident high energy electrons. The design of the electron beam evaporator uses tantalum in the vicinity of the electron filament, where interaction with stray electrons is possible causing localised heating. Indeed tantalum deposits were detected on ceramic insulators on the electron beam hearth module using EDAX.

(ii) Chemical reactions giving rise to volatile reaction products. Possible reactants are oxygen, hydrogen, (Gulbransen & Andrew 1950), or boron. This later reaction could be occurring between the tantalum heater strips of the substrate heater and leaching of boron from the pyrolytic boron nitride (pBN) insulator tubes used to isolate them. At the maximum operating temperature of the tantalum strips ~1100°C, boron will leach from pBN, (Ostram & Allen 1986).

6.2.4 *Trace metallic contamination.*

Table 6.3 shows the contamination levels due to the other metals detected, manganese, tungsten, gold, and sodium. Only gold and sodium were consistently present in all the epilayers. Possible sources of these metals include the filaments in the ion gauges and trace contaminants in the chemicals used to clean the substrate.

6.2.5 *Concentration of deep levels.*

The electrical activity of the metallic impurities was assessed by measuring the deep level concentration of the epilayers using DLTS, (see table 6.4). The concentration varies from 6×10^{11} to 2×10^{14} traps cm^{-3}.

Sample	Mn (cm^{-3})		W (cm^{-3})		Au (cm^{-3})	Na (cm^{-3})
	SIMS	NAA	SIMS	NAA	NAA	NAA
74/11	$<1x10^{14}$	$1x10^{15}$	$<1x10^{14}$	$7x10^{13}$	$1x10^{13}$	$1x10^{16}$
	$3x10^{14}$					
77/8	$<1x10^{14}$	$<1x10^{16}$	$<1x10^{14}$	$<8x10^{14}$	$4x10^{13}$	$2x10^{16}$
79/2	$<1x10^{15}$		$1x10^{15}$			
79/4	$7x10^{15}$	$<1x10^{15}$		$<6x10^{20}$	$4x10^{13}$	$6x10^{15}$
79/8, Substrate heated in the growth chamber		$<1x10^{15}$		$<3x10^{13}$	$3x10^{13}$	$4x10^{15}$
Substrate		$<5x10^{15}$	$<1x10^{14}$	$<1x10^{11}$	$<1x10^{10}$	$7x10^{13}$

Table 6.3. Trace metallic impurities in SI-MBE material. Note that both Mo and Co were below the detection limit of SIMS, < $1x10^{16}$atoms cm^{-3}

These levels are ~2 decades below the estimate for the total metallic impurity content. Comparing this value with the total metal impurity content, indicates that a maximum of 0.002% of the metal impurities are on electrically active sites in the epilayer. The rest are presumably on inactive sites such as interstitial sites or in precipitates at crystallographic defects. This is consistent with Sidebottom et al (1988), who concluded; (a) the deep level concentration increases to a maximum at the substrate-epilayer interface and (b) the deep level concentration decreases with increasing temperature. Both these conclusions also indicate the presence of an internal gettering mechanism centred at the substrate-epilayer interface, (as suggested by the SIMS profile of the copper contamination shown in figure 6.2).

As pointed out in appendix A, identification of deep levels is a complicated process and positive identifications are rare. The deep levels observed in these epilayers have been variously associated with, tantalum, nickel, gold, manganese, nitrogen and point defect complexes. An interesting point is that despite the high level of

copper contamination, no deep levels have been associated with copper, which forms an electron trap at 199 meV, (Akhmedova et al 1976) and hole traps at 240, 370 & 520 meV, (Keenan & Larrabee 1983). The possibility of point defects in the silicon lattice causing deep levels indicates that despite the importance of removing metallic impurities, other imperfections in the silicon lattice can be just as detrimental and need to be removed before a significant reduction in the deep level concentration can be achieved.

Epilayer	Growth temperature (^{o}C)	Total deep level concentration (cm^{-3})
77/8	570	7.4×10^{13}
77/9	626	8.9×10^{12}
78/2	690	4.0×10^{12}
79/2	790	6×10^{11}
79/3	512	1.2×10^{14}
79/4	489	2.1×10^{14}
89/3	760	1×10^{12}

Table 6.4. The total deep level concentration measured (using DLTS), in the same sample set used for the chemical analysis. The large variation has been shown to be dependant on the growth temperature by Sidebottom et al (1988), see figure 6.7.

6.3 Discussion.

6.3.1 *Comparison of metallic impurity levels found in Si-MBE material.*

Two separate studies carried out by Marsh (1988) and Delage et al (1988) both agree that the tantalum strip heater is a source of tantalum contamination. In both cases the tantalum heater used had no quartz shield separating the tantalum strips and the substrate,

unlike the heaters used in this study. Marsh observed an initial tantalum contamination level of $3x10^{16}$ atoms cm^{-3}, (almost a decade higher than the maximum level observed in this study). Using NAA, he observed a reduction to $8x10^{14}$ atoms cm^{-3} by shielding the substrate from the tantalum heater strips. The principle conclusion of Delage et al was that the tantalum contamination occurred principally at the back of the substrate. The contamination levels at the front of the substrate were found to be below the detection limit of NAA. Van Gorkum et al (1990), (using a V80 MBE system), also found the contamination levels of several metals were greater at the back of the substrate than at the front, in the epilayer. However, as they had a quartz shield in front of the tantalum strips, they concluded that the heater was not a source of tantalum! They also note that, after a year of operation of their MBE system, the tantalum levels in the epilayer dropped from $3.6x10^{16}$ atoms cm^{-3} to $2.2x10^{15}$ atoms cm^{-3}. (Note that their current contamination level is similar to that found in this study). This decrease with time was also observed with the other contaminants, eg. the chromium content in the back of the substrate decreased from $1.6x10^{15}$ atoms cm^{-2} to $4.4x10^{12}$ atoms cm^{-2}. No explanation for these observations was given.

6.3.2 *Comparison of minority carrier lifetimes in Si MBE material.*

Minority carrier lifetime is generally used as a "yardstick" to assess the effect of metallic impurities on the electrical properties of MBE epilayers. Smith et al (1990), measured minority carrier lifetimes on processed silicon epilayers grown in the MBE system used in this study, (see table 6.5). Four different methods were used, each (using different assumptions), gave differing results.

Author	Material	Method	Minority Carrier Lifetime		Comments
			gettered samples	ungettered samples	
Smith et al 1990	MBE	Forward characteristics of p-n diode		0.7 μs	Measuring recombination lifetime on processed p-n diodes grown by MBE.
		(2)		> 10 μs	
		Reverse current recovery		1.1 μs	These two techniques are influenced by the substrate.
		(1)		0.4 μs	
Delage et al 1988	MBE	-		>36 μs	no deep levels detected by DLTS
Bean 1984	MBE	-		100 μs	
Marsh 1988	MBE	(1)		2 ns	
Ota 1983	MBE	(2)		70 μs	diode formed by diffusion into an epilayer
		(1)		15 μs	oxidation via heating in steam at >1000°C
Salih et al 1986	CVD	(1)	1000 μs	10 μs	
Rath et al 1985a	CZ substrate	deduced from the diffusion length	19-28 μs 0-8 μs 3-5 μs 4-6μs		measurments over different batches of substrates
Borland 1985	Bulk	(1)	0.8-10 ms 30-60 μs 15-60 μs 1.5-3000 μs		lifetime dependent on the thermal processing used to getter the impurities
Varker & Ravi 1974	Measured at a defect in a bulk sample.	(2)		4-400 ps	measured in the space charge region around a decorated stacking fault.

(1) Zerbst method, (measures the generation lifetime of minority carriers)
(2) Reverse characteristics of a p-n diode, (measures the generation lifetime of minority carriers).

Table 6.3. Comparison of minority carrier lifetimes measured in bulk and CVD grown silicon with those measured in Si-MBE material.

The average recombination lifetime of minority carriers measured at room temperature of ~0.1 μs, was considered to be indicative of good quality material.

The two main methods used by other groups are analysis of either the reverse characteristics of a p-n diode or the capacitance time transient characteristic of a MOS device ie. Zerbst method, (both measure the generation lifetime of the minority carriers). Using these methods a variety of groups have measured a variety of minority carrier lifetimes in Si-MBE epilayers. These are also shown in table 6.5, together with measurements of CVD epilayers and bulk silicon samples. The large discrepancy between the minority carrier lifetimes measured by different authors, could be entirely due to the MBE epilayers containing different concentrations and types of metallic impurities. However, as noted earlier the measurement technique can also influence the final result.

Despite these problems the minority carrier lifetimes measured in MBE epilayers are of the same order of magnitude as those measured for ungettered, bulk samples, thus indicating that despite the perceived drawbacks of MBE ie. inherently high metallic impurity levels, good quality devices can be produced. Indeed it has been claimed that the limiting factors for long minority carrier lifetimes are not the deep levels associated with metallic impurities at all. Huber et al (1986) studying bulk silicon, suggests that the limiting factor for minority carrier lifetimes are intrinsic point defects and the strain induced by high doping levels.

6.4 Reduction of unintentional impurities.

The above results suggest that the sources of impurities are associated with:

1) Stainless steel components.

2) The tantalum substrate heater.

3) The electron beam evaporator.

Two courses of action were taken to reduce these sources.

(i) *Use of silicon components*. All components that interacted with either the substrate or the electron beam evaporator were either shielded with silicon wafers or machined out of silicon. Therefore the transfer trolly, the water cooled collimator and the top surface of the electron beam hearth were lined with silicon wafers. Unfortunately the areas in the electron beam hearth proposed as the most likely source of copper, could not be shielded during the course of this study. Therefore, as expected the level of copper in the epilayers remained high, at $\sim 1 \times 10^{17}$ atoms cm^{-3}. During transfer in the MBE system, the substrate was carried in a 4" silicon ring and the heater stage and the substrate shutter were manufactured out of silicon to avoid the close proximity of hot metal.

(ii) *Replacement of the tantalum strip substrate heater*. This should allow the extent of contamination arising from the tantalum heater to be assessed. To this end a new substrate heater incorporating a non-metallic heating element was designed and built. The feasibility of using silicon itself as the heating element was investigated. However, it is a brittle material and at the temperatures envisaged for the heating element (>1200°C), it has a significant sublimation rate (Tolomasov et al 1971), which reduces its lifetime. The material chosen was graphite, (see chapter 2).

6.4.1 *Results and Discussion.*

Introduction of the graphite substrate heater was a technical success, (see chapter 2), allowing significantly higher substrate temperatures to be reached than those possible with the tantalum strip

substrate heater. However, due to the high detection limits of the analytical techniques available, its effect on the metallic contamination levels was ambiguous. The tantalum contamination in epilayers heated by the graphite heater were found to be below the detection limit in SIMS, $<1x10^{14}$ atoms cm^{-3}. But, this low level remained in epilayers grown when the tantalum heater was replaced in the MBE system.

Analysis of annealed epilayers. To enhance the gettering mechanism at the substrate-epilayer interface (see figure 6.2), four epilayers grown while heated with the graphite heater, were subsequently annealed at 1000°C for 10 minutes in a nitrogen atmosphere. SIMS analysis for four elements, tantalum, chromium, molybdenum and copper, detected only copper, (see figure 6.6). The other three elements being below the detection limit of $\sim 1x10^{14}$ atoms cm^{-3}.

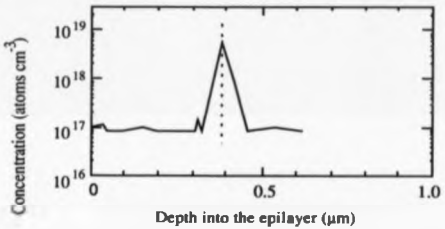

Figure 6.6. SIMS profile of an annealed epilayer, 86/5, (1000°C for 10 mins). The graphite heater was used to heat the epilayer during growth. The only element detected was copper, the ^{65}Cu isotope is illustrated here. The other elements searched for were, Ta, Cr, Mo. All were below the detection limit of $1x10^{14}$ cm^{-3}.
The peak in the concentration occurs at the substrate-epilayer interface, (ie. at the dotted line).

The failure to detect tantalum in epilayers heated by either the graphite or tantalum heaters indicates the difficulty in understanding

and controlling metal contamination in MBE material. It highlights the necessity for a greater understanding of all the possible sources of impurities and the mechanisms by which they reach the epilayer.

6.4.2 *Influence of the graphite heater on the deep level concentration*

Sidebottom et al (1988) showed that the deep level concentration in Si-MBE material was a strong function of the growth temperature. Thus this dependence has to be taken into account when assessing the influence of the graphite heater.

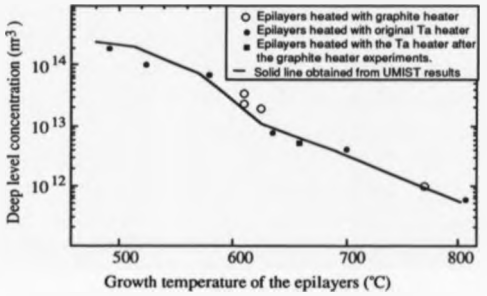

Figure 6.7. Graph showing the dependance of deep levels on the growth temperature. Note that no change in the total deep level concentration was observed when the graphite heater was used.

Figure 6.7 plots the deep level concentration observed in epilayers grown with both heaters, as a function of the growth temperature. There is no discernible difference between the two heaters, indicating that; a) in the configuration of the substrate heater used, the tantalum strips are effectively shielded from the substrate, or b) the tantalum contamination is electrically inactive, eg. in the form of precipitates.

6.5 Conclusion and Further work.

This chapter presented the results of a preliminary investigation into the metallic contamination levels in Si-MBE material. The principle and consistent contaminant was found to be copper, at concentration levels sufficient to have a detrimental effect on the properties of devices, ($5x10^{14}$ to $2x10^{17}$ atoms cm^{-3}). The evidence indicates a source intrinsic to the MBE process, probably due to copper diffusing into the hot silicon charge and/or stray electron bombardment of the copper hearth. It is hoped that the earthed collimator above the electron beam hearth and the future introduction of more comprehensive deflection electrodes (see chapter 3), will reduce the probability of charged species, caused by the electron beam evaporator, from reaching the growing epilayer.

Other contaminants found were iron, chromium and tantalum. The presence of tantalum at concentrations in the range $1x10^{15}$ to $5x10^{15}$ atoms cm^{-3} is surprising due to its very low vapour pressure. It is suggested that chemical reactions on the surface of tantalum, giving rise to volatile reaction products, could enhance the vapour pressure sufficiently to cause this level of contamination, a prime reaction site being the tantalum strips in the substrate heater. A replacement graphite meander heater was technically successful, in that the substrate temperature sufficient to fully desorb SiO_2 could now be achieved. However, the tantalum contamination levels during and after the introduction of this heater were below the detection limit of the analytical techniques used and no firm conclusion could be drawn. Further work, using thicker epilayers >10 μm to improve the detection limits, is required to positively identify the source of

tantalum contamination and more importantly the mechanism by which it reaches the substrate.

Surprisingly the deep level concentration remained unchanged irrespective of which substrate heater was used. In fact this study has shown that a maximum of ~0.002% of the metallic contaminates are electrically active, the exact level being dependant on the growth temperature. This result correlates with the long minority carrier lifetimes found in Si-MBE material by a variety of workers. Association of several of the deep traps with imperfections in the crystalline lattice as well as metallic complexes, indicates that unintentional impurities are not the only limiting factor preventing Si-MBE becoming a device production technology. Experiments using techniques that study the electronic environment of imperfections in the lattice, ie Electron Spin Resonance and the us of tuneable lasers, need to be undertaken to positively identify the composition of the deep levels present in Si-MBE material.

With respect to the questions posed in the introduction:
(a) Due to limitations in the available analytical techniques, the minimum contamination levels achievable in MBE material could not be identified. However, as the long minority carrier lifetimes show, the current Si-MBE material is of high quality. Further refinements in this quality could be achieved by changes in the technology. For example, the use of a gas source for the silicon flux, (Hirayama et al 1987).
(b) With regards to possible gettering techniques, this study has shown that a gettering process for copper already exists during growth. Quenched anneal experiments and examination of the substrate-epilayer interface by high resolution TEM would enable greater understanding of this process and whether or not it is feasible to adapt it for other contaminants without compromising dopant profiles.

Chapter 7

Conclusions and Future Work

Si-MBE is now "mature" growth technique, specialising in the growth of high resolution, abrupt profiles. Despite this there are still several areas in which improvement is required for it to take the next step and become integrated into device fabrication lines. This study has demonstrated significant advances in three of these areas, particulate contamination intrinsic to solid source MBE, understanding of the dopant segregation process and the restricted n-type doping capabilities. Significant advances were made in these cases. However, only a preliminary investigation was possible into another area of concern, that of metallic contamination, due to limitation of analytical techniques and external restrictions mentioned in the chapter 1.

Another area that has been neglected in Si-MBE is the presence of high levels of carbon. Carbon undergo several complex reactions in the bulk silicon, forming refractory metal carbides and point defects with impurities. These imperfections can significantly reduce the electrical activity and reliability of devices. The concentration of oxygen and carbon in Si-MBE material has been investigated in this study, however, its influence on electrical measurement has not. This aspect requires further work.

With regard to particulate contamination of the SI-MBE material, two distinct particulate-related defects were identified. One, due to microscopic particulates, causes crystallographic defects. The other, due to larger macroscopic particulates, cause disruptions to the epilayer growth. Assessment of the MBE growth process highlighted the energisation of the electron beam evaporator as being the prime cause

of particulate contamination. The particulates originate from the "flaky" deposits of silicon in the growth chamber, which gives rise to an "atmosphere" of silicon particulates in the growth environment. They reach the epilayer surface via the electrostatic fields originated at the electron beam evaporator. Particulate-related defect densities of $\sim 1 \times 10^4$ cm^{-2} were reduced by two decades to $\sim 1 \times 10^2$ cm^{-2} by forming stable deposits of the excess silicon flux in a water cooled collimator, lined with silicon. The collimator also had the added advantage of confining the charged species originating from the electron beam evaporator. An electrode was used to influence the trajectories of charged particulates reaching the substrate and although no net reduction in the defect densities was achieved, a design of a deflection electrode is suggested which should produce significant reductions.

With respect to the dopant incorporation process, an empirical model is proposed in chapter 4, which predicts the occurrence of surface accumulation of dopants in silicon and also in III-V semiconductors. In the latter case it accurately predicts the site occupancy of dopants. It was successfully tested against the available experimental data and used to predict the occurrence or absence of surface accumulation and the dominant site occupation (in the case of compounds) for all the common dopants in silicon, germanium and III-V MBE, to provide a basis for further tests of this hypothesis. One of the predictions being that phosphorus doping in Si-MBE will not exhibit any surface accumulation. The model is based on the relative atomic size of a dopant and its lattice site and does not rely on any specific mechanism for dopant incorporation. However, it is proposed that the nature of the local equilibrium at the growing surface and the nature of the strain (compressive or tensile), caused by the incorporation of a dopant atom

are key factors that need to be included in a quantitative description of the dopant incorporation process in MBE.

The feasibility of achieving phosphorus doping by co-evaporation in Si-MBE has been demonstrated for the first time, in this study. The tin phosphide dopant source used provided a fairly stable dopant flux allowing doping levels of at least 1×10^{19} cm^{-3} to be achieved. Phosphorous was found to be a relatively well behaved dopant in MBE, and abrupt dopant profiles would seem to be possible. Electron mobility levels comparable to values observed in bulk silicon were achieved despite the less then unity activation coefficients observed. Fears of unacceptable memory doping affects arising from the high vapour pressure of phosphorus at room temperature were shown to be unfounded, as deposits of silicon over the phosphorus deposits significantly reduced background doping levels. Preliminary evidence indicates that phosphorus does not accumulate on the surface of silicon during MBE growth, thereby providing support for the above model. Further studies are needed to investigate the processes phosphorus undergoes on the growing silicon surface, as it has an unusually low substrate temperature dependence.

Chapter 6 presented the results of investigations into the metallic contamination in Si-MBE material. A persistent impurity was found to be copper, at concentrations in the range 5×10^{14} to 2×10^{17} atoms cm^{-3}. Iron ($\sim 3 \times 10^{15}$ atoms cm^{-3}), chromium ($\sim 7 \times 10^{14}$ atoms cm^{-3}), and tantalum ($\sim 3 \times 10^{15}$ atoms cm^{-3}) were also found. Experiments aimed at reducing the contaminant levels were either not successful or produced conflicting results. Despite the relatively high levels of metallic contamination, minority carrier lifetimes of ≥ 1 µs were observed in this material. An encouraging sign, was that the substrate-epilayer interface appears to act as a getter, at least for copper, during

MBE growth. Optimization of localised gettering processes could produce further improvements in the electrical quality of Si-MBE material.

Possible future work has already been discussed in detail in each of the chapters, as each problem requires specific solutions. Problems associated with particulate contamination can be alleviated by technological improvements. Limitations due to lack of dopant controllability and metallic contamination are more fundamental, but improved understanding of the incorporation process may lead to improvements.

In summary, this study has demonstrated that Si-MBE can become a viable technology for the production of novel devices requiring nanometre control over the dopant profile. However, due to its complexity and its cost, it is likely to become the production technique for high cost, specialised devices, rather than become integrated into standard device production lines.

Appendix A

Analysis techniques.

A variety of analysis techniques were used during the course of this study. In the main these were standard techniques, however, in a few instances the peculiarities of the technique as applied to silicon MBE epilayers, had an influence on the conclusion drawn from the results obtained. Therefore these techniques will be briefly reviewed and the peculiarities discussed.

A.1 Direct measurement techniques.

A.1.1 *Neutron Activation Analysis.*

There are many descriptions of neutron activation analysis (NAA), as used in analysis of bulk and epilayer silicon (Domenici et al 1986, Rath et al 1985). In essence the technique involves irradiating the sample with thermal neutrons and detecting the gamma ray (γ) radiation produced

$$ {}^{A}_{z}E + n_{(thermal)} \rightarrow {}^{A+1}_{z}E^{*} + \gamma $$

E = the element of interest, A is its atomic weight and z is its atomic number. Each element gives of a characteristic set of gamma rays, the relative intensities and their absolute energies provide a "fingerprint" of the element.

The standard sample preparation technique is to irradiate the solid sample, then to etch off the epilayer and analyse the solution. The etching is carried out in two stages. The first few hundred angstroms are removed to give an indication of the surface contamination, then the "majority" of the epilayer is removed and

analysed. Measurement of the solid sample is possible, however it is not quantitative, (Delage et al 1988).

Calibration is generally carried out with standard solutions and computer predictions of the activity expected for each element.

Factors affecting the Detection Limit.

(i) The irradiation time and the flux density of the applied neutrons. Obviously the longer the irradiation time the greater the count rate, however this has to be balanced against the extended turn-around time. The samples in this study were irradiated for 14 hrs at a nominal flux of 1.3×10^{13} neutrons cm^{-2} sec^{-1}.

(ii) The purity and the efficiency of the etchant. In general the etchant contains "hold-back" carriers such as non-radiative copper and gold to minimise back plating of the etched material.

(iii) Volume of sample. In the case of epilayers this is extremely limited and is the main factor which affects the detection limit with respect to bulk silicon.

Detection limits in bulk silicon are $\leq 1 \times 10^{11}$ atoms cm^{-3} (Rath et al 1985), however for epilayers this increases significantly, eg. to $\sim 1 \times 10^{13}$ atoms cm^{-3} for gold and $\sim 1 \times 10^{19}$ atoms cm^{-3} for nickel. The variability in the detection limits, (eg. for molybdenum it varied from 7×10^{15} to 3.5×10^{16} atoms cm^{-3}), is due to variation in the signal to noise ratio, (Domenici et al 1986).

Due to lack of facilities in this country the NAA analysis was carried out at Texas Instruments, Houston, USA. Therefore a long turn-around time was unavoidable.

A.1.2 *Atomic Adsorption Spectroscopy.*

As with NAA, Atomic Adsorption spectroscopy (AA) is a routine tool for analysis of bulk silicon (Stewart & Newton 1983, Phelan 1986, Rath et al 1985). The technique is very similar to NAA, it

involves etching of the epilayer and subsequent analysis of its atomic absorption spectrum in a furnace.

The factors which influence the detection limit are similar to those listed for NAA ie. purity of the etching chemicals, containers and contamination from the furnace and volume of sample. In bulk silicon the detection limits are similar to NAA, eg. $\sim 1 \times 10^{9}$ atoms cm^{-3} for iron (Stewart & Newton 1983), however this rises to between 1×10^{14} and 1×10^{15} atoms cm^{-3} (Phelan 1986) for epilayers.

The AA analysis was carried out at the Hirst Research Centre, Wembley, Middx.

A.1.3 *Secondary Ion Mass Spectrometry.*

Secondary Ion Mass Spectrometry (SIMS), may be used to provide a depth profile of the impurities, (Wittmaack 1982, Bennighovan et al 1987). The sample is bombarded by a beam of primary ions typically (1 to 20 KeV), resulting in material being sputtered from the top layers of the sample surface. Some of the material will be secondary ions, which may be extracted towards a mass spectrometer. If the primary beam is "rastered" over the sample surface, the sputter erosion can be controlled and hence the intensity of one or more species of secondary ions may be determined as a function of erosion time. Subsequent measurement of the crater depth, using a surface profilometer, allows a depth scale to be calculated. Reference to standard samples allows quantification of the profile.

Factors affecting the depth resolution and detection limit.

(i) "Mixing" of incident ions with the sample surface can lead to broadening of the depth profile. Lowering of the energy of the primary ions will reduce this effect, but will also increase the time required to complete the profile. Accounting for other possible

factors, such as a chemical reaction between the primary ions and the sample, the depth resolution is generally 3 → 10 nm, (Mcphail 1989).
(ii) The secondary ion yield is dependant on the primary ion species and the target elements. The higher the yield the higher the detection limit. The use of electronegative elements such as oxygen and electropositive element such as caesium, for the primary ion beam is known empirically to enhance the yield by up to 1000x over that obtained with a noble gas primary beam.
(iii) The relationship of the secondary ion yield to the concentration of the element in the sample can vary with the experimental conditions, therefore an empirical technique to analysis the results has evolved. This involves determining the ion yield of a sample with a known concentration for *each* element of interest before the unknown sample is analysed (keeping the experimental conditions constant). This fact limits SIMS to be being a spectrometry technique.
(iv) The detection limits varies with the element, ranging from $\sim 1 \times 10^{17}$ atoms cm^{-3} for phosphorus to $\sim 1 \times 10^{14}$ atoms cm^{-3} for most of the transition elements. The detection limits can also vary with the SIMS instrument. Mass interference from species with similar masses can reduce the sensitivity significantly, especially in a quadrupole instrument, (Mcphail 1989). For example the mass of SiH_2 is very close to that of phosphorus. Providing the standards are done at the time of the analysis the accuracies obtained for routine SIMS analysis is ± 10% at a concentration of 1×10^{17} atoms cm^{-3}, though this can be as high as ± 50% in some cases.

Two SIMS instruments were used to analysis the samples in this study. The EVA 2000 quadrupole instrument in the ASR group at Warwick University and the Cameca 3F magnetic sector instrument at Loughborough Consultants.

A.1.4 *Comparison of direct measurement techniques.*

NAA and AA are very similar techniques and provide similar results, however, these results occasionally appear contradictory to those supplied by SIMS. NAA and AA rely on a chemical etching process to isolate the epilayer. It is difficult to "lift off" all the epilayer without removing part of the substrate. Therefore in general the NAA and AA results are measurements of the "bulk" of the epilayer ie. not including the interface region. Metallic impurities will getter at strain sites such as the interface, leading to very high localised concentrations, (see figures 6.2 and 6.6), which are detectable by SIMS. If this interface contamination is removed during analysis then the total impurity content found by NAA and AA will be significantly higher. On the other hand, SIMS analysis a region ~20 μm^2 and therefore is sensitive to variations in the impurity concentration across the epilayer, which NAA and AA will average out. The defect distribution (ie. possible gettering sites), could also cause fluctuations in the SIMS results from sample to sample.

A.2 Electrical Characterisation techniques.

A.2.1 *Deep Level Transient Spectroscopy.*

DLTS is a "high frequency capacitance transient thermal scanning technique" developed by Lang (1974), capable of detecting energy levels down to ~1×10^{12} cm^{-3} . It is used widely in the semiconductor industry as a monitor of the quality of device fabrication processes.

A transient is excited by repeatedly switching a diode, fabricated on the sample, from a forward, or zero bias to a reverse bias

at frequencies in the MHz range. The forward bias pulse fills the deep levels with electrons (or holes) due to the collapse of the depletion layer. On switching the bias the electrons will be thermally emitted out of the levels. Changing the occupancy of the deep states in the depletion region changes the capacitance. The transient response of the capacitance is related to the deep level.

The spectral output of DLTS is obtained by sampling the transient at two points in time, t_1 and t_2. As the rate of emission of the electrons from the deep level is temperature dependant, increasing the temperatures will increase the emission rate until a point is reached when it is so fast that the capacitance appears constant between the sampling times t_1 and t_2. Decreasing the temperature, the emission rate will decrease allowing a difference to be detected between the sampling times. This difference will rise to a maximum at a specific temperature dependant on the "rate window" $(t_1 - t_2)$. Decreasing the temperature further, will decrease the emission rate to a level where the change in capacitance is too slow to register during the chosen rate window.

The "peak" temperature is indicative of the environment of the deep level and serves to differentiate the deep levels, allowing a spectrum of the deep levels to be obtained. The trap concentration is related to the height of the capacitance peak and the sign of the peak gives the type of trap, hole or electron.

Identification of the deep levels.

In principle, indentification of the species causing the deep level is straight forward. The capture cross section and the Arrenhius energy of a deep level, together with its characteristic temperature defines the deep level.

To relate a deep level to a particular species requires comparison with library data. This, however, can give ambiguous results due to the myriad of factors which can influence the characteristics of the deep level. These are related to the fundamental nature of a deep level as well as experimental problems and the nature of the sample, (Jaros 1982, Bachelet 1986). For example:

(i) Due to the nature of deep levels, local rearrangements or lattice relaxations, associated with crystallographic and point defect, can influence the deep level. Therefore in the production of standards, care has to be taken to avoid contamination which might change the character of the deep levels associated with the impurity of interest.

(ii) The thermal history of the sample will also influence the deep level observed. For example enhanced precipitation/gettering of an impurity by thermal cycling will give poor reproducibility as will the presence of metastable/surface states, (Schultz 1974). Therefore assignment of deep levels requires correlation of results from other techniques eg. SIMS (Xie et al 1986).

(iii) Experimental difficulties such as, inaccurate temperature measurement of the sample and fluctuations in the background capacitance of the DLTS instrument will influence the accuracy of concentration measurement of the deep traps (Leong & Robbins 1989).

(iv) Possible contamination introduced during the preparation of the schottky diode would also influence the deep level.

In summary, it can be said that DLTS is essentially a survey technique, it is not precise and is open to misinterpretation, but nevertheless, it can be an extremely valuable monitor of the influence of a variety of factors on the impurity content of samples.

Appendix B

Related Growth techniques.

A variety of methods have been used to grow silicon epilayers. The majority use a carrier molecule to transport silicon to the substrate eg. Metal Organic Chemical Vapour Deposition (MOCVD) (Kukimoto 1989). The presence of which increases the complexity of the processes occurring at the growing surface. The technique of UHV Sublimation, on the other hand, produces a flux of "pure" silicon. Due to this similarity with MBE, the results obtained with this growth technique are discussed for comparison with those obtained in this study. Here the basic principles of the technique are presented for completeness.

B.1 UHV Sublimation.

This technique has been in use since the early sixties (Nannichi 1963), however due to its inflexibility in producing doping profiles with a wide range of carrier concentrations it is not used widely today.

B.1.1 *Experimental Method.*

The source of the silicon flux is a silicon bar held in metal clips, heated up to temperatures between 1200°C and 1400°C. At these temperatures the silicon will sublime and subsequently condense on the substrate, held ≥10 mm away. The details of the technique can vary. For example Tolomasov et al (1971) used silicon substrates, 20 to 35 mm in diameter, mounted on tantalum clips, as both the substrate and the source. Each was radiatively heated using tantalum strip heaters. Due to this "closeness" of the source to the substrate,

temperatures ≤ 800°C were obtained solely by radiation from the source. Growth rates between 0.4 μm hr^{-1} and 9.5μm hr^{-1} were obtained by varying the source-substrate separation, as well as the temperature of the source. Thomas & Francombe (1969) used an array of six closely spaced silicon bars, (2.5 mm x 1.7 mm^2), as the source and rectangular substrates (13 mm x 7.5 mm x 0.4 mm). In this case both were resistively heated.

Doping is generally achieved by using doped substrates as sources, though Tolomasov et al (1971) experimented with a separate elemental source for evaporating antimony.

B.1.2 *Dopant Incorporation.*

Bennett & Parish (1975) have reported a detailed model describing the transfer of dopants from the source to the substrate. The essential conclusion being that the transfer rate is dependent on the distribution of dopant in the source, which is a function of the diffusion coefficient of the species involved. Their source-substrate geometry allowed unrestricted pumping, to the extent that they assume an infinite pumping speed in this region.

The more enclosed geometry used by other workers makes this assumption invalid and hence leads to different dopant incorporation kinetics and modifies the local equilibrium at the growing surface. For example, a dopant such as phosphorus re-evaporating from the substrate surface has a high probability of doing so in a trajectory that will take it back to the source. In this situation the dopant will undergo several "bounces" between the source and substrate before it either escapes or gets incorporated into the epilayer, resulting in an increasing partial pressure of phosphorus over the substrate, eventually reaching a steady state situation. The feasibility of this mechanism is indirectly acknowledged by Bennett & Parish (1975),

who site low pumping speeds and enclosed geometry in the growth region as a possible reason for the differences between their results and those reported by Thomas & Francombe (1969) for dopant transfer.

Other differences between MBE and UHV Sublimation that could provide a clue to the dopant incorporation process in MBE are: (i) the lack of any charged species in UHV Sublimation due to the electron beam evaporator in MBE and (ii) the dopant fluxes in UHV Sublimation are generally atomic, as opposed to the molecular species prevalent from the separate sources used in MBE, eg. Sb_4 and P_2.

Bibliography.

Abraham. F.F & Brundle. C.R, (1981), Surface segregation in binary solid solutions: A theoretical and experimental perspective, *J. Vac. Sci. Technol.* *18(2)*, *p506-519*.

Akhemedova. M.M, Berman. L.S, Kostina. L.S, Lebedev. A.A, (1976), Investigation of the parameters of copper levels in silicon by capacitance methods, *Sov. Phys. Semicond.*, *10(12)*, *p1400-1401*.

Allen. F & Kasper. E, (1988), Models of Silicon Growth and Dopant Incorporation, *Chapter 4 in Silicon Molecular Beam Epitaxy Vol 1, Kasper. E, Bean. J.C (ed), CRC Press Inc, Florida.*

Alexandre. F, Rasin. C, Abdalla. M.I, Brenac. A, Masson. J.M, (1980), Influence of growth conditions on tin incorporation in GaAs grown by molecular beam epitaxy, *J. Appl. Phys.* *51(8)*, *p4296-4304*.

Atkins. P.W, (1982), Chapter 2 in Physical Chemistry, *2nd Edition, Oxford University Press, Oxford.*

Bachelet G.B, (1986), Electronic States and Structural Properties of Deep Centers in Semiconductors, *Chap. 7 in Crystalline Semiconductors Materials and Devices, eds Butcher P.N, March N.H and Tosi M.P, Plenum Press, New York.*

Bajor. G & Greene. J.E, (1983), Model calculations for accelerated As ion doping of Si during molecular beam epitaxy, *J. Appl. Phys.* *54(3)*, *p1579-1582*.

Barnett. S.A & Greene. J.E, (1985), Si Molecular Beam Epitaxy: A Model for Temperature Dependant Incorporation Probabilities and Depth Distributions of Dopants Exhibiting Strong Surface, *Surf. Sci.* *151*, *p67-90*.

Beall. R.B, Clegg. J.B, Harris. J.J, (1988), Migration of Si in delta-doped GaAs, *Semicond. Sci. Technol.* *3*, *p612-615*.

Bean. J.C, (1984), Silicon MBE: From Strained-layer Epitaxy to Device Application, *J. Crys. Growth*, *70*, *p444-451*.

Becker, G.E & Bean, J.C, (1977), Acceptor dopants in silicon molecular-beam epitaxy, *J. Appl. Phys. 48(8), p3395-3399.*

Bedrossian, P, Meade, R.D, Mortensen, K, Chen, D.M, Golovchenko, J.A, Vanderbilt, D, (1989), Surface Doping and Stabilization with Boron, *Phys. Rev. Lett., 63(12), p1257-1260.*

Bellavance, D & Liu J, (1987), Summary Abstract: Particulates in silicon molecular beam epitaxy, *J. Vac. Sci. Technol, B5(3), p.751.*

Bennett, R.J & Parish, C, (1975), Determination of Diffusion, Partition and Sticking Coefficients for Boron, Phosphorus and Antimony in Silicon, *Solid State Elec 18, p833-838.*

Benninghoven, A, Rudenauer, F.G, Werner, H.W, (1987), Secondary Ion Mass Spectrometry, *John Wiley, New York.*

Borland, J.O, (1985), Influence of Micro-Defect Morphology on Intrinsic Gettering Effectiveness and Durability in CMOS Epitaxial Processing, *p269-274 in Impurity Diffusion and Gettering in Silicon, Vol 36 of Mat. Res. Soc. Sym. Proc., Materials Research Society, Boston.*

Bronner, G. B, Plummer, J. D, (1985), Physical Modelling of Backside Gettering, *p50-54 in Impurity Diffusion and Gettering in Silicon, Vol 36 of Mat. Res. Soc. Sym. Proc., Materials Research Society, Boston.*

Burton, W.K, Cabrera, N, Frank, F.C, (1951), The Growth of Crystals and the Equilibrium Structure of their Surfaces, *Philos. Trans. R. Soc. London Ser A 243, p299-358.*

Chai, Y.G, (1984), Tin Phosphide as a Phosphorus Beam Source for Molecular Beam Epitaxy, *Appl. Phys. Lett. 45(9), p985-987.*

Chai, Y.G, Chow, R, Wood, C.E.C, (1981), The effect of growth conditions on Si incorporation in molecular beam epitaxial GaAs, *Appl. Phys. Lett. 39(10), p800-803.*

Chang, C, Ludeke, R, Chang, L.L, Esaki, L, (1977), Molecular-beam epitaxy (MBE) of $In_{1-x}Ga_xAs$ and $GaSb_{1-y}As_y$, *Appl. Phys. Lett. 31(11), p759-761.*

Cho. A.Y & Hayashi. I, (1971), P-N Junction Formation during Molecular-Beam Epitaxy of Ge-Doped GaAs, *J. Appl. Phys.* 42(11). p4422-4425.

Chow. R & Chai. Y.G, (1983), A PH_3 cracking furnace for molecular beam epitaxy, *J. Vac Sci. Technol* A1(1). p49-54.

Collie. C.H, (1982), Kinetic Theory and Entropy, *Longman Group Ltd, UK.*

Collins. D.M, Miller. J.N, Chai. Y.G, Chow. R, (1982), Sn and Te doping of Molecular Beam epitaxial GaAs using a SnTe source, *J. Appl. Phys.* 53(4). p3010-3018.

Craven. R.A, (1985), Internal Gettering in Czochralski Silicon, *p159-174 in Impurity Diffusion and Gettering in Silicon, Vol 36 of Mat Res Soc Sym. Proc., Materials Research Society, Boston.*

Dean. J.A (ed), (1985), Table 3-10 in Lange's Handbook of Chemistry 13th ed, *McGraw-Hill Book Company.*

deCogan. D, (1988), Chapters 13.10-13.12 in Properties of Silicon, *published by INSPEC, The Institution of Electrical Engineers, London.*

deFresart. E, Rhee. S.S, Wang. K.L, (1986), Boron oxide interaction with silicon in silicon molecular beam epitaxy, *Appl Phys. Lett., 49(14). p847-849.*

deFresart. E, Wang. K.L, Rhee. S.S, (1988), Boron surface segregation in silicon molecular beam epitaxy, *Appl Phys Lett 53(1). p48-50.*

Delage. S.L, Iyer S.S, Scilla G.J, (1988), Unintentional Impurities in Silicon Layers grown by Molecular Beam Epitaxy, *Proc. 2nd Int. Conf. on Si-MBE, Honolulu, J. Electrochem. Soc. 88-8. p459-469.*

Domenici. M, Malonvemi P, Pedrotti M, (1986), Purification and Impurity Detection in Silicon for Microelectronics, *J. Crys. Growth, 75. p80-87.*

Duffalo. J.M & Monkowski J.R, (1984), Particulate Contamination and Device Performance, *Solid State Tech., March. p109-114.*

Eykholt. R & Srolovitz. D.J, (1986), Surface segregation during deposition, *J. Appl. Phys. 60(5). p1793-1796.*

Farrow, R.F.C. (1974), Growth of indium phosphide films from In and P_2 beams in ultra-high vacuum, *J. Appl. Phys. D.*, 7, *pL121-L124*

Forbes, L, Whitwer, F.D, Peng, J.D, Oxygen Precipitation in CMOS wafers, *p257-262 in Impurity Diffusion and Gettering in Silicon*, Vol 36 *of Mat. Res. Soc. Sym. Proc., Materials Research Society, Boston.*

Ghez, R & Iyer, S.S, (1988), The kinetics of fast steps on crystal surfaces and its application to the molecular beam epitaxy of silicon, *IBM J. Res. Develop., 32(6), p804-818*

Goorsky, M.S, Lagowski, J, Gatos, H.C, (1988), The Contrastive Behaviour of Fe and Cr during the intrinsic gettering of silicon, *J. Appl. Phys.*, 64(12), *p6716-6720.*

van Gorkum, A.A, Nakagawa, K, Shiraki, Y, (1989), Growth and Characterisation of atomic layer doping structures in Si, *J. Appl. Phys. 65(6) p2485-2492*

van Gorkum, A.A, Van de Walle, G.F.A, van den Heuvel, R.A, Gravesteijn, D.J, Fredrikaz, (1990), Performance and Processing Line integration of a Silicon Molecular Beam Epitaxy System, *Thin Solid Films, 184, p207-219.*

Gosele, H & Tan, T.Y, (1985), The Influence of Point Defects on Diffusion and Gettering in Silicon, *p105-116 in Impurity Diffusion and Gettering in Silicon, Vol 36 of Mat. Res. Soc. Sym. Proc., Materials Research Society, Boston.*

Graff, K, (1983), The Precipitation of Transition Metals in Silicon Crystal Wafers, *Proc. Electrochem. Soc.*, 83-4, *p121-133.*

Gravesteijn, D.J, Zalm, P.C, van de Walle, G.F.A, Vriezema, C.J, van Gorkum, A.A, Ijzendoorn, L.J, (1989), Ge Segregation During Molecular Beam Epitaxial Growth of $Si_{1-x}Ge_x$/Si Layers, *Thin Solid Films, 183, p191-196.*

Gschneider Jr. K.A. (1964). p344 in Solid State Physics: Advances in Research and Applications Vol 16. *Seitz. F, Turnbull. D (ed), Academic Press, New York.*

Gulbransen. E.A & Andrew. K.F. (1950). Reactions of Columbium and Tantalum, *J. Metals, Transactions AIME, 188. p586-599.*

Hanson. M & Anderko. (1958). Constitution of Binary Alloys, *McGraw-Hill, New York, p1088-1090.*

Harris. J.J, Ashenford. D.E, Foxon. C.T, Dobson. P.J, Joyce. B.A. (1984). Kinetic Limitations to Surface Segregation During MBE Growth of III-V Compounds: Sn in GaAs, *Appl Phys. A33. p87-92.*

Hasan. M.A, Sundgren. J.E, Hansson. G.V, Markert. L.C, Greene. J.E. (1990). Incorporation Probabilities and Depth Distributions of Aluminium Co-evaporated during Si(100) Molecular Beam Epitaxy, *Thin Solid Films, 184. p61-67.*

Hartzell. R.A, Schaake. H.F, Massey. R.G. (1985). A Model that Describes the Role of Oxygen, Carbon and Silicon Interstitials in Silicon Wafers During Device Processing, *p217-222 in Impurity Diffusion and Gettering in Silicon, Vol 36 of Mat Res. Soc Sym. Proc., Materials Research Society, Boston.*

Headrick. R.L, Robinson. I.K, Vlieg. E, Feldman. L.C. (1989). Structure Determination of the Si(111): B($\sqrt{3}$x$\sqrt{3}$)R30° Surface Subsurface Substitutional Doping, *Phys. Rev. Lett., 63(12). p1253-1256.*

Heggie. M, Jones, R, Umerski. A. (1989). Interaction of Phosphorus with Dislocation Cores in Silicon, *Poster OS47 at the I.O.P. Solid State Conf., Warwick University, England, 19th - 21st Dec*

Herman. M.A. (1982). Physical problems concerning effusion processes of semiconductors in molecular beam epitaxy, *Vacuum. 32(9). p555-565.*

Higgs. V. (1989). Private Communication.

Hirayama. H, Tatsumi T, Ogura A, Aizaka. N, (1987), Gas source silicon molecular beam epitaxy using silane, *Appl. Phys. Lett. 51(26), p2213-2215.*

Hoeven. A.J, van Loenen. E.J, Dijkkamp. D, Lenssinck. J.M, Dieleman. J, (1989), Reflection high energy electron diffraction and scanning tunnelling microscopy study of single-domain growth during silicon molecular beam epitaxy on Si(100), *Thin Solid Films, 183, p263-271.*

Hopkins. R.H & Rohatgi. A, (1986), Impurity effects in Silicon for High Efficiency Solar Cells, *J. Crys. Growth, 75, p67-79.*

Horn. M, Gotter. U, Henzler. M, (1988), Low-energy electron diffraction investigations of Si molecular-beam epitaxy onto Si(100), *J. Vac. Sci. Technol., B6(2), p727-730.*

Houghton. R.F, (1989), Phd Thesis, *Warwick University, UK.*

Houghton R.F, Patel G, Leong W.L, Whall T.E, Parker E.H.C, Kubiak R.A.A, Naylor R, (1987), A Preliminary Study of Impurities and Defects in Si-MBE Layers, *J. Crys. Growth, 81, p326-331.*

Hu. S.M, Fahey. P, Dutton. R.W, (1983), On models of phosphorus diffusion in silicon, *J. Appl. Phys. 54(12), p6912-6922.*

Huber. D, Bachmeier. R, Whlich. R, Herzer. H, (1986), Minority Carrier Diffusion Length and Doping Density in Non-degenerate Silicon, *p45-50 in Scientific Publications, Wacker-Chemitronic GmbH, Burghausen.*

Huheey. J.H, (1978), Appendix A & p820-821 in Inorganic Chemistry: Principles of structure and reactivity, *2nd ed, Harper & Row Publishers, New York.*

Ishizaka. A, Nakagawa. K, Shiraki. Y, (1982), Low-Temperature Surface Cleaning of Silicon and its Application to Silicon MBE, *Collected Papers MBE-CST-2, Tokyo, p183-186.*

Iyer. S.I, (1986), Silicon Molecular Beam Epitaxy, *Chapter 2 in Epitaxial Silicon Technology, Baliga. B.J ed, Academic Press Inc, New York.*

Iyer, S.S, Metzger, R.A, Allen, F.G, (1981), Sharp profiles with high and low doping levels in Silicon grown by Molecular Beam Epitaxy, *J Appl. Phys. 52(9), p5608-5613*.

Jaros, M, (1982), Deep Levels in Semiconductors, *The University Press (Belfast) Ltd*.

Jorke, H & Kibbel, H, (1986), Doping by secondary implantation, *J. Electrochem Soc., 133, p744*.

Joyce, B.A, Dodson, P.J, Larsen, P.K, (1988), Molecular Beam Epitaxy of III-V Compounds. Aspects of Growth Kinetics and Dynamics, *Chapter 7 in The Chemical Physics of Solid Surfaces and Heterogeneous Catalysis, King D.A, Woodruff, D.P, (ed), Elsievier Science Publishers, Amsterdam*.

Kasper, E, (1982), Private communication.

Kasper, E & Bean, J.C, (ed), (1988), Silicon Molecular Beam Epitaxy, *Vol I. CRC Press Inc, Florida*.

Katayama, Y, Shiraki, Y, Kobayahi, K.L.I, Komatsubara, K.F, Hashimoto, N, (1979), An MOS field-effect transistor fabricated on a molecular-beam epitaxial silicon layer, *Appl. Phys. Lett., 34, p740-741*.

Keenan, J.A & Karrabee, G.B, (1983), Chapter 1 in VLSI Electronics Microstructure Science, *Vol 6, Materials and Process Characterization, eds. Einsruch, N.G and Larrabee, G.B, Academic Press, New York*.

Kikuchi, H, Kitakata, M, Toyokawa, F, Mikami, M, (1989), New gettering using misfit dislocations in homoepitaxial wafers with heavily boron-doped silicon substrates, *Appl. Phys. Lett., 54(5), p463-465*.

Knall, J & Sundgren J.E, Markert, L.C, Rockett, A, Greene, J.E, (1989), Influence of the Si evaporation source on the incorporation of In during Si molecular-beam epitaxy: A comparative study of magnetically and

electrostatically-focused electron-gun evaporators, *J. Vac. Sci. Technol.* *B7(2), p204-209*

Konig U, Kasper E, Herzog H.J, (1981), Molecular Beam Epitaxy of Silicon: Effects of Heavy Sb Doping, *J. Crys. Growth, 52, p151-158*

Kubaschewski. O & Alock. C.B, (1979), Chapter 5 in Metallurgical Thermochemistry, *5th ed, Pergamon Press, Oxford.*

Kubiak R.A.A, (1985), Unpublished Data.

Kubiak. R.A.A, Leong. W.Y, Parker. E.H.C, (1985a), Enhanced sticking coefficient and improved profile control using Boron and Antimony as co-evaporated dopants in Si-MBE, *J. Vac. Sci. Technol. B3(2), p592-595.*

Kubiak. R.A.A, Leong. W.Y, Parker. E.H.C, (1985b), Potential enhanced Doping of Si Grown by Molecular Beam Epitaxy, *J. Electrochem. Soc. 132(11), p2738-2742*

Kubiak R.A.A, Leong W.Y, Houghton R, Parker E.H.C, (1985c), Factors Affecting Defect Densities in Si Grown by Molecular Beam Epitaxy, *Proc. First Int. Sym. Si-MBE, Electrochem. Soc. Proc., 85-3, p.124-132*

Kubiak. R.A.A, Patel. G, Leong. W.Y, Houghton. R, Parker. E.H.C, (1986), Co-evaporation Phosphorus Doping in Si Grown by Molecular Beam Epitaxy, *Appl. Phys A41, p233-235*

Kubiak. R.A., Newstead. S.M, Leong. W.Y, Houghton. R.F, Parker. E.H.C, Whall. T.E, (1987), The Electrical Properties of Doped Silicon, Grown by Molecular-Beam-Epitaxy (MBE), *Appl. Phys. A42, p197-200.*

Kubiak. R.A.A & Parker. E.H.C, (1988), Molecular Beam Epitaxy of Silicon and Related Materials, *Chapter 8 in The Chemical Physics of Solid Surfaces and Heterogeneous Catalysis, King. D.A, Woodruff D.P, (ed), Elsievier Science Publishers, Amsterdam*

Kukimoto. H, (1989), MOCVD - Current State and Future, *J. Crys. Growth, 95, p360-362*

Kuznetsov, V.P & Postnikov V.V, (1974), Transfer of the impurities P, As and Al from silicon sources into films obtained by vacuum sublimation, *Sov. Phys. Crystallogr.*, *19(2)*, *p211-213*

Kwo, J, Hong, M, Trevor, D.J, Fleming, R.M, White, A.E, Farrow, R.C, Korian, A.R, Short, K.T, (1988), *in situ* epitaxial growth of $Y_1Ba_2Cu_3O_{7-x}$ films by molecular beam epitaxy with an activated oxygen source, *Appl. Phys. Lett.*, *53(26)*, *p2683-2685*

Lang D.V, (1974), Deep-level transient spectroscopy: A new method to characterize traps in semiconductors, *J. Appl. Phys.*, *45*, *p3023-3032*.

Lau, F & Gosele, U, (1986), Two-Dimensional Phosphorus Diffusion for Soft Drains in Silicon MOS Transistors, *Appl. Phys. A*, *40*, *p101-107*

Lecrosnier, D, Paugam, J, Richou, F, Pelous, G, Beniere, F, (1980), Influence of phosphorus-induced point defects on a gold gettering mechanism in silicon, *J. Appl. Phys.*, *51(2)*, *p1036-1038*.

Leong, W.Y, (1985), PhD Thesis, *CNAA, UK*.

Leong, W.Y & Robbins, D.J, (1989), Anomalous DLTS Signals Due to Small Fluctuations in the Reverse Bias Voltage on a Si Diode, *J. Phys. E*, *22*, *p1051-1052*.

Leong, W.Y, Robbins, D.J, Young, I.M, Glasper, J.L, (1988), P- and N-Type doping in UHV/CVD Si epitaxy, *UK IT'88 Conf. Publication, University College, Swansea, 4th-7th July*, *p382*

Lippens, D, Constant, E, Friscourt, M.R, Rolland, P.A, Salmer, G, (1982), Simulation of Non Steady State Transport in GaAs and InP Millimetre Impatt Diodes, *IEEE Electron Device Lett.* *EDL3(7)*, *p213-215*

Luy, J.F, (1990), Silicon-Based Millimeter-Wave Integrated Circuits, *Thin Solid Films*, *184*, *p185-197*

Lyo, I.-W, Kaxiras, E, Avouris, Ph, (1989), Adsorption of Boron on Si(111): Its effect on the surface Electronic States and Reconstruction, *Phys. Rev Lett*, 63(12), p1261-1264.

Marsh, O.J, (1988), Status of the Si MBE Process, *Proc. 2nd Int. Conf. on Si-MBE, Honolulu, J. Electrochem. Soc.* 88-8, p333-346.

Maruno, S, Morishita, Y, Isu, T, Nomura, Y, Ogata, H, (1987), Molecular Beam Epitaxy of InP Using Low-Energy P+ Ion Beam, *J. Crys. Growth* 81, p338-343.

Mathiot, D & Pfister, J.C, (1982), Influence of the nonequilibrium vacancies on the diffusion of phosphorus into silicon, *J. Appl. Phys.* 53(4), p3053-3058.

Matsumoto, S, Ishihara, I, Kaneko, H, Harada, H, Abe, T, (1985), Effect of Dopant Concentration on the Growth of Oxide Precipitates in Silicon, p263-268 in *Impurity Diffusion and Gettering in Silicon*, Vol 36 of *Mat. Res. Soc. Sym. Proc., Materials Research Society, Boston.*

Matteson, S & Bowling R.A, (1988), Particulate contamination in atomic molecular-beam deposition systems, *J. Vac Sci. Technol.* A6(4), p2504-2507.

Mattey, N.L, Hopkinson, M, Houghton, R.F, McPhail, D.S, Whall, T.E, Parker, E.H.C, (1990), P- Type Delta Doping in Silicon MBE, *Thin Solid Films*, 184, p15-19.

McPhail, D.S, (1989), SIMS depth profiling of semiconductors, *chapter 5 in Secondary Ion Mass Spectrometry, Principles and Applications, eds Vickerman J.C, Brown, A, Reed, N.M, Clarendon Press, Oxford.*

Mendelson S, (1964), Stacking Fault Nucleation in Epitaxial Silicon on Variously Orientated Silicon Substrates, *J. Appl. Phys.* 35, p1570-1581.

Metzger, R.A & Allen, F.G, (1984a), Evaporative antimony doping of silicon during molecular beam epitaxial growth, *J. Appl. Phys.* 55(4), p931-940.

Metzger. R.A & Allen. F.G, (1984b), Antimony Adsorption on Silicon, *Surf. Sci.* 137, *p397-411*.

Morin. F.J & Maita. J.P, (1954), Electrical Properties of Silicon containing Arsenic and Boron, *Phys. Rev.*, 96(1), *p28-35*.

Mullins. W.W, Hirth. J.P, (1963), The Microscopic Kinetics of Step Motion in Growth Processes, *J. Phys. Chem. Solids*, 24, *p1391-1404*.

Nakagawa. K & Shiraki. Y, (1986), Anomalous Mobility Enhancment in Si Doping Superlattices, *Surf. Sci.*, 174, *p646-650*.

Nannichi. Y, (1963), Epitaxial Growth of Silicon by Vacuum Sublimation, *Nature*, 200(4911), *p1087-1088*

Nauka. K, Lagowski. J, Gatos. H.C, (1985), Intrinsic Gettering in Oxygen-Free Silicon, *p175-180 in Impurity Diffusion and Gettering in Silicon, Vol 36 of Mat. Res. Soc. Sym. Proc., Materials Research Society, Boston*.

Neave. J.H, Joyce. B.A, Dobson. P.J, Norton. N, (1983), Dynamics of Film Growth of GaAs by MBE from RHEED Observations, *Appl. Phys.*, A31, *p1-8*

Newstead. S.M, (1989), Private communication.

Ni. W. -X, Knall. J, Hasan. M. A, Hansson. G. V, Sundgren. J. -E, Barnett. S. A, Markert. L. C, Greene. J. E, (1989), Kinetics of dopant incorporation using a low-energy antimony ion beam during growth of Si(100) films by molecular-beam epitaxy, *Phys. Rev. B*, 40(15), *p10449-10459*

Nobili. D, (1988), Chapters 13.9, 13.4-13.16 in Properties of Silicon, *published by INSPEC, The Institution of Electrical Engineers, London*.

Nodili. D, Armigliato. A, Finetti. M, Solmi. S, (1982), Precipitation as the phenomenon responsible for the electrically inactive phosphorus in silicon, *J. Appl. phys.* 53(3), *p1484-1491*.

Oh. J.E, Bhattacharya. P.K, Chen. Y.C, Tsukamoto. S, (1989), Molecular-beam epitaxial growth of high-quality InSb on InP and GaAs substrates, *J. Appl. Phys.* 66(8), *p3618-3621*.

Ostram. R.M & Allen. F.G, (1986), Boron doping in Si molecular beam epitaxy by co-evaporation of B_2O_3 or doped silicon, *Appl. Phys. Lett.* *48(3)*. *p221-223*.

Ota. Y, (1977), Si Molecular Beam Epitaxy (n+ on n) with Wide Range Doping Control, *J. Electrochem. Soc.* *124(11)*. *p1795-1802*.

Ota Y, (1980), Silicon molecular beam epitaxy with simultaneous ion implant doping, *J. Appl. Phys.*, *51*, *p1102-1110*.

Ota y, (1983), Silicon Molecular Beam Epitaxy, *Thin Solid Films* *106*, *p1-136*

Panish. M.B & Arthur. J.R, (1970), Phase equilibria and vapour pressures of the system In+P, *J. Chem. Thermodynamics* *2(3)*. *p299-318*.

Parker. E.H.C (ed), (1985), The Technology and Physics of MBE, *Plenum Press, New York*.

Parker. E.H.C & Whall. T.E, (1988), The Reduction of Silicon Molecular Beam Epitaxy to Real World Industrial Practice, *Proc. 2nd Int. Conf. on Si-MBE, Honolulu, J. Electrochem. Soc* *88-8*. *p347-354*.

Payne. M.C, Roberts. N, Needs. R.J, Needels. M, Joannopoulos. J.D, (1989), Total Energy and Stress of Metal and Semiconductor Surfaces, *Surf. Sci.*, *211/212*. *p1-20*.

Pearce. C.W & McMahon. R.G, (1977), Role of metallic contamination in the formation of "saucer" pit defects in epitaxial silicon, *J. Vac. Sci. Technol.*, *14(1)*. *p40-43*

Phelan V.J, (1986), Determination of Impurities in Silicon Epitaxial Layers, *GEC Hirst Research Centre Internal Report No MSI17804*

Phillips. J.C, (1970), Ionicity of the Chemical Bond in Crystals, *Rev. Mod. Phys* *42(3)* *p317-356*.

Phys/PD3, (1989), Preparation of Ph.D. Thesis, *Department of Physics, University of Warwick, UK*.

Pidduck. A.J, Robbins. A.J, Young. D.J. Patel. G. (1990). Rippled Surface Topography Observed on Silicon Molecular Beam Epitaxial and Vapour Phase Epitaxial Layers, *Thin Solid Films*, *184*, *p255-262*.

Ploog. K & Fishcer A, (1978), Surface segregation of Sn during MBE of n-type GaAs established by SIMS and AES, *J. Vac Technol 15(2)*. *p255-259*

Polignano. M.L, Cerofolini. G.F, Bender. H, Claeys. C, (1988), Gettering mechanisms in silicon, *J. Appl Phys.*, *64(2)*. *p869-876*

Rath H.J, Stallhofer P, Huber D, Eichinger P, Ruge I, (1985), Assessment of Metallic Trace Contaminates on Silicon Wafer Surfaces, *Mat. Res. Soc Sym. Proc.*, *16*, *p13-18*.

Ravi, K.V, (1981), Chapter 3 & 5 in Imperfections & Impurities in Semiconductor Silicon, *John Wiley & Sons Inc, New York*.

Richardson. W.B & Mulvaney. B.J, (1988), Plateau and kink in P profiles diffused into Si: A result of strong bimolecular recombination?, *Appl Phys Lett. 53(20)*. *p1917-1919*.

Robbins D.J, Ganson D.B, Hardeman R.W, Chew N.G, Cullis A.G, Warwick C.A, (1985), Luminescence and TEM of Defects in Silicon MBE Layers, *Proc. First Int. Sym. Si-MBE, Electrochem. Soc. Proc*., *85-3*, *p.57-67*.

Rockett. A, Barnett. S.A, Greene. J.E, Knall. J, Sundgren. J.E, (1985), Dopant depth distribution as a function of growth temperature in In-doped (100) Si grown by Molecular Beam Epitaxy, *J. Vac. Sci. Technol. A3(3)*. *p855-859*.

Rockett. A, Klem. J, Barnett. S.A, Greene. J.E, Morkoc. H, (1986), Si incorporation probabilities and depth distributions in $Ga_{1-x}Al_xAs$ films grown by molecular-beam epitaxy, *J. Appl. Phys. 59(8)*. *p2777-2783*

Sadana. D.K, (1985), Gettering & Precipitation Phenomena in Semiconductors, *p245-255 in Impurity Diffusion and Gettering in Silicon*, *Vol.*

36 of Mat. Res. Soc. Sym. Proc., Materials Research Society, Boston.

Sakamoto, T, Kawai, N.J, Nakagawa, T, Ohta, K, Kojima, T, (1985), Intensity oscillations of reflection high-energy electron diffraction during silicon molecular beam epitaxial growth, *Appl. Phys. Lett, 47(6). p617-619.*

Salih, A.S, Kim, H.J, Dacis, R.F, Rozgonyi, G.A, (1985), Extrinsic gettering via the controlled introduction of misfit dislocations, *Appl. Phys Lett., 46(4). p419-421.*

Salih, A.S.M, Ryu, J.S, Rozgonyi, G.A, Bean, K.E, (1986), Extrinsic Gettering via Epitaxial Misfit Dislocations: Electrical Characterisation, *Electrochem Sci. Tech., 133(3). p475-478.*

Schimmel, D.G, (1979), Defect Etch for <100> Silicon Evaluation, *J. Electrochem. Soc., 126. p479-483.*

Schimmel, D.G & Elkind, M.J, (1978), An Examination of the Chemical Staining of Silicon, *J. Electrochem Soc., 125(1). p152-155.*

Schulz M, (1974), Determination of Deep Trap Levels in Silicon Using Ion-Implantation and CV-Measurements, *Appl. Phys., 4. p225-236.*

Seah, M.P, (1979), Quantitative Predication of Surface Segregation, *J. Catalysis, 57. p450-457.*

Shannon, J.M, (1979), A majority-carrier camel diode, *Appl. Phys. Lett., 35(1). p63-65.*

Shimura, F, Tsuya, H, Kawamura, T, (1981), Thermally Induced Defect Behaviour and Effective Intrinsic Sink in Silicon Wafers, *J. Electrochem Soc., 128(7). p1579-1583.*

Sidebotham, E.C, Peaker, A.R, Hamilton, B, Hopkinson, M, Houghton, R, Patel, G, Whall, T.E, Parker, E.H.C, (1988), The Effects of Substrate Temperature on Deep States in MBE Silicon, *Proc. 2nd Int. Conf. on Si-MBE, Honolulu, J. Electrochem. Soc. 88-8. p360-367.*

Sirota. N.N, (1968). Chapter 2 in Semiconductors and Semimetals. *Vol 4, Physics of III-V compounds, Willardson. R.K, Beer. A.C (ed), Academic Press, New York.*

Smith. D.W, Houghton. R.F, Parker. E.H.C, Whall. T.E, (1990). The p-n Diode as a Diagnostic Tool for Silicon Molecular Beam Epitaxy, *Thin Solid Films, 184, p177-183*

Sparks. D.R, Chapman. R.G, Aivi. N.S, (1986). Anomalous diffusion and gettering of transition metals in silicon, *Appl Phys. Lett., 49(9), p525-527.*

Sparks. D.R & Randall. G.C, (1986). The Use of Rapid Thermal Annealing for Studying Transition Metals in Silicon, *J. Electrochem Soc., 133(6), p1201-1205.*

Stacy. W.T, Allison. D.F, Wu. T.C, (1981). The Role of Metallic Impurities in the Formation of Haze Defects, *p334-335 in Semiconductor Science, Huff H.R, Kreigler. R.J, eds, Electrochemical Society*

Stanley. C.R, Farrow. R.F.C, Sullivan. P.W, (1985). MBE of InP and Other P-Containing Compounds, *Chapter 9 in The Technology and Physics of Molecular Beam Epitaxy, Parker. E.H.C ed, Plenum Press, New York.*

Stenin. S.L, (1986). Molecular beam epitaxy of semiconductor, dielectric and metal films, *Vacuum, 36(7-9), p419-426*

Stewart D.A & Newton D.C, (1983). Determination of Iron in Semiconductor-grade Silicon by Furnace Atomic-absorption Spectrometry, *Analyst, 108, p1450-1458*

Stoll. L, Hedstrom, J, Sigurd. D, (1985). Coevaporation with a rate control system based on a quadrupole mass spectrometer, *J. Vac Sci. Technol., A3(2), p403-407*

Street. R.A, (1982). Doping and the Fermi Energy in Amourphous Silicon, *Phys. Rev. Lett., 49(16), p1187-1190*

Subbanna. S, Tuttle. G, Kroemer. H, (1988), N- Type Doping of Gallium Antimonide and Aluminium Antimonide Grown by Molecular Beam Epitaxy using Lead Telluride as a Tellurium Dopant Source, *J. Electronic Materials 17(4), p297-303*

Sugiura. H & Yamaguchi. M, (1981), Growth of dislocation-free silicon films by molecular beam epitaxy (MBE), *J. Vac. Sci. Technol. 19(2), p155-160.*

Sze. S.M, (1985), Chapter 1 & 8 in Semiconductor devices, physics and technology, *John Wiley and Sons, New York.*

Tatsumi T, Hirayma H, Azaki N, (1989), Si particle density reduction in Si molecular beam epitaxy using a deflection electrode, *Appl Phys Lett. 54(7), p.629-631*

Tatsumi, T, Naoaki. A, Tsuya. H, (1985), Advanced Techniques to Decrease Defect Density in Molecular Beam Epitaxial Silicon Films, *Jap. J. Appl Phy., 24(4), pL227-L229.*

Thomas. R.N & Francombe. M.H, (1969), Low-Temperature Epitaxial Growth of Doped Silicon Films and Junctions, *Solid-State Electronics, 12, p799-811.*

Tobin. S.P, Greenwald. A.C, Wolfson. R.G, Meir. D.L, Drevinsky. P.J, (1985), Rapid Diffusion of Molybdenum Trace Contamination in Silicon, *p43-48 in Impurity Diffusion and Gettering in Silicon, Vol 36 of Mat. Res. Soc. Sym. Proc., Materials Research Society, Boston.*

Tolomasov. V.A, Abrosimova. L.N, Gorshenin. G.N, (1971), Epitaxial Films of n-Type Silicon Obtained by Vacuum Sublimation, *Sov. Phys. Crystallogr., 15(6), p1076-1080.*

Tsang. W.T, Miller. R.C, Capasso. F, Bonner. W.A, (1982), High quality InP grown by molecular beam epitaxy, *Appl. Phys. Lett. 41(5), p467-469*

Tsuya, H, Shimura, F, Ogawa, K, Kawamura, T, (1982), A Study on Intrinsic Gettering in CZ Silicon Crystals: Evaluation, Thermal History Dependance and Enhancement, *J. Electrochem. Soc.*, *129(2)*, *p374-379*.

Uhrabera, R.I.G, Brinqans, R.D, Bachrach, R.Z, Northrup, J.E, (1986), Electronic and atomic structure of arsenic terminated Si(100), *J.Vac. Sci. Tech.* *A4*, *p1259-1264*.

Varker, C.J & Ravi, K.V, (1974), Oxidation-induced stacking faults in silicon. II. Electrical effects in *PN* diodes, *J. Appl. Phys.*, *45(1)*, *p272-287*.

Vivian, A.C, (1920), Tin-Phosphorus Alloys, *Institute of Metals Journal*, *23*, *p325-360*.

Weast, R.C, (1988), ed, Table F115 - F123 in CRC Handbook of Chemistry and Physics, *1st Student Edition, CRC Press Inc, Florida*.

Weber, E.R, (1985), Diffusion, Complexing and Precipitation of Transition Metals in Silicon, *p3-11 in Impurity Diffusion and Gettering in Silicon, Vol 36 of Mat Res. Soc. Sym. Proc., Materials Research Society, Boston*.

Werkhoven C.J, (1983), Source, Transport and Precipitation of Metallic Impurities in Si Epitaxy, *Proc. Electrochem. Soc., Vol. 83-4, p144-154*.

Wittmaack, K, (1982), Design and performance of quadrupole-based SIMS instrument: A critical review, *Vacuum*, *32(2)*, *p65-89*.

Wong, C.-C.D, Malwah, M.L, Pollock, L, (1985), Nucleation Time Effects on Intrinsic Gettering, *p239-44 in Impurity Diffusion and Gettering in Silicon, Vol 36 of Mat Res. Soc. Sym. Proc., Materials Research Society, Boston*.

Wood, C.E.C, (1985), Molecular Beam Epitaxial III-V Compounds: Dopant Incorporation, Characteristics and Behaviour, *Chapter 4 in The Technology and Physics of MBE, Parker, E.H.C (ed), Plenum Press, New York*.

Wynblatt. P & Ku. R.C, (1977). Surface Energy and Solute Strain Energy Effects in Surface Segregation, *Surf. Sci.* 65, *p511-531*.

Xie Y.H, Wu Y.Y, Wang K.L, (1986). Deep level defect study of molecular beam epitaxially grown silicon films, *Appl. Phys. Lett.*, 48(4), *p287-289*.

Zeindl. H.P, Wegehaupt. Eisele. I, (1987). Growth and Characterisation of a delta-function doping layer in Si, *Appl. Phys. Lett*, 50(17), *p1164-1166*.

Zhu. J, Chaussemy. G, Barbier. D, (1989). Rapid thermal annealing: An efficient means to reveal chromium profiles in Si after diffusion and gettering, *Appl. Phys. Lett.*, 54(7), *p611-613*.

TITLE Silicon Molecular Beam Epitaxy: Doping and Material Aspects

AUTHOR Govind Pindoria
(formally Govind Patel)

INSTITUTION and DATE University of Warwick, 1990